Directing the self-assembly of short peptide derivatives

Maria Paola Conte

Thesis presented to the Department of Pure and Applied Chemistry, University of Strathclyde, in fulfilment of the requirements for the degree of Doctor of Philosophy.

2017

Declaration

This thesis is the result of the author's original research. It has been composed by the author and has not been previously submitted for examination which has led to the award of a degree.

Signed:

Date:

“I cannot remember the books I have read any more than the meals I have eaten; even so, they have made me.”

R. W. Emerson (Dubious attribution)

Acknowledgements

As I have undertaken this journey, the record of which is detailed in this thesis, I have been given unique opportunities and I have encountered dozens of remarkable individuals who I wish to acknowledge.

Firstly, I would like to express my sincere gratitude to my supervisors, Prof. Rein V. Ulijn and Dr. Aaron Lau, for giving me the opportunity to undertake this research project and for all of their continuous support and guidance. In particular, I would like to thank Prof. Rein V. Ulijn for giving me the chance to spend six months in his lab at the ASCR in NYC, which is an amazing place to work.

I would also like to show my gratitude to Dr. Alastair Wark for his patience and assistance with the operation of his microscope and to Dr. Elisa Riedo for the work done in collaboration at the ASRC in NYC. I am also grateful to Margaret Mullin from Glasgow University for her help with the TEM and to Isabel Scott for her positive attitude in every circumstances.

I give many thanks to the Ulijn Lab and Lau Lab members, in Glasgow and in New York, for their help and support, for the warm welcome at the very beginning and for being good friends and not just good colleagues: Jugal, Yousef, Gary, Nadeem, Mona, Mohit, Nadeesha, and all the other current and former members that I know. It was great sharing the lab with all of you during the last three and a half years.

I would like to acknowledge the Marie Curie Actions program for funding my project and all the fellow students and the supervisors in the SMARTNET: Ana Catarina, Jorge, Kars, Laura, Marco, Matija Nishant, Philip, Serhii, Tomasz and Vânia. Thank you for all the constructive discussions and the great time we always had during our meetings and our trips around Europe.

I sincerely thank all of you, for I cannot imagine any Ph.D. to be a better experience than this.

There are many people whose direction, encouragement, support and company have proved invaluable along the way and that I wish to thank.

My deepest gratitude goes to all the members of our “Glasgow Family”: Andreia, Kiko, Flo, Ivan, Laura, Miguel, Nuno and Paula. Thank you for your support, for your company and for all the wonderful memories we share. I will forever remember fondly our time together. Davide, thank you for always being there for me, your support throughout the years has been invaluable.

My PhD would have not been the same without some of my office and lab mates throughout the years:

Inês, who has been a true friend since we began (almost) together this adventure, and who has been such a great company (and roommate!) during our wonderful tours around Europe; Ana, for always being there, for our chats and lunches together, for her support and company throughout the years; Krystyna, who was there whenever I needed a break and made every day in the lab more entertaining!

Babis, thank you for being there in such a special moment of my life, for being “The Hero” and making my time in NYC even more exciting. I miss our conversations about philosophy, love, life and supramolecular death.

Annalisa, working with you has been a pleasure and a blast! I have never laughed so much in the lab! Thank you for your company and for exploring The City with me. Ana Pina, Carina, Sara, Vanesa and Sureyya, my amazing flatmates in the Towers, thank you for the unforgettable time we spent together.

Most of all, I would like to thank my parents, for their unconditional love throughout my life. They have cherished with me every great moment and supported me whenever I needed.

My biggest acknowledgement goes to the people who cannot read these pages, and to whom I wish to dedicate my work: my grandparents, Babbo e la Nana.

Finally, I would like to thank Dan, for affecting my life in ways I could have never predicted. Thank you for always being understanding, encouraging and entertaining. Every day I spend with you, my love gains strength.

Grazie.

A Babbo e alla Nana

Abstract

Self-assembly of molecular building blocks has attracted increasing interest as an effective bottom-up approach for the design of functional nanomaterials. Amongst the variety of known molecular building blocks, very short (di- and tri-) peptides and their derivatives are of particular relevance in this context due to their chemical simplicity, low cost and remarkable properties.

In this thesis, we first investigate the behaviour of the well-known self-assembling dipeptide diphenylalanine (FF) and its amidated derivative (FF-NH_2) in a predominantly aqueous environment. We demonstrate that these molecules can form metastable hydrogels upon a combination of solvent switching and sonication of the dipeptide solutions. The hydrogels show instantaneous syneresis upon mechanical contact resulting in rapid expulsion of water and collapse into a semi-solid gel. Thanks to the highly hydrophobic nature of the fibres formed, the gels can be employed as selective scavengers for small hydrophobic molecules.

Combining biocatalysis and molecular self-assembly provides an effective approach for processing of self-assembled materials, directing the assembly kinetics by means of catalysis which results in the controlled formation of hierarchical nanostructures. Herein, we investigate the possibility to achieve localised self-assembly of peptide derivatives exploiting different strategies to immobilize enzymes, thereby adding spatial control over the self-assembly process.

We functionalised surfaces with bioinspired polydopamine and polyphenol coatings to study the effects of enzyme surface localisation and surface release on the self-assembly process. We demonstrate how these coatings could be conveniently used to release protease enzyme thermolysin into a pre-gelator (Fmoc-T and F-NH_2) solution for bulk gelation as well as to irreversibly immobilize the enzyme for localizing the self-assembly to the surface.

Enzyme-(magnetic)nanoparticle conjugates were employed to trigger the self-assembly and gelation of peptide derivatives in two different systems, an equilibrium system and a far from equilibrium one. For both systems, the self-assembly results in the formation of stable

hydrogels. We were able to visualise the self-assembled nanostructures at the site of enzyme immobilization by electron microscopy. Moreover, employing magnetic nanoparticles allows for an additional level of control on the properties of the hydrogels, which can be manipulated with an external magnetic field.

Finally, we employed a soft-lithographic technique (microcontact printing) to transfer a pattern of enzymes onto a modified substrate. The surfaces with the patterned thermolysin were used to trigger the localized formation of the gelator Fmoc-TF-NH_2 through direct condensation of two non-assembling precursors Fmoc-T and F-NH_2. Fluorescence microscopy was employed to confirm the localized formation of self-assembled structure by staining the β-sheet fibres with Thioflavin T.

The thesis concludes with a number of overall conclusions that can be drawn from the work presented, as well as some possible directions for future work.

Publications

1* Spatially controlled biocatalytic self-assembly on magnetic nanoparticles

M. P. Conte, J. Sahoo, K. H. A. Lau and R. V. Ulijn

ACS Appl. Mater. Interfaces, **2017**, In Preparation

2* Biocatalytic self-assembly using reversible and irreversible enzyme immobilization

M. P. Conte, K. H. A. Lau and R. V. Ulijn
ACS Appl. Mater. Interfaces, **2017**, 9, 3266-3271

3* Metastable hydrogels from aromatic dipeptides

M. P. Conte, N. Singh, I. R. Sasselli, B. Escuder, R. V. Ulijn
Chem. Commun., **2016**, 52, 13889-13892

4 Insight into the esterase like activity demonstrated by an imidazole appended self-assembling hydrogelator

N. Singh, **M. P. Conte**, R. V. Ulijn, J. F. Miravet and B. Escuder
Chem. Commun., **2015**, 51, 13213-13216

Publications directly related with this thesis indicated with *.

Oral Presentation

2016 *Spatio-temporal control of Biocatalytic Self-Assembly via immobilized enzymes*

Gels, Formulations and Supramolecular Materials

Solvay, RIC, Paris

Posters

2016 Bio-Nano-Med

City University of New York, New York, USA

2015 Active and Adaptive Materials

City University of New York, New York, USA

2015 Nanopeptide 2015: International Meeting on Peptide and Protein based Materials and Technologies

University of Strathclyde, Glasgow, UK

2014 ERC Grantees Conference 2014

Humboldt University, Berlin, Germany

Abbreviation list

µCP	Microcontact Printing
2D	Two-dimensional
3D	Three-Dimensional
AFM	Atomic Force Microscopy
CCD	Charge-Coupled Device
CLEAs	Cross-Linked Enzymes Aggregates
CLECs	Cross-Linked Enzymes Crystals
DA	Dopamine
DCL	Dynamic Combinatorial Library
DOPA	3,4-dihydroxyphenylalanine
DPN	Dip-pen Nanolithography
ECM	Extra Cellular Matrix
FITC-BSA	Fluorescein Isothiocyanate labelled Bovine Serum Albumin
Fmoc	9-Fluorenylmethyloxycarbonyl
FRET	Förster Resonance Energy Transfer
HPLC	High Performance Liquid Chromatography
IgG	Immunoglobulin G
ISISP	Ink Subtract Ink Subtract Print
ISP	Ink Subtract Print
LMWG	Low Molecular Weight Gelator
MSCs	Mesenchymal Stem Cells
nCP	Nanocontact Printing
PG	Pyrogallol

PMMA	Poly(methyl methacrylate)
RP-HPLC	Reverse Phase High Performance Liquid Chromatography
SAMs	Self-Assembled Monolayers
SFINKS	Single Feature INKing and Stamping
TA	Tannic acid
TCNL	Thermochemical Nanolithography
TEM	Transmission Electron Microscopy
ThT	Thioflavin T
UV-vis	Ultra Violet – visible

Table of Contents

1. Chapter 1 - Introduction

1.1. Introduction to the Thesis

Molecular self-assembly is a process widely employed by nature. It is a mechanism through which large and complex nanoscale molecular assemblies are formed, via weak intermolecular interactions. This mechanism allows for the formation of the double helix of the DNA, the folding of proteins, and the formation of lipid bilayer membranes.[1]

Naturally occurring proteins have the inherent ability to self-assemble into secondary structures such as β-sheets, α-helices and coiled coils. The understanding of the rules that govern the self-assembly of naturally occurring proteins have inspired design of synthetic analogues that can mimic this tendency to self-assemble.[2, 3]

Peptide-based systems have been proven to assemble through non-covalent intermolecular interactions into highly organised nanostructures.[4, 5, 6] The self-assembly of these molecules typically gives rise to nanofibers or nanotubes, which entangle to form a network. This network of fibers can in turn trap water resulting in the formation of a hydrogel. The self-assembly of peptide derivatives into supramolecular hydrogels can either occur spontaneously or can be triggered by a variety of external stimuli, including pH, salt concentration, temperature, mechanical triggers or UV-vis light.[7-9]

An alternative and more sophisticated trigger is the catalytic action of enzymes. Compared to chemical or physical stimuli, enzymatic triggering operates under physiological conditions of pH, temperature and ionic strength and is thus particularly attractive for biological and biomedical applications. The combination of molecular self-assembly and (bio-)catalysis provides a powerful means for the controlled fabrication of complex nanostructures. This approach has been inspired by biological systems, where self-assembly is often coupled to catalysis.[10] In addition to applications that take advantage of biological function of enzymes, there is scope for the use of enzyme assisted self-assembly for the biofabrication of nanostructures with enhanced complexities, by taking advantage of selectivity, spatiotemporal control of nucleation and structure growth, with a wide range of biotechnological applications.

1.2. Motivation of the project

The motivation of this research was to investigate the self-assembling behaviour of very short, purely peptidic systems and of peptide derivatives and to direct the assembly with various external triggers. This was achieved by a combination of mechanical and chemical stimuli in the first instance, and then by employing enzymes to trigger the self-assembly. Moreover, we aimed to introduce an additional level of control in systems that employ biocatalysis to trigger the self-assembly of peptide amphiphiles. To achieve this goal, we investigated the possibility to exploit immobilised enzymes, on flat surfaces or onto nanoparticles, which may allow for spatially selective self-assembly.

1.3. Layout of the Thesis

This thesis is split into 7 separate Chapters. The literature review chapter consists of three different sections related to the three main topics involved in the project. The first section focuses on supramolecular self-assembly of peptide-based nanomaterials, which includes an overview of the enzymatically triggered self-assembly of aromatic peptide amphiphiles. The second section focuses on various strategies for enzyme immobilisation, explaining the benefits of employing these systems instead of their soluble counterparts and analysing the effect of immobilisation on the performance of the catalysts. The third and final section of the literature review is related to the strategies to realise a controlled pattern of enzymes or other biomolecules with micro- and nanometre resolution, giving examples of a few relevant techniques that have been applied for this purpose.

The experimental chapters are presented separately, each with its own introduction, discussion, experimental section and conclusion. This layout allows readers to consult individual Chapters.

The first experimental Chapter (Chapter 3) describes the formation of metastable dipeptide hydrogels obtained upon sequential solvent switching and sonication of dipeptide solutions. All the following experimental chapters investigate different strategies to achieve localised biocatalytic self-assembly exploiting immobilised enzymes.

In Chapter 4, surfaces functionalised with polydopamine and polyphenol coatings are employed to study the effects of enzyme surface localisation and surface release on the self-assembly process. These coatings are conveniently used to release enzymes for bulk gelation as well as to irreversibly immobilise enzymes for localising the self-assembly to the surface.

In Chapter 5, enzymes immobilised onto magnetic nanoparticles are used to trigger the self-assembly of peptide derivatives. This approach allows for the visualisation of self-assembled nanostructures at the site of enzyme immobilisation and for an additional control of the resulting hydrogel by an external magnetic field.

In the last experimental Chapter (Chapter 6), a soft-lithographic technique (microcontact printing) was employed to transfer a pattern of enzymes on polydopamine or polyphenol coated substrates. The printed enzymes are employed to trigger the localised self-assembly of aromatic peptide amphiphiles.

The experimental Chapters are followed by an overall conclusion.

2. Chapter 2 - Literature Review

2.1. Supramolecular Gels

2.1.1. Introduction

Supramolecular chemistry is a highly interdisciplinary field of science that focuses on chemical systems made up of assembled molecular components held together and organised by means of weak intermolecular (non-covalent) interactions. In the last decades there has been a growing interest towards the possibility of producing functional materials exploiting supramolecular chemistry. A sub-branch of this field is focused on supramolecular gels.

A gel is a two-phase material with solid-like behaviour, in which the main component is a liquid (or gaseous) phase. The second constituent of a gel is a solid phase, which forms a three-dimensional cross-linked network in the liquid (or gas). The gel state has been recognised since the 1860's, when Thomas Graham (Professor of Chemistry at what is now the Universtiy of Strathclyde) gave a first description of these materials;[11] in the following years, scientists attempted to provide more rigorous definitions in order to better describe the physical properties of these materials and to link them to their microscopic features.[12, 13, 14] The major component of gels is the gaseous or liquid phase, nevertheless they exhibit solid-like behaviour, since the bulk phase is trapped by the entangled three dimensional matrix.[15] Gels can be classified according to the chemical nature of their components (assembled small molecules or polymers), the type of interactions that lead to the formation of the network (physical or chemical) or the physical state of the medium entrapped (*i.e.* gas or liquid).

In supramolecular gels, the network components are small organic compounds, known as Low Molecular Weight Gelators (LMWGs). These molecular gelators self-assemble into a supramolecular structure, which constitutes the solid component of the gel. LMWGs can be classified as organogelators or hydrogelators, depending on whether the liquid phase is an organic solvent or water.[16] A wide range of gelators are known, with very different molecular structures and inspiration for the design of synthetic gelators often comes from

the biological world. Supramolecular hydrogelators share common features with certain self-assembled structures in biology, such as amphiphilicity and reliance on specific supramolecular interactions. Regardless of their structural diversity, their self-assembly is driven by non-covalent interactions, such as π-π stacking, hydrogen bonding, electrostatic and hydrophobic interactions.[17] Supramolecular gels are physical gels, since the formation of the 3D network occurs due to entanglements of the network components (typically fibres) and weak non-covalent interactions that arise between them, so that these gels are generally thermo-reversible.[13, 14] Polymers, proteins, small organic molecules are examples of substances that can form *physical* gels.[13] By contrast, *chemical* gels are formed by covalent cross-linking between the network components, resulting in an irreversible structure (unless the chemical bonds are broken). Examples of chemical gels include many polymeric gels, which consist of covalently cross-linked networks that swell due to the absorption of solvent molecules.[13, 18]

Following the rise of supramolecular chemistry in the 1970s and 1980, since 1990 the number of publications on supramolecular gels has rapidly increased.[13, 19, 20] This interest has been driven by the number of existing, and potential applications these materials may have (e.g. chemical sensing, cosmetics, drug delivery, tissue engineering).[21, 22, 23]

2.1.2. Low Molecular Weight Gelators

Traditionally, gel chemistry has been dominated by polymer-based materials; more recently however, interest has shifted towards gels obtained from LMWGs.[24, 25] These type of gels display a responsive behaviour towards external stimuli such as pH, temperature, chemicals, light or sound waves.[26] The main advantage that supramolecular gels offer compared to polymer gels is the 'designability' of the building blocks: the possibility to design LMWGs and to introduce different functionalities, allows for the potential tailoring of the properties of the materials that result, for several different applications, ranging from tissue engineering and drug delivery to molecular electronics and sensing.[24]

In recent decades, many different LMWGs have been studied, covering a wide structural diversity. Most of them have been discovered serendipitously, but in the last years the finding of new gelators has been progressing towards a more rational design.[27, 28] Examples

of LMWGs have been reported for the gelation in both organic solvents[16, 29, 30] and water.[31, 32] The ability for these molecules to gelate solvents is often related to their amphiphilic behaviour. A variety of chemically diverse structures have been employed as LMWGs. A comprehensive review of the different LMWGs is outside the scope of this thesis since the main focus is on peptide-based hydrogelators.

2.1.2.1. Peptide-based Hydrogelators

Peptides and derivatives thereof are of particular interest as building blocks for molecular self-assembly.[33] Nature provides an extremely powerful toolbox for the fabrication of protein and peptides: exploiting only the 20 gene-encoded amino acids, 20^n different peptide sequences can be obtained (*n* being the number of amino acids in the sequence).[17] A huge variety of structures can thus be achieved through the combination of different amino acid sequences. A number of these sequences are known to assemble into nanoscale fibres, giving rise to nanostructured gels. All of the 20 gene-encoded amino acids are chiral (except for glycine) and occur in nature mainly in the L-form (Fig. 1). They all have the same backbone (except of proline, which is an imino acid), bearing different side chains, which dictate the different properties of the molecules.

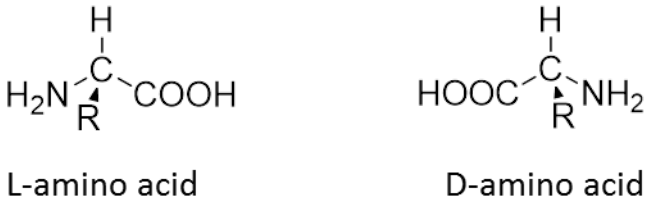

Figure 1 L- and D- amino acid configurations.

According to the different functional groups of the side chains, amino acids can be classified into different categories: hydrophobic (aromatic and aliphatic), hydrophilic, positively or negatively charged[34] (Fig. 2). Glycine, cysteine and proline do not fall under any of these categories and are therefore classified as "others". The minimal steric hindrance of the R group in glycine will introduce high flexibility in the peptide chains containing this residue; in contrast, a proline residue will confer backbone rigidity to the chain. The SH functional group on cysteine side chain can be exploited for the crosslinking of peptides by oxidative formation of disulphide bonds between cysteines.[35] The position of the amino acids relative to one another in the peptide chain influences the final peptide configuration. Peptide chains interact with one another by means of various non-covalent interactions, such as

hydrogen bonding, π-π stacking, electrostatic and hydrophobic interactions. These local interactions between residues lead to the formation and help the stabilisation of secondary structures and subsequently tertiary structures in proteins.[23] Throughout this review, amino acids and peptide sequences will be referred to using the one letter amino acids code.

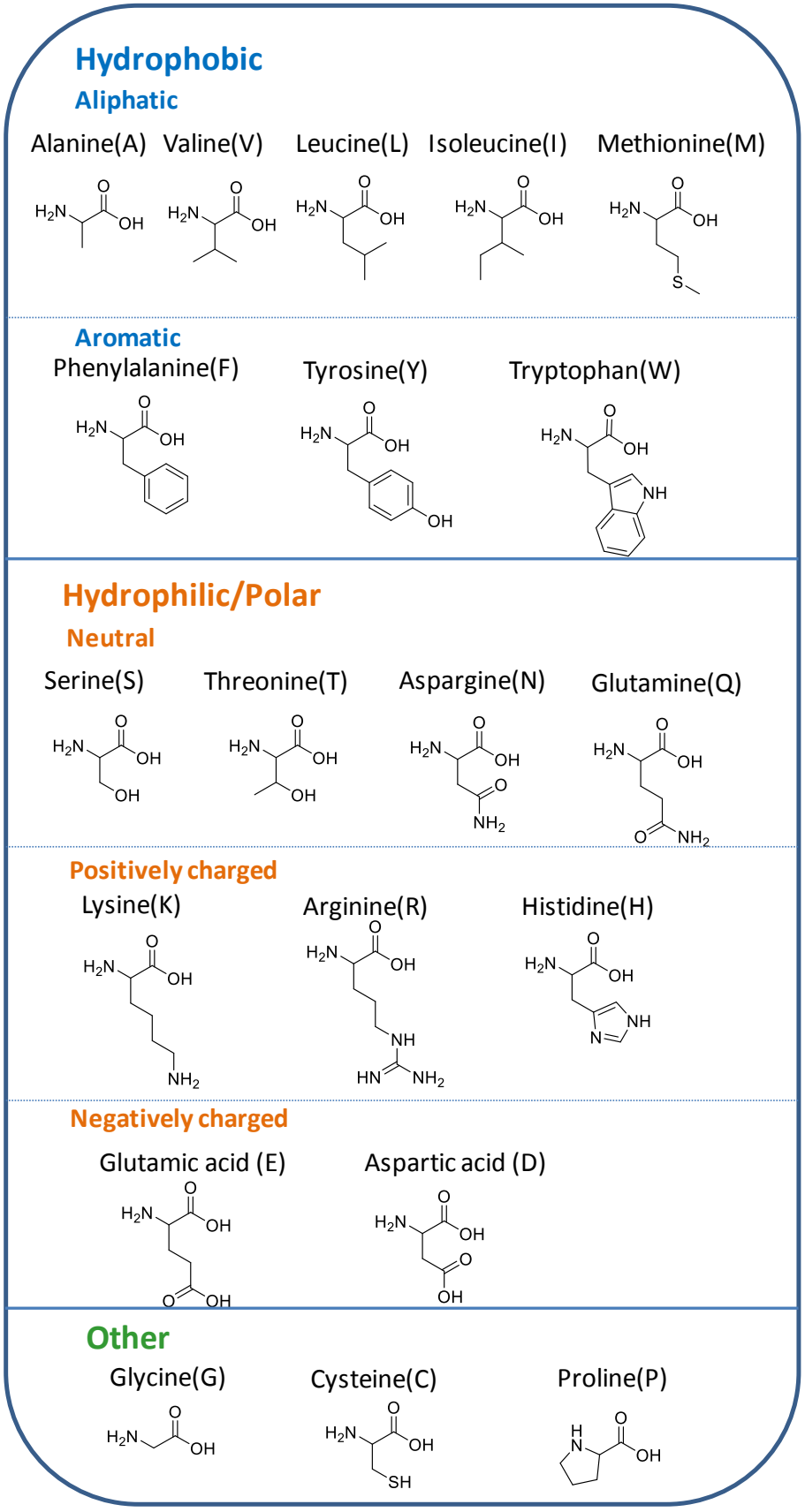

Figure 2 Chemical structures of 20 gene-encoded amino acids. Modified from reference 17.

2.1.3. Non-covalent Interactions in Supramolecular Chemistry

Non-covalent interactions are the driving forces for the formation of supramolecular structures. Compared to covalent bonds, non-covalent interactions are weaker, nevertheless they are of critical importance in maintaining the three dimensional structure of large molecules such as proteins or nucleic acids and in biochemical processes such as driving the association of two strands of DNA to form a double helix. Electrostatic interactions, hydrogen bonding, van der Waals interactions, π-π interaction and hydrophobic interactions are fundamental non-covalent bond types. They are characterised by different geometry, strength and specificity and they can be affected by the presence of water.[36]

Electrostatic interactions arise when a charged group interacts with another charged group either with opposite polarity (attraction) or with the same polarity (repulsion). The energy of these interactions is given by Coulomb's law:

Eq 2.1. $$E = kq_1q_2/Dr^2$$

where E is the energy, q_1 and q_2 are the charges on the two atoms, r is the distance between the two atoms, D is the dielectric constant and k is a proportionality constant. Ion-ion interactions are the strongest electrostatic interactions, with bond energies ranging from ca. 100 to 350 kJ mol^{-1}.[37] Ion-dipoles interactions are somewhat weaker, ranging between ca. 50 and 200 kJ mol^{-1}. Interactions between two dipoles are even weaker, with energies ranging from 5 to 50 kJ mol^{-1}. As opposed to the ion-ion interactions where there is no particular directionality, the orientation of the dipole with respect to the charge and the orientation of the two interacting dipoles play an important role in ion-dipole and dipole-dipole interactions.[37]

Hydrogen bonding is partially governed by electrostatic interactions. When a hydrogen atom is covalently linked to an electronegative atom, the latter pulls electron density away from the hydrogen atom, which consequently develops a partial positive charge. An electrostatic interaction can hence arise between the partial positive charge on the hydrogen and an atom bearing a partial negative charge. Hydrogen bonding is crucial in biochemistry and for instance is responsible for specific base-pair formation in the DNA double helix.[36] Hydrogen bonds are relatively weak interactions, with energies ranging from

4 to 20 kJ mol^{-1}. The strength of this interaction varies according to the orientation of the hydrogen-bond acceptor and donor, the strongest hydrogen bonds being approximately straight, with the hydrogen-bond donor and acceptor and the hydrogen atom lying on a straight line. Moreover, hydrogen bonds involving charged species are usually significantly stronger than hydrogen bonds between neutral molecules. For example, the strongest hydrogen bond known is the F-H···F^- hydrogen bond, with an energy of ca. 160 kJ mol^{-1}.[37]

van der Waals interactions are amongst the weakest non-covalent interactions, with typical energies <5 kJ mol^{-1}. These forces involve interactions between permanent or induced dipoles, including attractive or repulsive electrostatic interactions between permanent dipoles (Keesom force), attractive interactions between a permanent dipole and an induced dipole (Debye force) and attractive interaction between two induced dipoles (London force).

π-π interactions are associated with the interaction between π-systems. An example of these interactions is the benzene-benzene interaction. Benzene has a permanent quadrupole moment, which arises from the sum of six $C^{\delta-}$- $H^{\delta+}$ bond dipoles. Under the symmetry of benzene, these dipoles add up to a quadrupole moment with a region of negative electrostatic potential parallel to the face of the ring and a region of positive electrostatic potential on the edge of the ring. Because of the repulsion between the two negatively charged faces, two rings do not tend to overlap in a face-to-face manner, but they will position in an edge-to-face orientation (Fig. 3). Another possible configuration is a face-to-face orientation with the two molecules shifted sideways to reduce the repulsive forces. The energy associated with π-π interactions is ~8 kJ mol^{-1} for the edge-to face and ~10 kJ mol^{-1} for the displaced face-to-face configuration.[38]

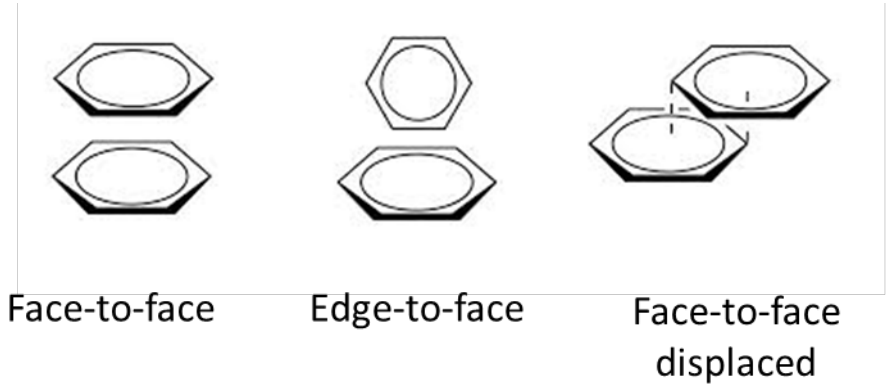

Figure 3 Schematic representing the possible orientations of two benzene rings in π-π stacking.

The Hydrophobic effect is a manifestation of the influence of the environment on intermolecular interactions. Most biochemical reactions take place in water, which is a polar solvent. When a non-polar molecule is placed in aqueous solution, the solute cannot form hydrogen bonds with the water molecules. Therefore, the solvent must rearrange to accommodate the solute and there is evidence that at ambient temperatures a more ice-like structure is formed at the interface.[36] The overall enthalpy change is small with van der Waals interactions still present between solute and solvent. However, there is an overall decrease in entropy as the rotational and translational freedom of interfacial water molecules is reduced. The hydrophobic effect arises because when two or more non-polar molecules interact in water the total surface area that needs to remain in contact with the solvent will be reduced. This releases the "ordered interfacial water molecules" back into the bulk solvent leading to an increase in entropy. The strength of the hydrophobic effect is therefore proportional to the overall reduction in the solvated non-polar surface areas of the interacting molecules.[36] The hydrophobic effect is responsible for the separation of a mixture of oil and water into its two components and is considered to be one of the dominant driving forces for protein folding. In globular proteins in aqueous solution, the hydrophobic residues are normally buried in the core of the protein, stabilizing the folded state. Charged and polar side chains are situated on the water-exposed surface where they interact with surrounding water molecules. Minimizing the number of hydrophobic side chains exposed to water is the principal driving force behind the folding process, although formation of hydrogen bonds within the protein also stabilizes protein structure.[36]

2.1.4. Supramolecular Assembly of Peptides and their Derivatives

Peptides and their derivatives have been proven to assemble into highly organised structures. One important class of these (nano)structures are nanofibers which, provided they have the ability to interact favourably with the solvent, can trap water or solvent molecules resulting in gels.

Naturally occurring proteins have the inherent ability to self-assemble into secondary structures such as β-sheets, α-helices and coiled coils. These types of protein conformations were first characterised in the early 1950s by Pauling, Corey and Crick.[2, 3] The formation of β-sheets occurs when multiple peptide chains, referred to as "strands", are aligned with their backbones parallel to each other. The carbonyls and NH in amide moieties on two adjacent strands can interact via hydrogen bonding and thus stabilise the structure. β-sheets are further classified as parallel or antiparallel, depending on the orientation of the strands in the β-sheet (Fig. 5a and b). In a parallel configuration, the C-termini of all the strands are found at the same end of the chain, in contrast with the antiparallel configuration, where the N-terminus of one strand is adjacent to the C-terminus of the next one. The backbone dihedral angles ϕ and ψ are respectively -119°, +113° for parallel and -139°, +135° for antiparallel β-sheet (Fig. 4).[39, 40]

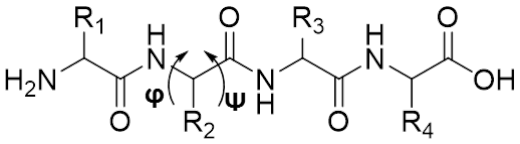

$$\varphi \equiv C'_{i-1} - N_i - C^{\alpha}_i - C'_i$$

$$\Psi \equiv N_i - C^{\alpha}_i - C'_i - N_{i+1}$$

Figure 4 Schematic representation of a peptide chain with the dihedral angles ϕ and Ψ.

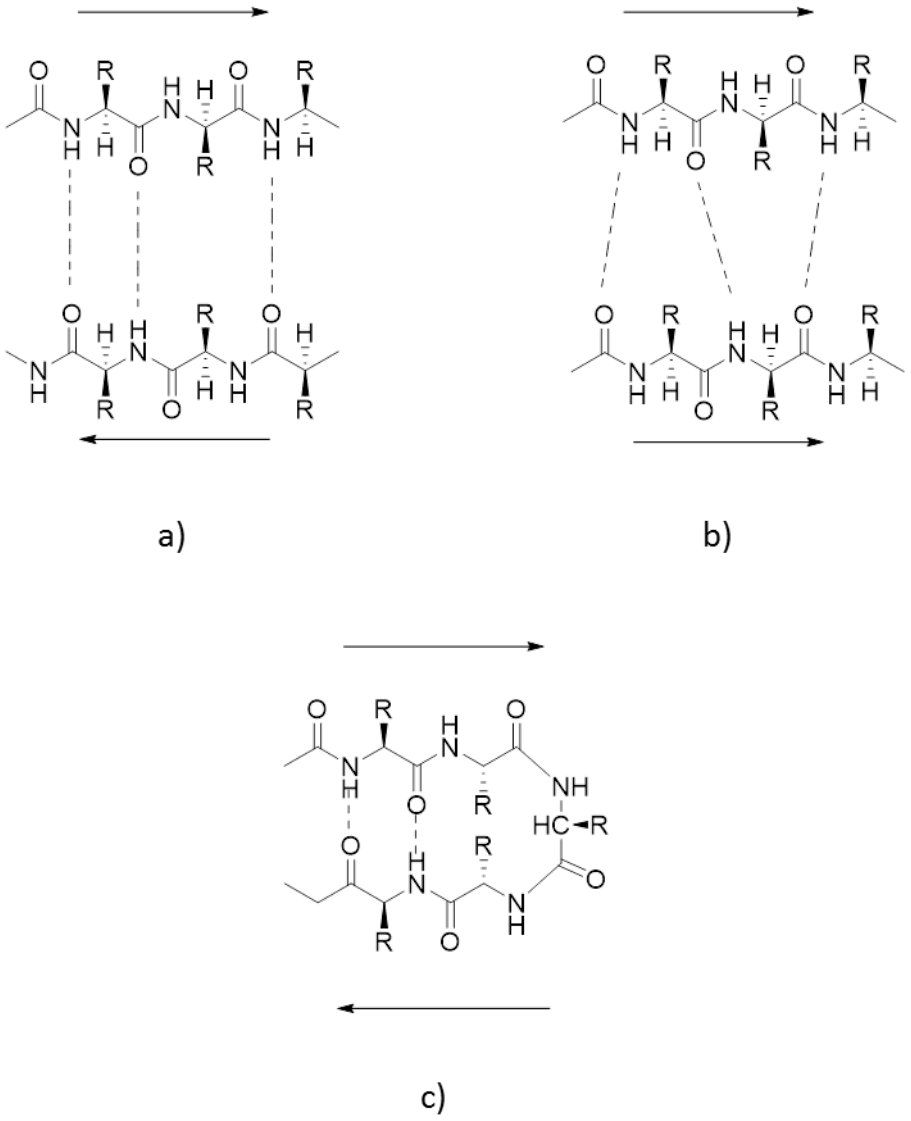

Figure 5 (a) Anti-parallel β-sheet, (b) parallel β-sheet, and, (c) β-hairpin. (The arrow indicates the direction of peptide (N-C)).

Antiparallel β-sheets are slightly more stable than parallel β-sheets because the hydrogen bonding is favoured in this conformation (Fig. 5b). When a single peptide chain folds back on itself, a β-hairpin is formed. This can occur when the amino acid sequence in the peptide chain includes residues that can form hydrogen bond between each other (Fig. 5c). This assembly gives rise to an anti-parallel β-sheet.[17, 34, 35]

In a α-helix, the amino acid sequence forms a right-handed helical structure; this conformation can occur when the backbone dihedral angles ϕ and ψ are respectively 60° and 45°. The structure is stabilised by hydrogen bonds parallel to the helix axis and formed between groups along the peptide chain itself: the amide group of an amino acid forms a hydrogen bond with the carbonyl group of the amino acid four residues earlier. Every two turns of the helix there are 7 amino acid residues, labelled *a* to *g* and known as a heptad.[17, 35]

Coiled-coils consist of at least two helices that come together to bury a hydrophobic interface. This can be achieved thanks to the pair-wise interaction between four residues in position *a, d, e* and *g*. The residues at positions *a* and *d* are hydrophobic and interact forming the hydrophobic core of the coil, while the charged residues *e* and *g* further stabilise the structure through electrostatic interactions. The solvent exposed residues *b, c, f*, dictate the interactions of the fibres with the solvent as well as the inter-fibres interactions, which can significantly affect the final gelation properties[17, 41] (Fig. 6).

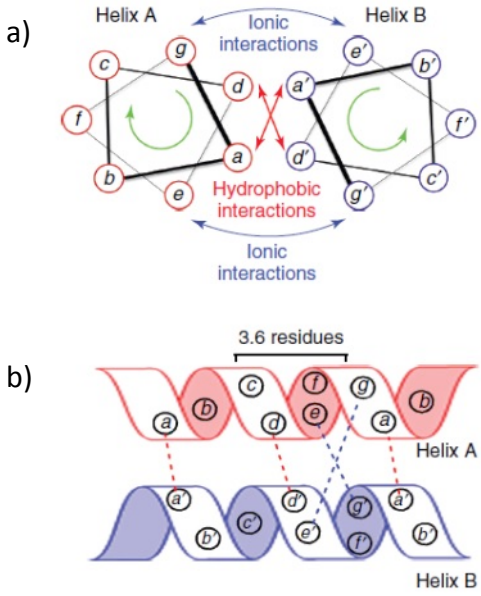

Figure 6 Schematic representation of the interactions between two α-Helices of a coiled-coil (a) and side view of the two α-Helices (b). Reproduced from reference 17.

The identification of the supramolecular structures formed by naturally occurring proteins inspired the possibility to design synthetic peptide derivatives that could mimic natural proteins tendency for self-assembly.

The first example of a designed self-assembled peptide nanostructure was reported in the 1970s when St-Pierre and Hodges designed a heptapeptide that assembles in an α-helical coiled-coil structure in aqueous solution.[42] In the mid '80s DeGrado *et al*. published a series of papers describing an approach to the design of a four-helix bundle protein.[43-46] The naturally occurring four-helix bundle proteins consist of four sequential α-helices, packed antiparallel to one another. DeGrado *et al*. designed and characterised a 16 residues peptide that forms an amphiphilic α-helical structure that in turn can form tetrameric aggregate in which the hydrophobic residues point towards the interior of the aggregate to limit the interactions with water. In the following phase, they inserted a single hairpin loop between two identical helices. Finally, they constructed the covalent tetramer connecting four helices by three loops. This designed globular protein was able to adopt a stable, folded structure in aqueous solution (Fig. 7).

a)

b)

c)

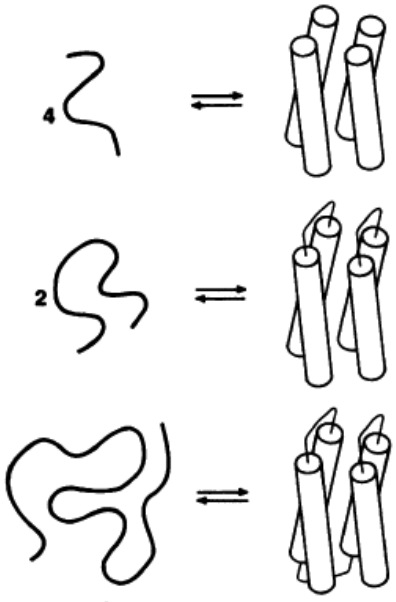

d)

Helix sequence: G-E-L-E-E-L-L-K-K-L-K-E-L-L-K-G
Loop sequence: P-R-R

Figure 7 Schematic illustration of the three stages in the design of a four-helix bundle protein: (a) a designed amphiphilic α-helix associates into a tetramer; (b) two helices are connected by a peptide linker; (c) the covalent tetramer is realised linking four helices by three loops; (d) amino acid sequence of the helix and the loop used to connect the helices. Reproduced from reference 46.

In the 1990s, the first examples of synthetic nanostructures based on β-sheet arrangements were reported. Ghadiri *at al.* described the design of an eight-residue cyclic peptide based on the sequence $(_DAE_DAQ)_2$ that is not found in nature. These subunits stack in an antiparallel fashion and interact with each other by hydrogen bonding, producing a β-sheet structure that in turn gives rise to a tubular structure. Thanks to the alternating D- and L- stereochemistry, peptide side chains must be located on the outside of the structure, thus allowing for the formation of a hollow tubular shape.[47] In the same year, Zhang *et al.* reported that a 16-residue peptide (EAK16) adopts a β-sheet structure in water and aggregates to give filaments with an average diameter between 10 and 15 nm. The interwoven network of filaments in turn gives an insoluble macroscopic membrane, stable and resistant to the digestion of several enzymes.[48] Aggeli *et al.* reported an alternative approach for β-sheet design;[49] they started from the observation of a 24-residue peptide

K24, whose sequence is found in the transmembrane domain of the IsK protein and is able to form β-sheet structures in lipid bilayers and in amphiphilic solvents. By observing the behaviour of this peptide and from previous results in the relevant literature, Aggeli *et al.* deduced a criterion for the rational design of a β-sheet forming peptide. They inferred that attractive forces and lateral recognition between adjacent strands (hydrogen bonding, π-π interaction, coulombic attraction) as well as the interaction of the strands with the solvent to control solubility are of primary importance for the generation of tapes. According to these rules, they designed the de novo peptide DN1 (Fig. 8), which indeed adopts a β-strand configuration in water and produces self-supporting hydrogels. In this peptide, the glutamine residues provide the hydrophobic interactions; intermolecular recognition is provided by phenylalanine and tryptophan by π-π interaction and by arginine and glutamic acid by coulombic attraction. The coulombic attraction between arginine and glutamic acid favours the antiparallel arrangement of the strands; moreover, the charged residues make the β-sheet surface hydrophilic.

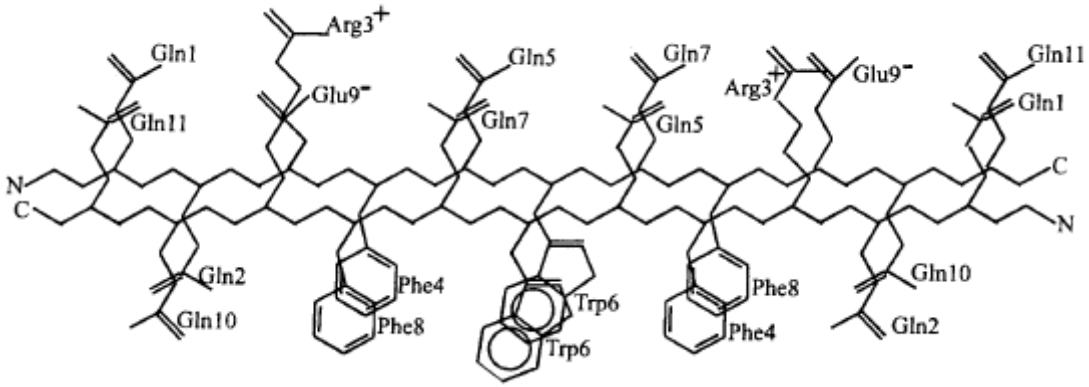

Figure 8 Schematic illustrating the designed peptide DN1 and the proposed antiparallel arrangement of two molecules Reproduced form reference 49.

Schneider and Pochan reported the example of the designed peptide MAX1 that forms β-hairpins thanks to the inclusion in the peptide chain of the turn sequence -V^{D}PPT-. The presence of the non-natural D-form of proline forces the structure to assume a *trans* configuration and prevents the formation of a *cis*-prolyl bond. Under basic conditions, the peptide forms β-hairpins, which can interact with each other to form a fibrous hydrogel. The presence of a *cis* configuration may result in an extended conformation which could undergo mixed self-assembly with folded hairpins[50] (Fig. 9).

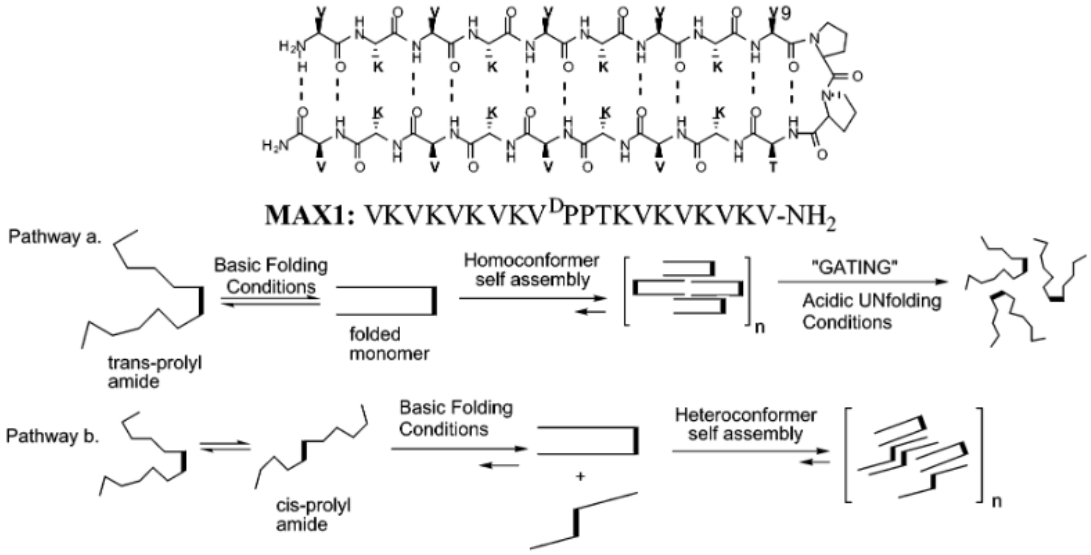

Figure 9 The designed peptide MAX1. The inclusion of the sequence –V^{D}PPT- forces a *trans* configuration, so that pathway (a) is followed. If a *cis* configuration was allowed, pathway (b) would be followed, with the consequent formation of a heterogeneous self-assembled structure. Reproduced from reference 50.

Shorter peptides have been shown to assemble as well. Gazit and co-workers analysed a variety of short peptide fragments from unrelated amyloid-forming proteins as a model system to decipher the mechanism of amyloid formation. They observed a remarkable occurrence of dyads of aromatic residues in these fragments and focused on the study of aromatic short peptides. By means of this reductionist approach they discovered that the core element in the β-amyloid polypeptide, the dipeptide sequence FF, self-assembles into vescicles and nanotubes.[6,51] This pioneering work highlighted how the π-π stacking of aromatic groups plays a crucial role in the stabilisation of self-assembled structures.

The aggregation behaviour of short, purely peptidic systems has been recently investigated by Tuttle and Ulijn *et al.* They exploited computational methods to screen the self-assembly properties of all possible combinations of canonical amino acids in tripeptides (20^3=8000). The simulation results led to the assessment of design rules that promote self-assembly. It was found that aromatic residues promote self-assembly when located in position 2 and 3, (position 1 being the N-terminus of the sequence), negatively charged amino acids and positively charged amino acids are favoured in position 3 and 1 respectively and hydrogen-bond-donating amino acids are favoured in position 1. The design rules inferred computationally were exploited to synthesise new sets of potentially self-assembling

tripeptides. This study led to the discovery of the first unprotected tripeptides that form hydrogels (KYF, KYY, KFF, KYW).[52]

2.1.5. Peptide Modification to Aid Assembly: Amphiphilic and Aromatic Peptide Amphiphiles

Using the insights gained from the understanding of natural and designed peptide self-assembly, a number of attempts have been undertaken in order to try and facilitate the self-assembly process and to set rules for a rational design of peptide-based nanostructures. It has been shown that linking non-peptidic components to the peptide chain, thus obtaining an amphiphilic structure, can aid the self-assembly process. The inspiration for this kind of peptide modification comes from the observation of self-assembly tendency of naturally occurring amphiphilic systems, such as phospholipids. Peptides are the "head" groups in these amphiphilic structures, and they can be linked to different "tail" groups. Two examples of peptide-based building blocks are aliphatic peptide amphiphiles and aromatic peptide amphiphiles. Aliphatic peptide amphiphiles are composed of oligopeptide head groups modified with aliphatic tails. In these structures, the length of the aliphatic tails plays an important role in the control of the self-assembly by modulating the hydrophobic effect[4, 53]; a quite long aliphatic tail (minimum of 10 carbon atoms) is needed to enable the formation of self-supporting gels. Interactions between the head groups contribute to the self-assembly thanks to a combination of non-covalent forces like interpeptide hydrogen bonding, electrostatic interactions and non-specific van der Waals interactions. All of these interactions promote the association of the amphiphilic molecules to form aggregates and help stabilise the structures formed; hence, the longer the peptide chain, the more non-covalent bonds will be present to stabilise the structure.[54, 55] Fields and Tirrell[56, 57] carried out one of the first systematic investigations on peptide modification with hydrocarbon chains. Their studies showed that alkyl chains conjugation can help the stabilisation of protein-based self-assembled structures. With a pioneering series of papers, Stupp's group gave an important contribution to the elucidation of self-assembling systems obtained with aliphatic peptide amphiphiles. The systems they developed typically consisted of multiple domains: the hydrophobic chain; a structural peptide sequence capable of forming hydrogen bonding; a region with charged amino acids

to improve the solubility and to allow for pH and salt responsiveness; and a region which presents bioactive signals.[58] For instance, in 2001, they described a system consisting of a hydrophobic alkyl tail of 16 carbon atoms linked to the C terminus of a peptide chain. The peptide sequence included four cysteine residues, that may form disulphide bonds and polymerise the structure, three glycine residues to provide flexibility to the system, a phosphorylated serine residue, designed to interact with calcium ions in the intended environment, and finally the hydrophilic head with the sequence arginine, glycine, aspartic acid, which acts as cell adhesion ligand.[4] This system self-assembles in aqueous environment, to give cylindrical micelles with a hydrophobic core and the hydrophilic peptidic parts exposed on the surface and interacting via hydrogen bonding (Fig. 10). Stupp *et al.* demonstrated the use of peptide amphiphile self-assembled systems to a wide range of applications including drug delivery, magnetic resonance imaging, templates for mineralisation and tissue regeneration.

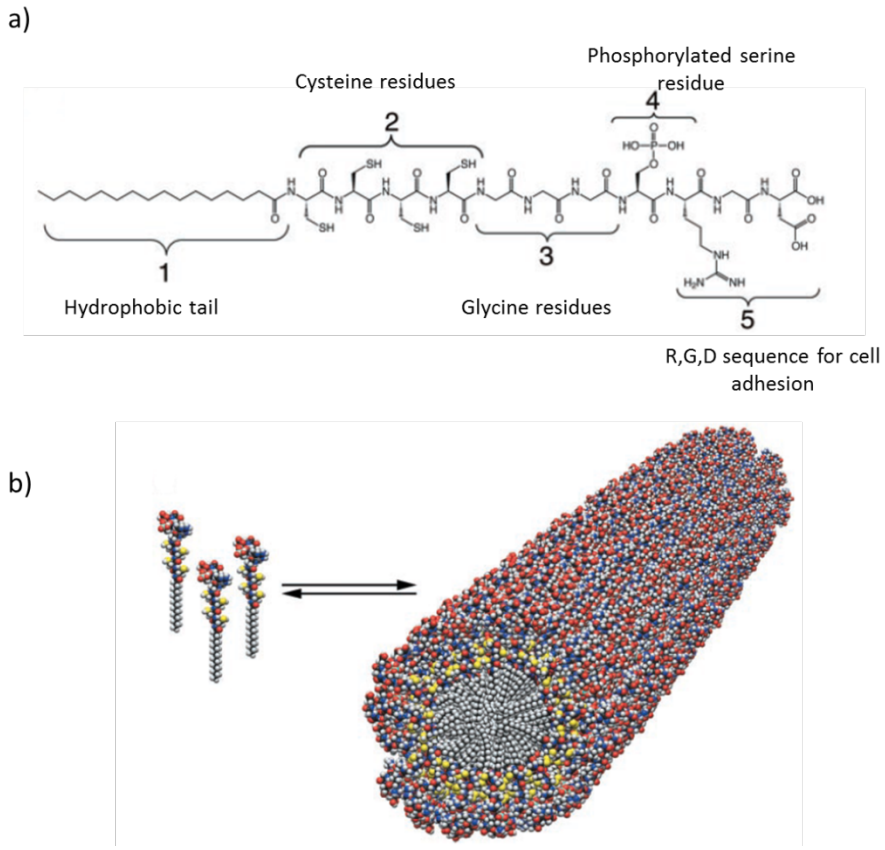

Figure 10 a) Chemical structure of the PA, highlighting the five key structural domains b) Schematic showing the self-assembly of PA molecules into a cylindrical micelle. Modified form reference 4.

An alternative approach to promote aggregation is introducing an aromatic moiety to the N-terminus of the peptide sequence, creating an aromatic peptide amphiphile. In these systems, self-assembled structures can be obtained starting from much shorter peptide chains, compared to other systems (such as for example the aliphatic peptide amphiphile previously described). In addition, aromatic stacking provides directionality to the self-assembly process, providing an element of architectural control, which is not the case for aliphatic amphiphile systems. Structure formation in aromatic peptide amphiphiles is driven by the combination of π-π stacking of the aromatic rings, combined with hydrogen bonding among peptide chains arranged in β-sheets like configurations. A number of different aromatic groups can be coupled to the N-terminus of peptide chains: amongst the most exploited aromatic moieties for protein modification are phenyl, naphthalene, fluorene and Pyrene.[59, 60] Varying the aromatic moiety and the peptide sequence, different self-assembled structures can be obtained, ranging from tubes[59] to fibers[4], tapes[61] and spheres[62]. In 1995 Vegners *et al.* reported that Fmoc-LD (Fig. 11a) formed a

thermoreversible gel after a heat-cool cycle.[5, 28] This was the first example of an aromatic peptide amphiphile hydrogelator. The gap between this paper and the next publications on aromatic peptide amphiphiles suggests that Vegners's work was not largely recognised by the scientific community. Fmoc-dipeptide hydrogelators were later rediscovered thanks to the work of Gazit and Xu's groups, from 2003 onwards.

Gazit *et al.* in 2003 proved that the peptide sequence FF self-assembles into nanotubes in aqueous environments, but does not form gels (Fig. 11b)[6] (as discussed in the previous section). This pioneering work highlighted how π-π stacking interactions between aromatic groups can be essential for the stabilisation the self-assembled structures. To explore the potential role of electrostatic interactions arising from the charged groups on FF, they studied two modified peptide analogues: NH_2-FF-NH_2, which has a net positive charge and the non-charged Ac-FF-NH_2.[63] These studies clearly demonstrated the ability of both systems to form highly ordered tubular structures similar to those formed by FF. This confirmed the importance of aromatic interactions in the self-assembly of amyloid fibrils. Moreover, upon making various modifications to the N-terminus of the FF system they discovered that the modified analogues Boc-FF-COOH, Z-FF-COOH and Fmoc-FF-COOH formed tubular structures as well, but with smaller diameters compared to the systems previously studied. This finding showed how a simple chemical modification can modulate the final self-assembled structure. Xu *et al.* have been widely investigating Fmoc-protected peptide self-assembly; almost concurrently with Gazit's work on diphenylalanine, they reported the first example of supramolecular hydrogel that responds to ligand-receptor interaction.[64] Following the serendipitous observation that Fmoc-^{D}A^{D}A forms hydrogels, they started synthesising a series of Fmoc-dipeptides (Fmoc-AA, Fmoc-GG, Fmoc-G^{D}A, Fmoc-GS, Fmoc-GT) and to investigate their response to a specific biological ligand-receptor, vancomycin (Van). All the systems investigated were able to form hydrogels in the range of concentration and pH investigated, except for Fmoc-GT. Upon addition of Van, the hydrogels showed a different behaviour, since different dipeptides bind Van with different affinities. As expected, Fmoc-^{D}A^{D}A (Fig. 11c) interacts with Van[65]; adding increasing amounts of Van to these hydrogels causes water expulsion and eventually a gel-sol transition. On the contrary, the hydrogel formed with Fmoc-AA showed no change upon addition of Van, in agreement with the fact that the L enantiomer of Alanine does not bind Van.

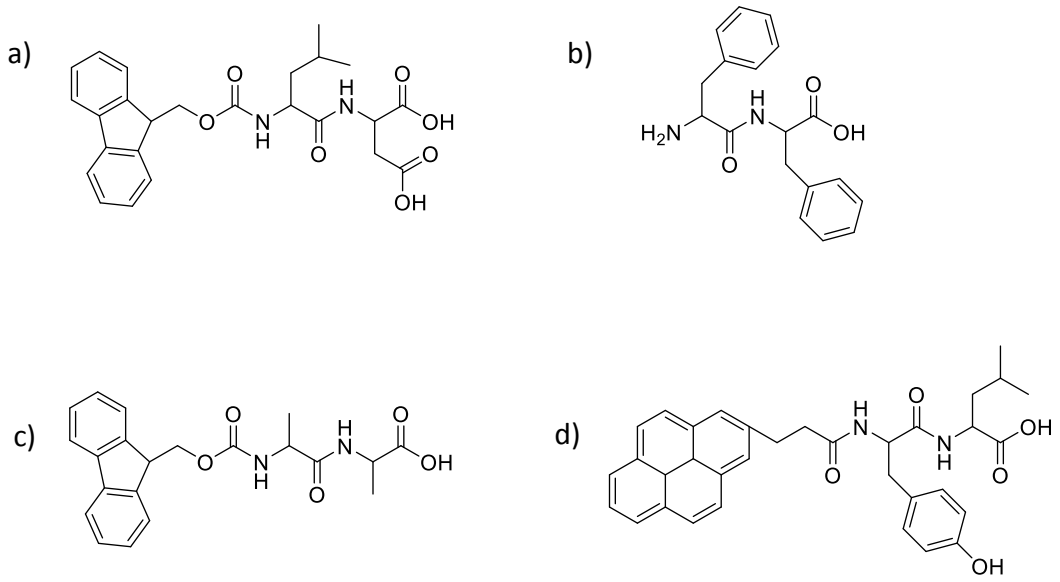

Figure 11 Examples of Peptide-based Self-assembling building blocks.

Ulijn and co-workers widely investigated the gelation properties of aromatic peptide amphiphiles, obtained by combining a number of different peptide chains and protective aromatic moieties. For instance, Jayawarna *et al.* investigated the gelation properties of a library of seven Fmoc-dipeptides, obtained from the combination of the amino acids A, G, F and L. Fmoc-FF and the mixtures Fmoc-FF + Fmoc-GG, Fmoc-FF + Fmoc-K were found to form stable gels at physiological pH and were subsequently tested and found to support cell culture of chondrocytes.[66] Fleming *et al.* reported the gelation of Pyrene peptide amphiphiles comparing them with analogous Fmoc-protected compounds and investigating the different co-assembly mode that could be obtained upon combining Fmoc- and Pyrene-protected compounds (Fig. 11d). The results highlighted that replacing Fmoc with Pyrene allows for increased aromatic stacking, which in turn can favour the self-assembly of the aromatic peptide amphiphile.[67]

A variety of different modes of assembly have been proposed to describe the supramolecular organisation of aromatic peptide amphiphiles, including parallel, antiparallel and interlocked antiparallel stacking.[28] As previously mentioned, aromatic peptide amphiphiles are modified with an aromatic moiety at the N-terminus, which constitutes a relatively hydrophobic region of the molecule, compared to the relatively

hydrophilic peptide sequence. The self-assembly of aromatic peptide amphiphiles is driven by two main contributions based upon the self-association of the two regions of the molecule: the aromatic functionalities can interact *via* π-π stacking, whereas the peptide chains can form hydrogen bonds. These supramolecular interactions can lead either to a parallel or an antiparallel conformation (Fig. 12). Evidence of the formation of both configurations have been shown in the literature. Examples of parallel stacking have been proposed for Fmoc-Y[68] and for side chain penta-fluorinated Fmoc-(F_5)-F.[69] Ryan *et al*. investigated the self-assembly and gelation properties of Fmoc-(F_5)-F. They proposed that the most energetically favourable packing mode for this molecule could be a parallel stacking in which Fmoc groups interact by π-π stacking and the F_5-phenyl also self-associates. The self-assembled structure could be further stabilised by hydrogen bonding between the carbamate carbonyl and the NH functionality. Moreover, with this arrangement, the association of multiple fibrils could be possible thanks to interactions between the Fmoc groups in two different fibrils. In this way, the hydrophobic functionality would be buried in the core, leaving the hydrophilic C-terminal carboxyl functionality exposed to the solvent. This packing mode is in agreement with the arrangement proposed by Xu *et al.* for Fmoc-T. Nevertheless, an antiparallel arrangement is also possible, in which Fmoc moieties participate in π-π stacking with the F_5-phenyl groups on the side chain.[28]

As previously mentioned, depending on the molecular structure, a distinct antiparallel arrangement can also form, whereby the exposed aromatic groups from different strands may interlock. This interlocked antiparallel stacking architecture has been initially proposed for Fmoc-FF[59] and Fmoc-LLL[70] and consists of an antiparallel arrangement of β-sheets in which the Fmoc moieties positioned on alternating sides of the sheets can interact via π-π stacking with the Fmoc moieties on an adjacent β-sheet (Fig. 12d). Due to the twist present in the β-sheet, the sheets are rotated in relation to one another; hence, four interlocking sheets give rise to a cylindrical structure.

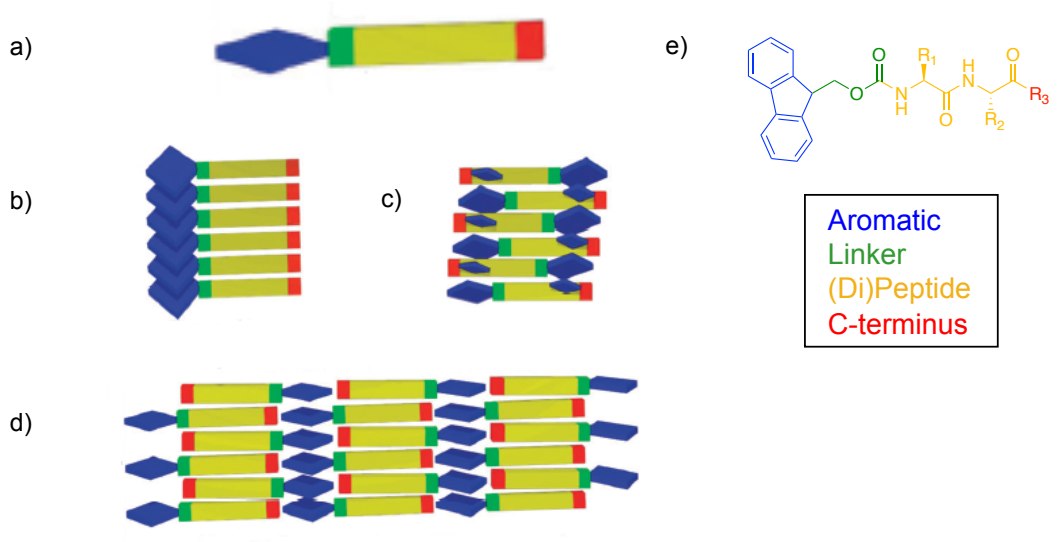

Figure 12 a) Schematic representation of a single aromatic peptide amphiphile self-assembling building block. The blue cuboid represents the aromatic moiety, the green rectangle is the linker to the peptide chain, depicted in yellow, and the red rectangle is the C-terminus of the peptide chain. The possible stacking arrangements for the aromatic peptide amphiphile building blocks are depicted. b) parallel arrangement, c) antiparallel arrangement. The small blue cuboids represent an aromatic side chain on the peptide; d) interlocked antiparallel arrangement. e) General chemical structure of an aromatic (Fmoc) peptide amphiphile self-assembling building block. Modified from reference 28.

2.1.6. Triggering the Self-Assembly

The self-assembly of peptides and their derivatives can either occur spontaneously or can be triggered by an external stimulus. There is significant interest in the design of stimuli-responsive supramolecular hydrogels, since directing the self-assembly by means of an external trigger allows for a better control over the process.[71] The self-assembly of molecular precursors into supramolecular hydrogels can be induced by a variety of external stimuli, both physical (temperature, mechanical triggers, UV-vis light) and (bio-)chemical (pH, salt concentration, redox agents and enzymes).[7-9]

The combination of (bio-)catalysis and molecular self-assembly provides a powerful means to direct supramolecular interactions. This approach has been inspired by biological systems, where self-assembly is often coupled to catalysis. The approach exploits enzymes to convert non-assembling precursors into self-assembling building blocks.[61, 72] Enzymes are biological catalysts involved in a multitude of different chemical processes that occur in

living systems.[73] They are able to catalyse reactions in very mild conditions (room temperature, aqueous media, no need of high pressures) and they generally have high stereo-, regio- and chemo-selectivity.[74] For biological and biomedical applications it is particularly attractive to utilise enzymes to trigger molecular self-assembly, because of their inherent biocompatibility. Compared to chemical or physical stimuli, enzymatic triggering operates under physiological conditions of pH, temperature and ionic strength. Moreover, enzyme assisted self-assembly allows for a better control of the process, since the synthesis of the self-assembling building blocks is spatially confined at the site of enzyme action, which may result in the localised nucleation and growth.[61, 75]

A molecule designed to act as an enzyme-responsive peptide gelator typically requires three different components: an enzyme sensitive component (substrate or substrate mimic); a component that directs the self-assembly (usually a self-assembling peptide moiety); and a molecular switch that initiates the self-assembly only upon enzyme action[75], usually by catalytic removal of a steric or charged group to readdress the amphiphilic balance required for self-assembly.

The action of the enzyme on the molecular switch component of the precursor modifies the amphiphilic balance within the molecule, converting the non-assembling precursor into a self-assembling molecule. This mechanism usually involves three steps[76]: the conversion of the precursor into a self-assembling building block (either by formation or by cleavage of covalent bonds); the self-assembly of the resulting building block molecules at the site of the enzyme action and the formation of nanostructures. In many reported cases the molecules used are gelators, which sequester water molecules resulting in formation of a supramolecular hydrogel (Fig. 13).

The conversion of a non-assembling precursor into the hydrogelator upon the enzyme action can proceed in two different ways: the enzyme can catalyse the formation of peptide bonds between two amino acid derivatives or peptide chains, or cleave a covalent bond through a hydrolysis reaction, allowing for the removal of functional groups that prevent the self-assembly (either causing electrostatic repulsion or because of their steric hindrance).[34, 35]

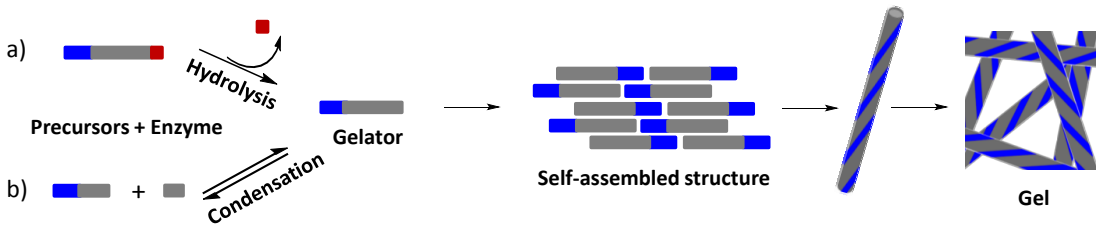

Figure 13 Conversion of the precursors into self-assembling molecules via hydrolysis (a) or condensation (b) reactions and resulting formation of the supramolecular gel.

A range of enzymes have been utilised to initiate self-assembly of peptide derivatives, including phosphatases, esterases and proteases (Fig. 14). Phosphatases catalyse the dephosphorylation of the precursor, that is the removal of a phosphate group by cleavage of the phosphate ester bond.[62, 72] The presence of negatively charged phosphate groups prevents the molecular self-assembly due to electrostatic repulsion. Upon removal of the phosphate group from the peptide chain, self-assembly is possible.[77] Xu *et al*. reported the first example of enzyme triggered self-assembly of an Fmoc amino acid: they exploited the dephosphorylation of the non-assembly precursor Fmoc-Yp (Fmoc-Tyrosine Phosphate) into the self-assembly hydrogelator Fmoc-Y, by means of alkaline phosphatase.[72] Following this example, dephosphorylation of Fmoc-protected peptides has been widely employed to trigger their self-assembly, and different supramolecular structures have been reported, depending on the amino acids included in the peptide chain. Phosphorylated aromatic peptide amphiphiles are surfactant-like and can form spherical micelles, as shown by Sadownik *et al.* In this work, the phosphorylated precursor Fmoc-FYp initially exists in a micellar form in a buffered water solution, with the hydrophilic phosphate groups in contact with the solvent. Upon addition of alkaline phosphatase, the dephosphorylation of the precursor causes the micelles to disassemble. The dephosphorylated Fmoc-FY self-assembles into fibrous structures, resulting in the formation of a hydrogel.

Ester-terminated non-assembling peptides can be converted into gelators upon the action of an esterase enzyme, that catalyses the hydrolysis of the ester group. Subtilisin is a protease enzyme with esterase activity that has been employed to trigger the self-assembly of Fmoc-dipeptides; self-assembly of these building blocks gives rise to networks of nanotubes or fibres, depending on the peptide sequence.[61]

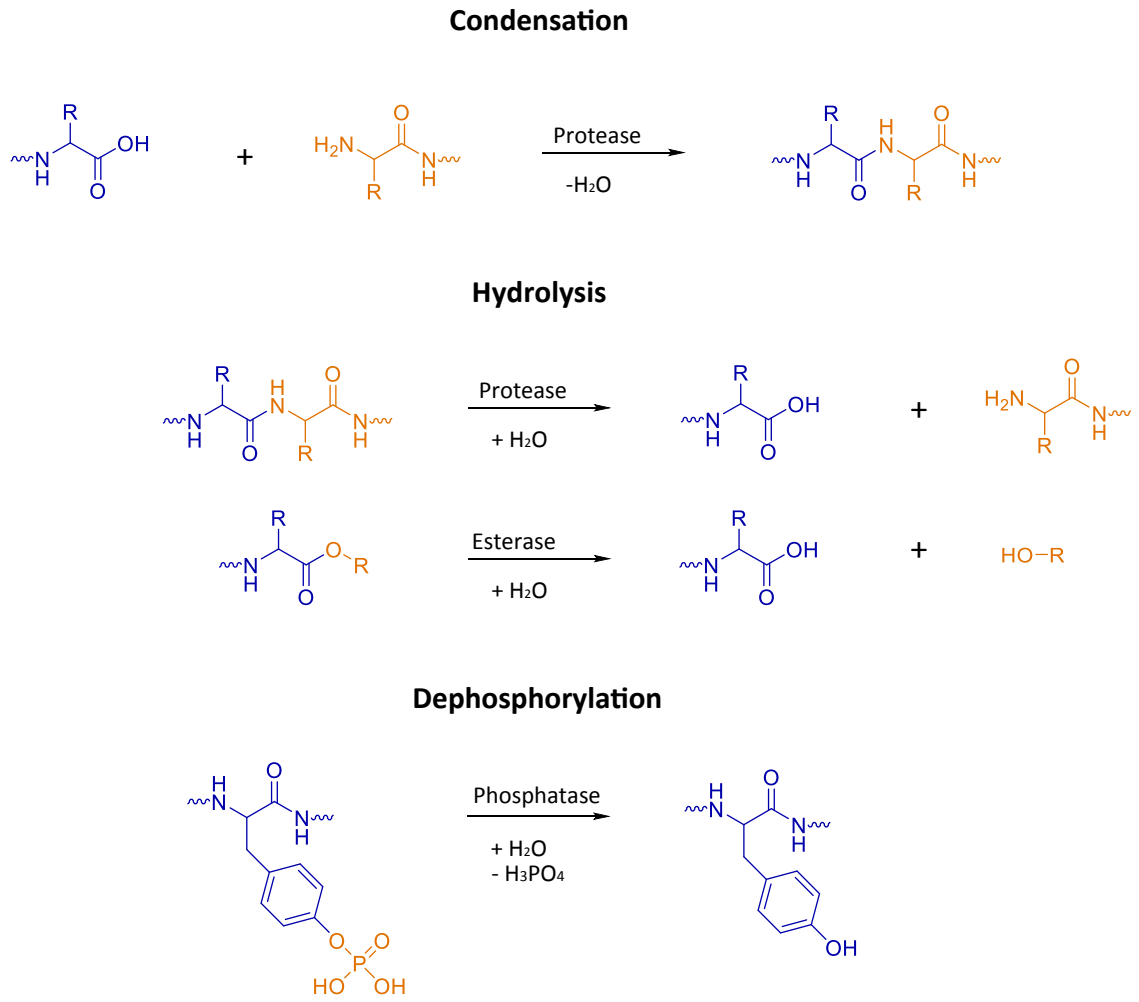

Figure 14 Examples of enzyme-catalysed reactions.

Proteases can be exploited to trigger the self-assembly of peptide derivatives in two different ways since these enzymes are able to catalyse both the cleavage and the formation of an amide bond; hence, they catalyse the formation of a self-assembling gelator either through the removal of a group that prevents the self-assembly[78], or by condensation of two non-assembling precursors. The preferred direction depends on the relative thermodynamic stability of the reactants and products, as discussed in the next section.

Thermolysin is a protease enzyme that can catalyse both the hydrolysis and the reverse hydrolysis of peptide bonds. Triggering the self-assembly *via* reverse hydrolysis provides a route towards a dynamic reversible process, ultimately allowing for defect correction.[79, 80, 18] This thermodynamic control of the self-assembly process will be further discussed in the next section.

2.1.7. Thermodynamic vs Kinetic Control of Self-Assembly

Depending on the enzyme selected for triggering the process, biocatalytic self-assembly may proceed under thermodynamic or kinetic control.

When the self-assembly is kinetically controlled, the enzyme action gives rise to "kinetically trapped" structures which are not the most thermodynamically favoured. This occurs when the formation of the self-assembling building blocks upon enzyme action and their subsequent organisation in self-assembled structures are both thermodynamically favoured and not coupled (Fig. 15). Kinetic control has been observed for example, for phosphatase[72] and subtilisin.[61]

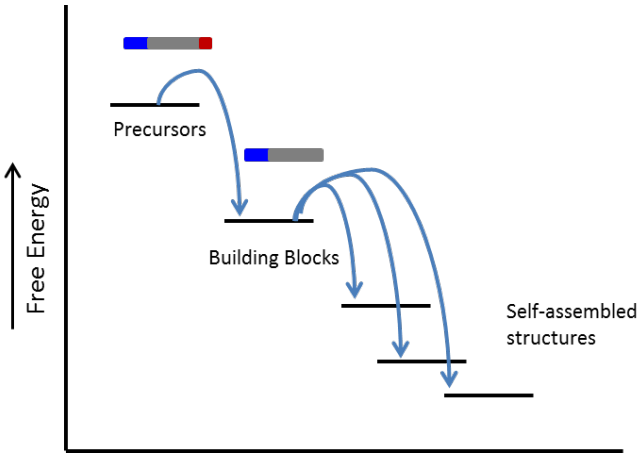

Figure 15 Free energy diagram of kinetically controlled enzymatic self-assembly.

Upon gelation, the system is fixed, since it would be too energetically unfavourable (i.e. the activation energy is too high) to rearrange the building blocks in the gel state. This process is referred to as "kinetic locking". As a consequence, the final supramolecular structure may

not be the most thermodynamically favoured and represents a local minimum in the free energy landscape.

In kinetically controlled systems, the final supramolecular structure is determined by the rate of the self-assembly, hence is related to the enzyme concentration. Changing the amount of catalyst, different local minima in the free energy landscape can be accessed. It has been shown that varying the rate of the self-assembly, different supramolecular arrangements are obtained; the properties of the resulting hydrogels will be affected, with higher rates (enzyme concentration) generally producing stiffer hydrogels, compared to similar systems obtained with lower enzyme concentrations.[81, 82] On the other hand, slower assembly rates have been related to final structures with fewer defects.[75]

An enzymatically triggered system operates under thermodynamic control when the enzymatic reaction in itself is energetically unfavourable, but the free energy change associated with the self-assembly compensates this increase in free energy due to the production of self-assembling building block, thus driving the reaction towards self-assembly (Fig. 16). The self-assembled structures obtained represent the global thermodynamic minimum for the system and the assembled systems obtained through this approach are dynamic and fully reversible, allowing for defect correction.[18, 35]

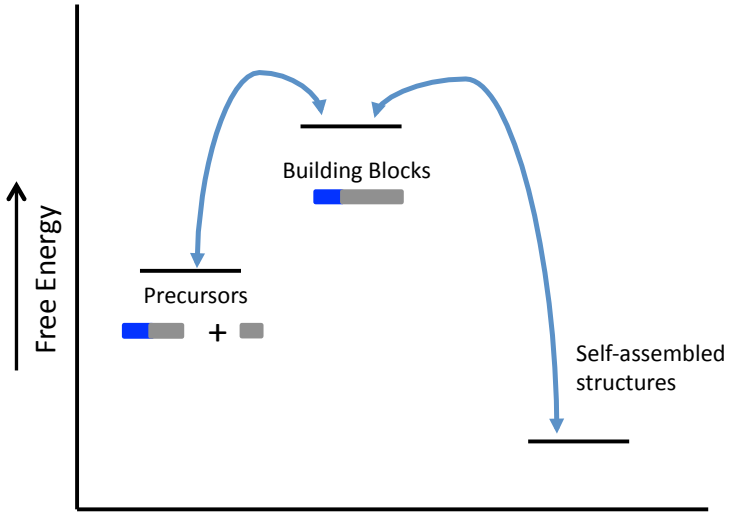

Figure 16 Free energy diagram of thermodynamically controlled enzymatic self-assembly.

Thermodynamically driven systems can be exploited to compare the relative stability of different building blocks: when different precursors are added to the same system, they will continuously interchange, finally self-selecting the most thermodynamically stable structure. This approach is known as dynamic combinatorial library (DCL).[83, 84] Nalluri and Ulijn applied the DCL approach to a library of naphtoxy-substituted dipeptides. The dipeptide derivatives were obtained by the enzyme-catalysed condensation of amino acid derivatives, the non-assembling precursors being Nap-Y and six different amino acid amide derivatives (F, L, V, Y, A and G). The objective of this study was to discover efficient energy transfer nanostructures, exploiting the donor-acceptor interactions between naphthalene and dansyl β-alanine. In order to do so, dansyl β-alanine was introduced to the library. The effect of the addition of the acceptor in the library and of the ratio between donor and acceptor was investigated, the results confirming that the additional interactions between donor and acceptor can favour the self-assembly of the most stable dipeptide sequence.[85] In a recent paper, Pappas *et al.* developed a methodology based on dynamic combinatorial peptide libraries to search the peptide sequence space to for self-assembling structures.[86] They employed unprotected homo- and heterodipeptides as the input dyads and added thermolysin to the mixture, initiating a sequence of exchange and selection by enzymatic hydrolysis and condensation. Over time, the most thermodynamically stable structures (*i.e.* the peptides that give rise to the formation of self-assembling structures) are amplified.

2.1.8. Applications of Peptide-Based Hydrogels

Peptide-based hydrogels are particularly attractive for applications in biology and experimental biomedicine.[87] The high water content of hydrogel makes them potentially biocompatible; moreover, they can be realised in a variety of physical forms (films, particles, etc.); they are deformable and suitable for subcutaneous injection; they can be designed to have chemical and mechanical properties similar to the extracellular matrix properties.

In biological systems, many dynamic nanoscale and macroscale processes are ultimately directed by the action of enzymes[88]; The enzyme-responsive hydrogel could be designed to respond to one of the enzymes already present in the body: the biological environment could hence trigger the material response, without the need to add the stimulus externally.[89] Diseases are often associated with abnormal activities or overexpression of

some specific enzymes, providing an additional cue that could be exploited to generate a suitable material response. Moreover, enzyme action is often localised to certain (diseased) sites, providing the means for spatio-temporal control of the changes induced in the material properties.

For these reasons, the main areas that have been investigated as possible applications of peptide-based materials include regenerative medicine[88, 90, 91, 92], controlled drug delivery[93], biosensing[94] and intracellular/pericellular gelation to direct a cell's fate. Drugs could be loaded into the gel matrix and they could be then released at a rate dependent on the diffusion coefficient of the drug molecule through the gel network. Hydrogels can also be biodegradable, since degradation can be triggered by a variety of stimuli (pH, temperature, enzymes).[94] These features can be exploited to design materials for controlled drug release and targeted action towards diseased tissues, reducing unwanted side effects. A few specific recent examples are discussed below.

Gao and co-workers described a drug delivery application of a supramolecular system in which a drug derivative is exploited as therapeutic agent and as gelator at the same time.[95] They included taxol, an antineoplastic agent, in a hydrogel precursor bearing an alkaline phosphatase cleavable group. Upon the action of the enzyme, the precursor is converted into a hydrogelator that self-assembles into fibers, forming a hydrogel that can slowly release the taxol derivative hydrogelator in water. Toxicology studies proved that this derivative has a similar activity to taxol itself.

Biocatalytic self-assembly may also be exploited to produce intracellular artificial nanostructures that can potentially help in understanding cellular activities and to predict or dictate their behaviour. The first example of cellular response to intracellular enzymatic hydrogelation was reported by Xu *et al.*[96] They designed a peptide-based gelator precursor which could enter *E. coli* cells by diffusion. The overexpressed enzyme phosphatase inside the bacterium catalysed the formation of the hydrogelator inside the cell, the subsequent formation of self-assembled nanofiber induced hydrogelation within the cell and the formation of the gel caused a sudden change in the viscosity of the cytoplasm, stressing the cells and inhibiting their growth.

The antimicrobial properties of self-assembling aromatic peptide amphiphiles were further investigated by Hughes *et al.*, where they treated *E. coli* with different aromatic peptide

amphiphiles to determine whether this would result in different anti-microbial properties. The *E. coli* cultures were exposed to a number of phosphorylated Fmoc-dipeptides, which are known to form different nanoscale morphologies. This resulted in a decreased cell activity, supposedly caused by the formation of a nanofibre network in the periplasmic space. Despite the different morphologies of the nanostructures formed, different aromatic peptide amphiphiles caused a similar response, regardless of their different chemical and nanoscale structure.[97]

In a more recent publication, Xu *el al.* described a new approach to control cell fate exploiting the formation of a hydrogel in the pericellular space. Surface and secretory phosphatases catalyse the dephosphorylation of the precursor, a naphtalene-capped D-peptide, to form a hydrogelator, which self-assembles into nanofibres. The subsequent formation of the hydrogel in the pericellular space decreases cell migration and adhesion, thus inducing cell apoptosis. Since surface and secretory phosphatases are overexpressed by cancer cells, the pericellular hydrogel will selectively form on the cancer cells thus inhibiting their growth.[98]

Peptide-based hydrogels are particularly attractive as scaffolds for cell culture and regenerative medicine applications since they provide a valid tool for the design of scaffolds with tunable properties and able to reproduce key features of the extracellular matrix (ECM) for an enhanced interaction with the cells.

Capito *et al.* combined a peptide amphiphile (PA, positively charged) solution with a hyaluronic acid (HA, negatively charged) solution, observing the formation of macroscopic sacs and membranes at the interfaces between the two solutions.[99] These highly ordered self-assembled materials are mechanically robust, self-healing and permeable to proteins. The PA-HA structures were employed for in-vitro studies using human mesenchymal stem cells (hMSC). The hMSC were incorporated in the sacs and cultured in cell growth media and remained viable for up to 4 weeks, confirming that the self-assembled sacs could provide a suitable environment for cell survival.

Zhou *et al.* employed Fmoc-protected di-peptides and tri-peptides for the fabrication of a bioactive hydrogel.[100] They used a mixture of Fmoc-FF, which forms hydrogels under physiological conditions, thus providing a stable structural support, and Fmoc-RGD, which besides being a structural component, promotes cell adhesion through the RGD integrin

binding sequence. Fmoc-FF/RGD gels were compared with Fmoc-FF/RGE gels, containing the RGE sequence, which does not promote cell adhesion. Both gels were tested for culturing human dermal fibroblasts (HDFa) three-dimensionally *in vitro.* Cell spreading occurred for the cells cultured on the Fmoc-FF/RGD hydrogels suggesting cell adhesion to the scaffold, whereas cells cultured on the Fmoc-FF/RGE hydrogel maintained a spherical shape.

Alakpa *et al.* employed a supramolecular peptide hydrogel with tunable stiffness to culture perivascular stem cells.[101] The hydrogel is based on the core-shell co-assembly of Fmoc-FF (the structural element) and Fmoc-S (surfactant-like molecule). The stiffness of the Fmoc-FF/S can be controlled by varying their concentration. The perivascular stem cells undergo stiffness-directed fate selection when cultured on gels of different stiffness, differentiating into neural cells, chondrocytes and osteoblasts on gels of increasing stiffness. Focusing on chondrogenesis and osteogenesis, they identified two lipids which are significantly depleted during the differentiation process. By feeding these lipids to standard stem cell culture, they induced differentiation into chondrocytes and osteoblast phenotypes, proving the key role of these lipid metabolites in driving cell differentiation.

2.2. Enzyme Immobilisation

2.2.1. Introduction

As already discussed in the previous section, enzymes are very attractive for a variety of technological applications, including biotechnological, pharmaceutical, food and chemical industries.[73] However, the industrial and commercial application of free enzymes is limited by a number of disadvantages: costs of production and isolation are still high, and when used in solution it can be very complex to recover and recycle enzymes. Hence, numerous efforts have been devoted to the development of strategies to improve enzymes viability for technical purposes. One of the most applied strategies to overcome these hindrances is the immobilisation of enzymes on a solid support. This technique could be of interest in bio-nanotechnological applications, such as nanosensing, diagnostics or localised nanostructure formation, but the majority of the literature in this field is focused on industrial applications of immobilised enzymes for biocatalysis.[102, 103, 104, 105] Enzyme immobilisation can be defined as the "confinement of enzyme to a phase (matrix/support) different from the one for substrates and products".[106] Employing immobilised enzymes rather than free enzymes in solution can be a powerful tool to improve enzyme stability, product separation and to reduce production costs by recycling the catalyst.[107]

The first application of immobilised enzymes was reported in early 1900 by Nelson and Griffin, who immobilised invertase on $Al(OH)_3$ and charcoal and showed that after the immobilisation the enzyme retained its catalytic activity.[105, 108] Although this discovery is now considered a fundamental contribution in the field, the potential of enzymes immobilisation was not appreciated until the 1940s. Since then, this subject has been widely investigated and a number of different methods to immobilise enzymes have been developed[106], including the physical methods that dominated the field until the 1950s, along with the covalent immobilisation techniques that were further explored in these years and the early studies on carrier free immobilised enzymes (cross-linking of crystalline enzymes) in the 1960s. In the succeeding decades all these methods were widely investigated and extended to a variety of enzymes that were expected to have great industrial potential. At the same time, it was increasingly acknowledged that the nature and properties of the substrate affect the final catalytic properties of the enzymes. Hence, along

with traditional materials (such as glass, alumina and a few synthetic polymers), new materials were specifically developed for enzyme immobilisation. Between the 1970s and 1980s it was also recognised that, under appropriate conditions, many enzymes retain their catalytic activity in organic solvents, although their activity and stability are usually lower in organic solvents than in aqueous media.[107] Consequently, in the following years much effort has been devoted on the development of immobilised enzymes that are active and stable in organic solvents. Since the 1990s to date, the major focus was on the development of rational design for enzyme immobilisation and strategies to improve the performances of immobilised enzymes. Most of the techniques currently employed are characterised by the rational combination of different methods to help and solve drawbacks that could not be solved by and individual method.[107]

2.2.2. Choice of Supports

It is acknowledged that the nature and properties of the support affect the final performance of the immobilised enzyme system.[107, 73] The interactions between the enzyme and the carrier affect the final biochemical, mechanical and kinetic properties of the immobilised enzyme.[109] The ideal support should meet a number of requirements: it should be hydrophilic, biocompatible and available at reasonable cost, depending on the application and scale[73]; stability, inertness and physical strength should also be taken into account.[106] A number of supports for enzyme immobilisation have been tested, including natural and synthetic polymers, silica gels, hydrogels, glass, metals and metal oxides (Table 1).[73, 109] Compared to non-porous supports, the higher surface area of porous materials allows higher loading of enzyme; hence, porous supports such as porous silica or zeolites are the most exploited so far. [103, 104]

In more recent years, nanotechnology-inspired biocatalytic systems have been developed. The physical characteristics of nanoscale materials, such as high surface area: volume ratio and enhanced diffusion and particle mobility, distinguish nanoscale biocatalyst system from traditional immobilised systems and give them unique behaviour. Several types of nanostructures have been employed for enzyme immobilisation, including nanospheres, nanorods, nanotubes and nanowires.[110, 111] Nanoparticles – based immobilised enzymes are further discussed in section 2.3.4.

Table 1

Classification of Supports

Natural Minerals:	betonite, silica
Natural Polymers:	cellulose, agar, agarose, alginate, collagen
Synthetic Polymers:	polystyrene, polyacrylates, polymethacrylates, polyamides, polyvinyl
Processed Materials:	glass (nonporous and controlled pore), controlled pores metal oxides, metals
Nanoscale Materials:	silica, gold, polymer (polystyrene, poly-acrylonitrile-co-methyl methacrylate), magnetic nanoparticles (Fe_3O_4, ZnO)

2.2.3. Methods for Enzyme Immobilisation

The possible strategies for enzyme immobilisation can be broadly classified in three categories:[102] binding to a support, entrapment and cross-linking(Fig. 17).

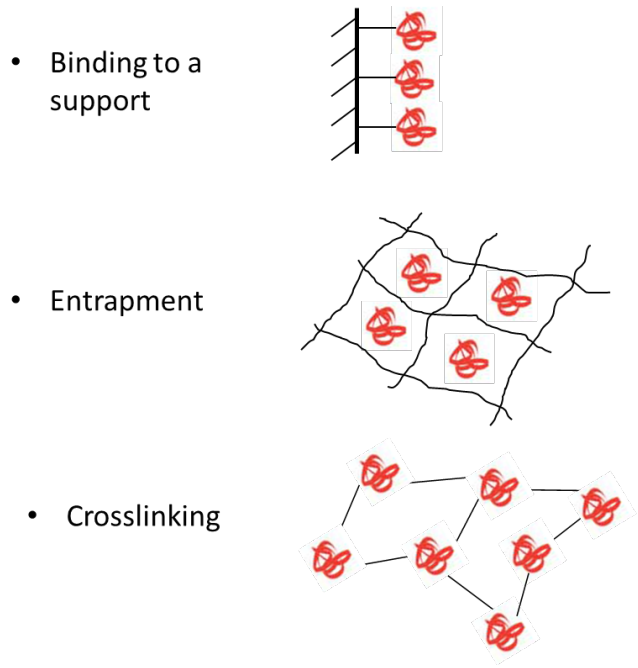

Figure 17 Different approaches for enzyme immobilisation.

2.2.3.1. Binding to a Support (Covalent or Non-Covalent)

Enzymes can be bound to a support by means of interactions ranging from non-covalent to covalent bonding. The forces involved in non-covalent immobilisation, such as physical adsorption and ionic binding, result in an interaction between the enzyme and support that can be modulated by changing conditions such as pH, ionic strength or solvent polarity. The stronger the binding force, the more difficult to detach the enzyme from the support without damaging either its catalytic activity or the support itself, hence, the immobilisation will be irreversible.[73] Non-covalent immobilisation methods usually involve mild processes in which the catalytic activity of the enzyme is better preserved; however, these methods often suffer the drawback of catalyst leakage since the interactions involved may not be strong enough to keep the enzyme fixed to the carrier.[102]

The formation of a covalent bond between the support and the enzyme is one of the most extensively used techniques in enzyme immobilisation.[112] This is the most suitable method when it is strictly necessary to avoid product contamination, since the strength of the bond between substrate and enzyme will prevent the latter from being easily released in solution. This approach is the most adequate for large scale industrial processes and has also found applications in the fabrication of biosensors and immobile phase for affinity chromatography.[112]

A wide variety of coupling methods have been employed, the choice depends on the functional groups available on the surface of the support and those accessible on the enzyme. The coupling reactions involve functional groups on the side chains of the amino acids present in the enzyme, for instance the carboxylic group on aspartic and glutamic acids, thiol on cysteine, amino group on lysine or arginine. These functional groups can either react directly with active groups on the support surface or be linked via a crosslinker. In the most commonly adopted procedures, the coupling will result in the formation of amide, ether or carbamate bonds.[73] Nucleophilic amine groups on the enzyme surface can, for instance, attack epoxides similar to covalently link enzymes on acrlylic resins (e. g. the commercially available Eupergit®)[109] or on modified glass or silica surfaces.[113] Mesoporous silicas are widely employed inorganic porous supports, enzymes are usually covalently linked on these materials through functionalisation of the support surface with amine groups; the amine-functionalised surfaces can then be coupled with the enzyme by means of crosslinking agents such as glutaraldehyde, glutaric anhydride or cyanuric chloride.[105]

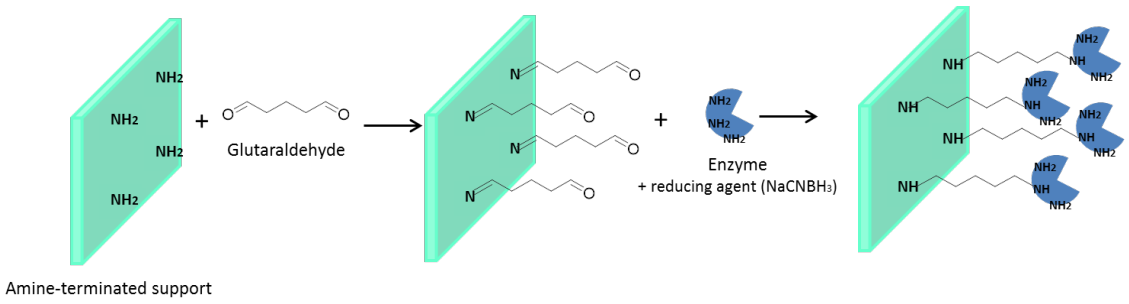

Figure 18 Protein immobilisation on amine-terminated supports pre-activated with glutaraldehyde.

Glutaraldehyde is the most popular crosslinking agent; under mild conditions it can crosslink the amine-functionalised surfaces with the amine groups on the enzyme surface

(Fig. 18); however, during this reaction the presence of a competitive inhibitor is normally required to prevent the reaction of glutaraldehyde with the enzyme's active site.[112] Hydroxyl containing polymeric supports (e.g. agaroses) are usually coupled to enzymes using a two-step process: the first step is the activation of the polymer by a modifying agent such as cyanogen bromide or tresyl chloride;[73, 112, 114] the second step is the coupling of the enzyme with the activated polymer (Fig. 19). Tresyl chloride has been proposed as an alternative to the potentially hazardous cyanogen bromide; moreover, it appears to provide a more stable bond between the polymer and the enzyme.[112] The major drawback of covalent linking is the potential loss of enzyme activity: the enzyme should withstand the reaction conditions and the amino acid residues in the enzyme active site should not be involved in the covalent bond with the surface.[73]

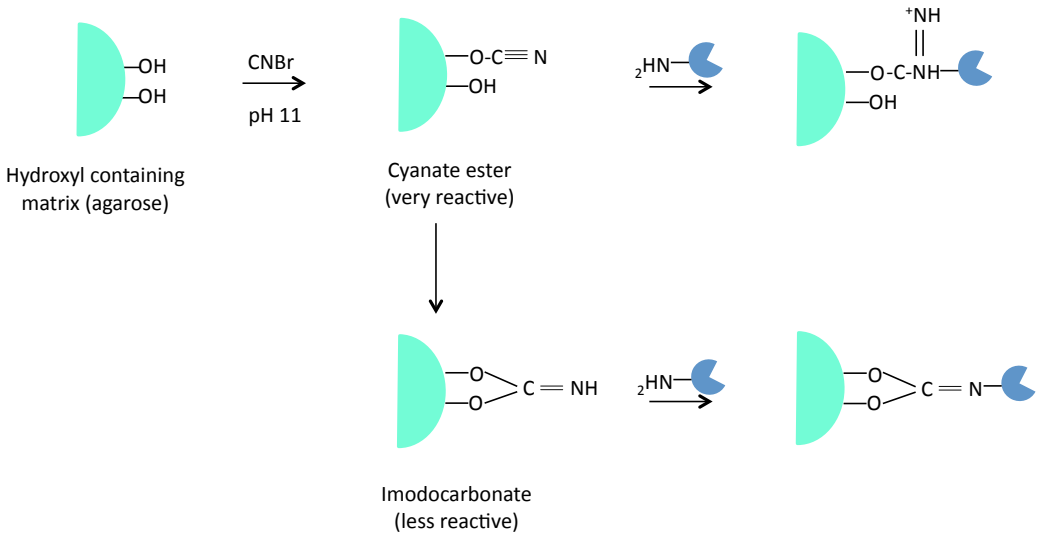

Figure 19 Illustration representing the covalent binding of enzymes on a surface activated by cyanogen bromide. Cyanogen bromide (CNBr) in alkaline conditions reacts with hydroxyl groups on the matrix to form cyanate esters or imidocarbonates. These groups in turn react with primary amines under mild conditions, resulting in the covalent coupling of the ligand (e.g. enzymes) to the matrix.

A simple and versatile alternative strategy to bind enzymes on a variety of different substrate is to exploit a polydopamine surface coating. Dopamine is a biomolecule that contains catechol and amine groups and has been employed as a structural mimic of the proteins responsible for mussel adhesive properties (Fig. 20).[115]

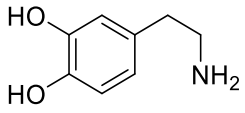

Figure 20 Illustration of the chemical structure of dopamine.

Under alkaline conditions dopamine polymerises to yield a polymer which is able to adhere on virtually any kind of substrate. This polymeric film can be exploited for biomolecule immobilisation, thanks to its reactivity towards nucleophiles. The polymerisation mechanism and the exact chemical composition of the polydopamine film are not precisely known;[116, 117] however, catechol and quinone functional groups are believed to be present in the coating. This equilibrium is shifted towards the quinone at alkaline pH, and the quinone is capable of covalent coupling to nucleophiles; thus, the enzyme immobilisation occurs upon immersion of the polydopamine coated substrate in an enzyme solution. This procedure presents a number of advantages compared to the other techniques for covalent binding since these treatments are normally tailored for a specific support and enzyme and they cannot be easily adapted to a different system. On the contrary, and as mentioned previously, the distinguishing feature of the polydopamine coating is its versatility and ability to adhere to a great variety of material, which facilitates enzyme immobilisation on different solid substrates.[118] Moreover, this (aqueous) method is much simpler compared to more traditional coupling methods, which normally require multistep procedures and may involve more expensive and aggressive surface treatments. For all these reasons, this approach presents a simple and versatile alternative for enzyme immobilisation.

2.2.3.2. Entrapment

In the case of the entrapment, the enzyme is physically confined within a matrix that allows the substrate to penetrate and reach the catalytic sites, but retains the enzyme. However, this physical confinement does not completely prevent enzyme leakage,[109] so additional covalent attachment may be required; hence, it can be difficult to distinguish between binding to a support and entrapment. Sheldon[102, 109] proposed a definition to discriminate between these two methods: he defined support binding as “the binding of an enzyme to a prefabricated support (carrier) irrespective of whether the enzyme is situated on the external or internal surface” whereas entrapment “generally requires the synthesis of the polymeric matrix in the presence of the enzyme”.[102, 109] According to this definition,

entrapment is a one-pot process in which the enzyme is added to the reaction mixture while the host matrix is formed.

Different supports have been employed for entrapping enzymes, including mesoporous silica[104, 103], silicon elastomers[119], polydimethylsiloxane membranes[120] and electrospun nanofibers.[121] Mesoporous silica materials have been widely exploited for enzyme entrapment. These materials are characterised by a high surface area-to-volume ratio and a uniform pore distribution, where pore dimensions can be tuned.[106] Porous silica materials can be easily prepared via the sol-gel method, a process that involves hydrolysis and condensation of metal alkoxides ($Si(OR)_4$) in the presence of acid or base as catalyst. This process occurs in mild conditions and is hence relatively harmless for many enzymes.[105, 122] A more recent approach exploits electrospun nanofibers. Electrospinning is the process of spinning polymeric fibres with the help of electrostatic forces and can be exploited to produce fibres with diameters in the nanometre range.[123] The electrospun nanofibers generally form a non-woven network that can be exploited as a membrane; hence, immobilising enzymes on these materials results in a system that can be employed at the same time for biocatalysis and for filtration, making these systems particularly suitable for applications such as membrane bioreactors, biosensors and biofuel cells. To achieve enzyme entrapment in the nanofibers network, the electrospinning is performed in the presence of the enzyme; since most of the enzymes are soluble in aqueous media, water soluble polymers are employed, including poly(vinylalcohol), poly(vinylpyrrolidone), poly(ethylene oxide).[121]

2.2.3.3. Cross-linking

The early studies on carrier-free immobilised enzymes were performed in the 1960s by Quiocho and Richards,[124] who were investigating solid phase protein chemistry to stabilise enzyme crystals for X-ray diffraction studies. Employing a bifunctional crosslinker (glutaraldehyde), which reacts with amine groups on the enzyme's surface, they obtained cross-linked enzyme crystals (CLECs), which retained catalytic activity. A few decades later, these systems were investigated for possible applications as industrial biocatalysts, as compared to their soluble counterparts, CLECs proved to have improved thermal stability and tolerance towards organic solvents.[125] However, this method had a few drawbacks, including low mechanical stability of the aggregates, low activity retention and above all,

the need to crystallise the enzymes, which can often be a long and difficult process.[109] Nevertheless, the development of carrier-free immobilised enzymes that combine the features of pure enzymes with improved stability and specific activity was very appealing. This inspired further research in the field, which led to the development of cross-linked enzymes aggregates (CLEAs®) by Sheldon *et al*. The addition of salts, non-ionic polymers or organic solvents such as alcohols to aqueous solutions of proteins induces the formation of aggregates of protein molecules. The proteins in the aggregates retain their original structure and, hence, their catalytic activity. This well-known effect is often exploited as a method to purify proteins, since these aggregates are held together by weak non-covalent interactions they can be easily re-dispersed in aqueous media. By cross-linking these physical aggregates, Sheldon *et al.* obtained permanently insoluble structures in which the enzyme catalytic activity was retained. For CLEAs glutaraldehyde is also the most employed cross-linking agent; however, due to its small size and high reactivity, glutaraldehyde can in some cases react with the amino acids residues in the catalytic core of the enzyme, thus unsurprisingly causing a loss of catalytic activity. For this reason, bulky polyaldehydes (like dextran polyaldehyde) have been exploited as alternative cross-linking agents.[109] The preparation of cross-linked enzyme aggregates is an interesting alternative methodology to obtain immobilised enzymes, since it combines enzyme purification and immobilisation in a single process, thus does not require highly pure enzymes and provides stable enzyme aggregates with highly specific catalytic activity.

2.2.4. Nanoparticle-based Immobilisation of Enzymes

As mentioned previously, nanoscale materials have attracted growing interest as supports for enzyme immobilisation. Compared to conventional immobilisation supports, nanoscale supports are characterised by a higher surface area-to-volume ratio. This can be advantageous for enzyme immobilization since it allows for high enzyme loading. This distinctive feature has been the driving force for the development of nanobiocatalysis.[110] The first examples of nanoscale materials as supports for biocatalysis date back to the late 1980s,[126, 127, 128] since then, a wide range of nanoscaffolds have been reported, consisting of different materials (silica, magnetite, gold, polymers) and shapes (nanospheres, nanorods, nanofibers, nanotubes). Different methods for enzyme immobilisation have been employed, exploiting either covalent binding or non-covalent interactions with the support, or a combination of both.

Nanoporous materials such as silica have been employed as hosts for enzyme immobilisation; most commonly, simple adsorption is employed to immobilise enzymes into nanoporous materials. As previously highlighted, adsorption is a relatively simple process; however, this approach has a serious drawback in enzyme leaching form the pores. In order to prevent enzyme leakage, additional covalent attachment may be required.[129] In a recent review, Bayne *et al*. analysed published data on enzyme immobilisation onto nanoporous materials to correlate pore dimensions with protein loading.[130] When the pore diameter is smaller than 10 nm, the enzymes encounter physical restrictions in accessing the pores, which results in a decrease of protein loading. On the other hand, a decrease in protein loading is observed when pore diameter is greater than 100 nm as well, due to a reduction in the available surface area. In the range between 10 and 100 nm the protein loading is expected to decrease while increasing the diameter, but in fact it remains constant. This is ascribed to protein-protein interactions, which block the pores and limit the access at decreasing pore diameters. No obvious correlations between pore dimension and retention of activity were observed.

Both magnetic and non-magnetic nanoparticles have been employed in biocatalysis. Together with the increased surface area-to-volume ratio, nanoparticles present an additional feature that can be exploited in enzyme immobilisation. When enzymes are immobilised on nanoparticles they still exhibit Brownian motion. This reduced diffusional limitation compared to enzymes immobilised on macro-scale matrices accounts for the apparent increased activities obtained when enzymes are immobilised on nanoscale hosts.[131] Gold and silver nanoparticles can be conveniently employed for enzyme immobilisation; enzymes and proteins can be adsorbed on gold and silver surfaces thus allowing for direct immobilisation without any modification, taking advantage of inherently present charged groups and thiols. Gold nanoparticles can also be easily modified with thiolated molecules or carboxylic groups, which can in turn be conjugated with the amino groups of the enzymes. The recovery of non-magnetic nanoparticles from the reaction medium can often be a difficult task, this drawback can be overcome by using magnetic nanoparticles as the magnetic properties of the nanoparticles can be exploited for efficient recovery of the enzyme-nanoparticle complex simply by means of a magnet. For this reason, magnetic nanoparticles (iron oxide in particular) are of great interest for applications in nanobiocatalysis.[131]

Nanoparticle size strongly influences protein structure and function. Dordick and co-workers investigated the structure and activity of lysozyme upon immobilisation on silica nanoparticles of different diameters (ranging from 4 to 100nm).[132] Circular dichroism proved that the α-helix content is lower for lysozyme adsorbed on larger silica nanoparticles, demonstrating that upon adsorption, the enzyme undergoes a considerable secondary structure modification and that this effect increases with increasing particle diameter. Measuring lysozyme activity as a function of nanoparticle size it was found that this was decreasing with increased particle size, as with the α-helix content. Since the surface curvature increases as the size of the nanoparticles decreases, there is less interaction (in this case mostly Coulombic interactions) between the protein and the smaller nanoparticles, which in turn results in a less significant perturbation of enzyme secondary structure and higher retention of activity (Fig. 21). These results were later confirmed for a number of different enzymes (lysozyme, human carbonic anhydrase, cytochrome C, soyabean peroxidase, ribonuclease A).[133-136] Thanks to the advantageous properties of nanobiocatalytic systems, it is anticipated that this approach for enzyme immobilisation might enable further technological applications of enzymes.

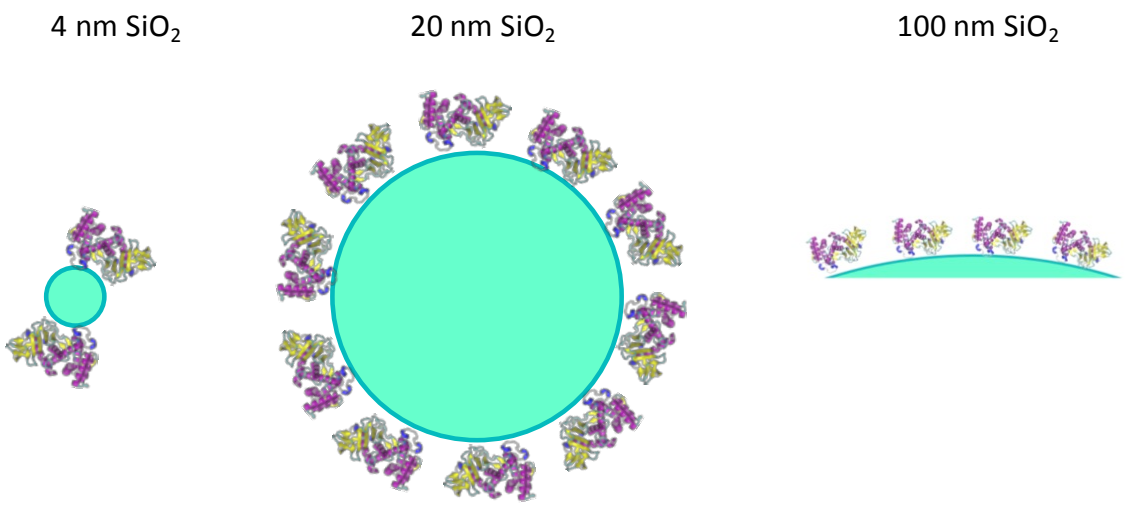

Figure 21 Illustration of lysozyme adsorption on silica nanoparticles of different diameters. The stronger interactions between protein and larger nanoparticles results in more protein unfolding and loss of activity. Modified from reference 132.

2.2.5. Final Properties of Immobilised Enzymes

As a result of the immobilisation, some properties of the enzymes may be different compared to their soluble counterparts. The final performance of the immobilised systems will depend on the conditions under which the enzyme was immobilised, the selected support and the nature of the enzyme (e.g. source from which it is obtained and purity).

The immobilised enzyme stability is affected by a number of factors involved in the immobilisation process, such as the interactions between the enzyme and the selected support, the chemical and physical properties of the support itself, the conditions under which the immobilisation occurred (*e.g.* pH, temperature, enzyme loading) the microenvironment and the number of bonds (in case of covalent binding with the matrix). In a number of examples, when an enzyme is immobilised, its stability is improved[73, 107] to an extent which depends on the immobilisation method (i.e. binding to a support, entrapment, crosslinking). The correlation between stabilisation and number of bonds for enzymes covalently bound to the carrier have been widely investigated and it is now generally accepted that a multipoint attachment can promote a stabilising effect.[73, 137, 138] When the enzymes are covalently bound to the support through many surface residues and by means of a short spacer, the rigidity of the attachment makes the enzyme more resistant to conformational changes that could be induced by external agents such as temperature or organic solvents (Fig. 22).

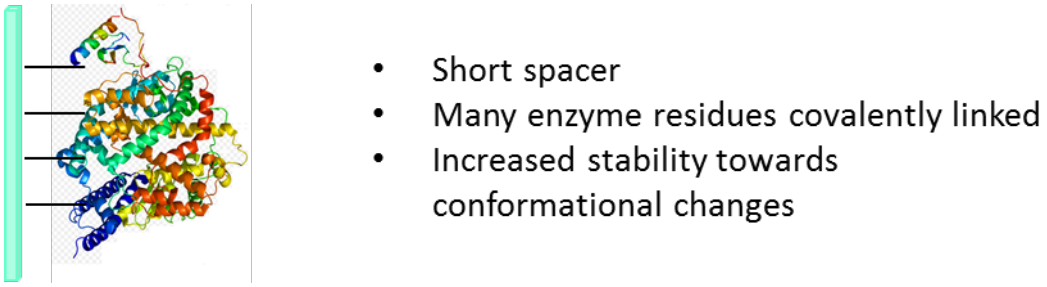

Figure 22 Protein stabilisation through multipoint covalent immobilisation.

Lopez-Gallego *et al.* developed a protocol for enzyme immobilisation via multipoint covalent attachment to aldehyde-terminated supports, where the aldehyde groups are separated from the support surface through a very short spacer (Support-O-CH_2-COH).[138]

The presence of a high number of aldehyde terminal groups and alkaline conditions (e.g., pH 10) promotes the multipoint covalent immobilisation through lysine residues on the surface of the enzyme (pK_a around 10.5).

One of the main drawbacks of enzyme immobilisation is the potential loss of catalytic activity, which may arise from limited access of the substrate to the catalyst or to an unfavourable orientation of the active site.[73] Nevertheless, an enhancement of enzyme activity upon immobilisation has been observed for a number of different enzymes and immobilisation techniques. A number of effects involved in the immobilisation process can affect the activity of the immobilised enzyme, including the microenvironment, conformational change, molecular orientation and binding mode.[107] The effect of the binding mode depends on the number, position and nature of the bonds. As opposed to the positive effect on enzyme stabilisation, a higher number of bonds between the enzyme and the carrier will lead to a lower activity[107]. For enzymes immobilised on porous supports, the substrate diffusion to the catalysts may be limited by steric hindrance. A reduction of apparent activity could also occur when the active site is not favourably oriented and hence it is more difficult for the substrate to reach it. In contrast with the positive effect that enzyme immobilisation generally has on the stability; the effect on the enzyme activity is hence more difficult to predict.

2.3. Micro- and Nanopatterning of Biomolecules

The possibility to realise a controlled pattern of enzymes or other biomolecules with micro- and nanometre resolution on solid surfaces is of great interest for a number of technological applications, ranging from fundamental studies of cell biology to the production of biosensors for molecular diagnostics.[139, 140] For example, protein nanoarrays facilitate the production of biosensors with more reaction sites, thus providing potentially greater sensitivity in diagnostic tests.[139] Studies of cell adhesion and motility may also benefit from progress in this area, since cell adhesion receptors are spatially organised at the nanoscale.[140]

The progress made in nanofabrication technology in the last decades allowed for the development of promising methodologies to produce submicron and nanoscale features on surfaces. Currently, a number of technologies have been reported, including microcontact/nanocontact printing (μCP, nCP),[141-143] traditional photolithography,[144] nanoimprint lithography[145] and atomic force microscopy (AMF)-based lithography techniques such as dip-pen nanolithography, nanographting and nanoshaving.[146, 147] These techniques have been successfully employed to print a variety of biological molecules, including proteins, DNA, enzymes, viruses and bacteria.[148] A comprehensive review of all these different techniques is beyond the scope of this thesis; however, a few relevant examples are reported below, which include two of the aforementioned methodologies.

2.3.1. Microcontact Printing

In the 1990s, Whitesides and co-workers developed a set of non-photolithographic microfabrication methods, as an alternative to the conventional photolithographic techniques. These methods are collectively referred to as “soft lithography”, since they all share the feature of using a soft elastomeric stamp rather than a rigid photomask to generate patterns on a surface.[149, 150]

Microcontact printing (μCP) is a soft lithographic technique that uses the relief patterns on an elastomeric stamp to form patterns of ink on the substrate surface through conformal contact. A master, or template, is created using traditional photolithography techniques. The master is typically created on silicon, but can be done on any solid patterned surface.

An elastomeric stamp having relief structures on its surface is the key element of soft lithography. The stamp is prepared by pouring a mixture of a silicon elastomer and a curing agent onto the silicon template and upon polymerisation of the elastomer the stamp can be peeled off, where the stamp is the negative of the silicon template and the material generally employed for the stamp preparation is polydimethylsiloxane (PDMS). Whitesides *et al*. initially applied this technique for micropatterns of self-assembled alkanethiol monolayers (SAMs) on gold surfaces.[149]

Since μCP is performed at room temperature in ambient conditions and requires no harsh chemicals, this technique is suitable to transfer patterns of biomolecules onto substrates and has been successfully employed for this purpose.[151, 152, 143] Delamarche and co-workers were pioneers in this field and in the late 1990s and early 2000s published a series of papers describing μCP and derivatives thereof for the immobilisation of proteins.[143, 152-155] They successfully employed μCP to create patterns of immunoglobulin G (IgG), rhodamine-labeled antibodies and alkaline phosphatase.[143] The printed alkaline phosphatase was used to convert a fluorogeinc substrate into an insoluble product that precipitates at the patterning sites, proving that the enzyme retained its activity upon immobilisation. Interestingly, Delamarche *et al*. also used μCP to print different proteins on a single substrate, they proved that patterns of different proteins can be obtained simply by successive printing: two different proteins have been subsequently printed onto the same glass substrate using different PDMS stamps (Fig. 23a).[143] Fluorescence images revealed that no loss of resolution occurred after the successive printing, proving that the stamp did not pick up those proteins already printed. In the same work, they showed an alternative approach to obtain multicomponent patterning of proteins. They exploited a microfluidic network to ink a planar stamp with 16 different proteins. This pattern was then transferred from the stamp to the polystyrene surface of a cell culture dish. The high molecular weight of the proteins and their affinity with the surface prevented any diffusion on the stamp before the printing (Fig. 23b).[143, 155]

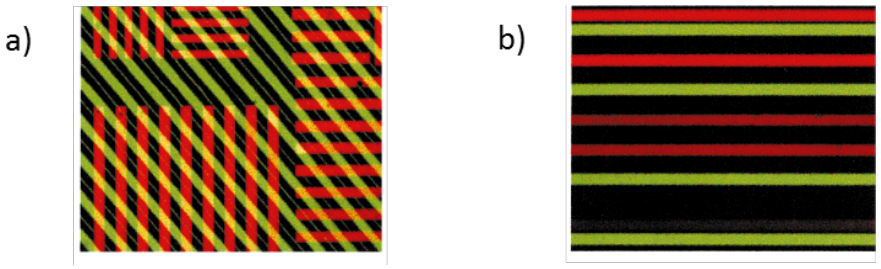

Figure 23 a) Fluorescence images of two different proteins printed onto a substrate. b) Fluorescence image of 16 different proteins (some of them without fluorescent label) patterned onto a plastic substrate using a stamp inked by means of a microfluidic network. Reproduced from reference 143.

Subsequently, Delamarche and co-workers proposed an alternative method to generate patterns of multiple proteins using a planar stamp.[156] This method is referred to as ISP, from the three main steps involved (Ink, Subtract, Print). A planar elastomeric stamp is inked with a protein solution and then brought in contact with a nanotemplate, which subtracts part of the proteins from the stamp, the stamp is then used to transfer the pattern onto a substrate. By adding two additional steps, this procedure can be used to print multiple proteins: the stamp is inked with the first protein, subtracted using the nanotemplate, inked again with a second protein, subtracted again and finally brought in contact with the substrate (Fig. 24). This strategy is referred to as (ISISP). The nanotemplate and the substrate should be less hydrophobic than the stamp in order to favour the protein transfer from a less wettable to a more wettable surface.

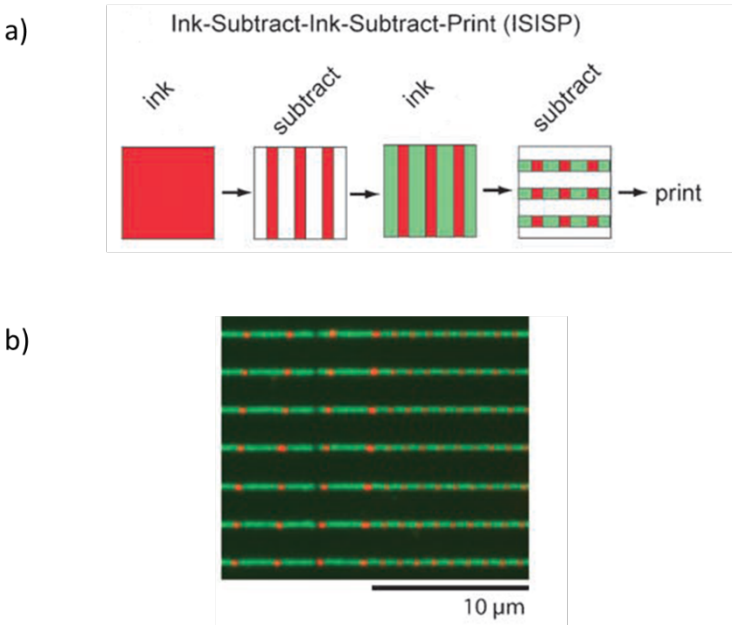

Figure 24 a) Schematic illustrating the ISISP strategy, consisting of the repeated inking and subtraction of two different proteins onto an elastomeric stamp, followed by the printing step. b) Fluorescence image on a pattern of two antibodies obtained by ISISP. Reproduced from reference 156.

More recently, Matsui and co-workers successfully employed microcontact printing to pattern enzymes on a glass surface.[142] The glass substrate was first modified to obtain an amine-terminated surface. The amine terminated glass surface was then treated in glutaraldehyde, obtaining aldehyde groups on the surface, which could react with the amine groups of the enzyme. The enzyme (urease) was added onto the PDMS stamp (previously modified to be hydrophilic), which was was then put in contact with the surface (Fig. 25). In this work Matsui and co-workers also proved that the immobilised enzymes retained their catalytic activity, by exploiting them to grow ZnO nanoparticles.

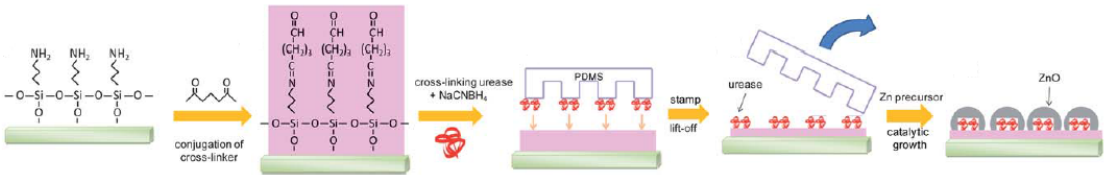

Figure 25 Schematic illustrating the procedure for urease immobilisation by micro contact printing. The glass substrate was modified to obtain an amine-terminated surface which was then conjugated with the cross-linking agent (glutaraldehyde). The enzymes were printed and exploited to grow ZnO nanoparticles to prove they retained catalytic activity upon immobilisation. Reproduced from reference 142.

2.3.2. Dip-Pen Nanolithography

Dip-pen nanolithography (DPN) is a scanning probe lithography technique, which employs an AFM tip to deliver chemicals to a substrate creating a pattern with nanometre resolution. The AFM tip is "inked" with the molecule that is to be deposited and is then brought into contact with the surface, where it can be scanned to create patterns. To stop the transfer of material, the tip is detached from the surface. This technique was firstly reported by Butt *et al.*[157] and then developed by Mirkin *et al.* in 1999 and has been initially employed to deliver alkanethiols to gold surfaces, allowing for the formation of (SAMs).[158, 159] DPN has since been extended to transfer a variety of inks (small organic molecules, polymers, biomolecules, colloidal particles)[160] to different substrates (gold, silicon and silicon oxide are among the most exploited).[159] The molecules of interest can be deposited in ambient conditions (or inert environment) and without the use of harsh chemicals or radiation. For these reasons, DPN has been employed as a tool for the immobilisation of biomolecules like proteins, DNA and enzymes.[139, 159]

One of the first examples that combined DPN and enzymatic catalysis was reported in 2004 by Hyun *et al*. In this work, they functionalised the gold substrate with an oligonucleotide SAM and subsequently employed DPN to pattern the substrate with DNase I. The adsorbed enzyme was then activated with a solution of Mg^{2+}, resulting in the digestion of the substrate (Fig. 26).

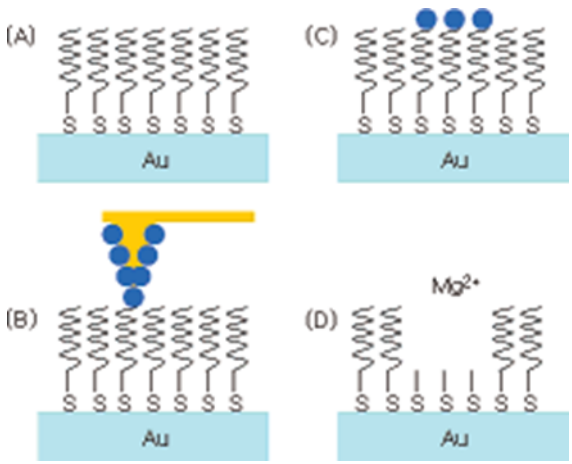

Figure 26 A) The gold substrate functionalised with oligonucleotides. B)-C) Enzyme DNase I is patterned on the SAM of oligonucleotides by DPN. D) Enzymatic digestion of the oligonucleotide upon activation with Mg^{2+} solution. Reproduced from reference 161.

AFM images showed the enzyme pattern on the surface and confirmed the digestion of the oligonucleotide upon enzyme activation (Fig. 27).

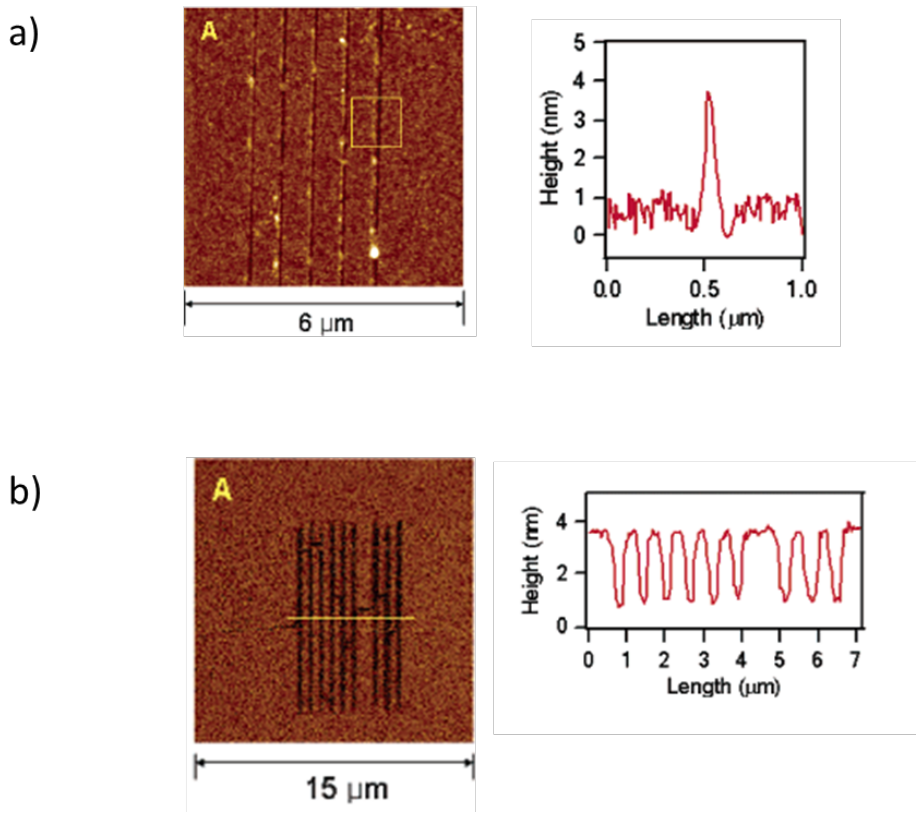

Figure 27 a) Tapping mode AFM images of DNase I patterned on an oligonucleotide SAM on a gold substrate. b) Tapping mode AFM image of the oligonucleotide SAM after digestion by DNase I. The line profiles show that the height of the trenches decreased on ~3nm after enzyme digestion of the SAM. Modified from reference 161.

Lee *et al*. proved that DPN can be employed to generate arrays of different proteins on the surface of interest.[162] To facilitate protein adsorption on the tip, they coated the conventional AFM tips with gold and then modified them with carboxylic acid-terminated SAMs. Au substrates were chosen due to the strong interaction between the cysteine residues on the protein and the gold surface, which provides a driving force for enzyme adsorption. Moreover, polyethylene glycol (PEG) can be used as a passivating agent to cover the areas not patterned with the protein. First, rabbit immunoglobulin-gamma (IgG) nanodot arrays were patterned on the gold surface by DPN; subsequently, lysozyme features were patterned between the IgG nanodots (Fig. 28).

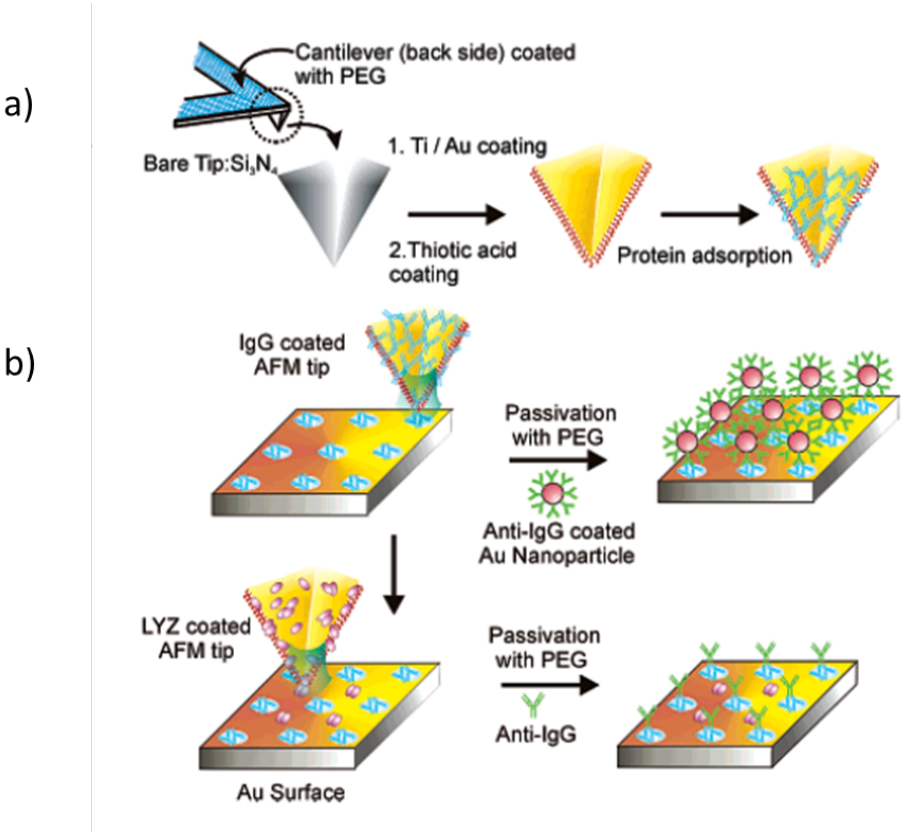

Figure 28 Schematic illustrating a) the tip modification procedure and b) the DPN process to pattern the gold substrate with two different arrays of proteins. Reproduced from reference 162.

To confirm that the IgG retained its biorecognition properties, the array was incubated in a solution containing anti-rabbit IgG. Line profiles showed a height increase, due to the binding of anti-rabbit IgG, exclusively on the IgG nanodots and not on the area patterned with lysozyme (Fig. 29).

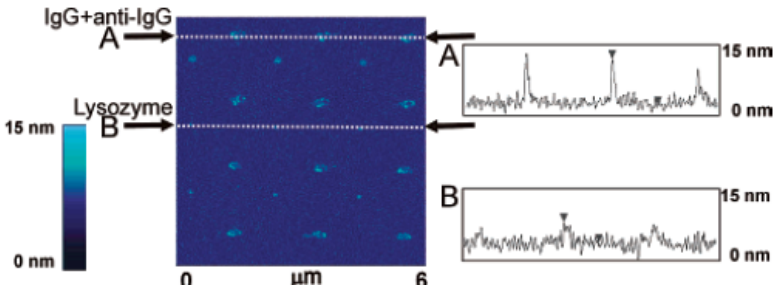

Figure 29 Tapping mode AFM image of the two-component pattern after reaction with anti-IgG and line profile. The line profile shows an increase of ~5nm in the areas patterned with IgG. Reproduced form reference 162.

An interesting approach was introduced by Van Orden and co-workers, who combined elements of DPN and μCP to generate multiple component patterns.[163] They used an AFM tip to ink individual features of a PDMS stamp. In this way, different components can be inked on a single stamp, the stamp is then brought into conformal contact with a substrate to transfer the pattern (Fig. 30). They referred to this technique as *s*ingle *f*eature *ink*ing and *s*tamping (SFINKS).

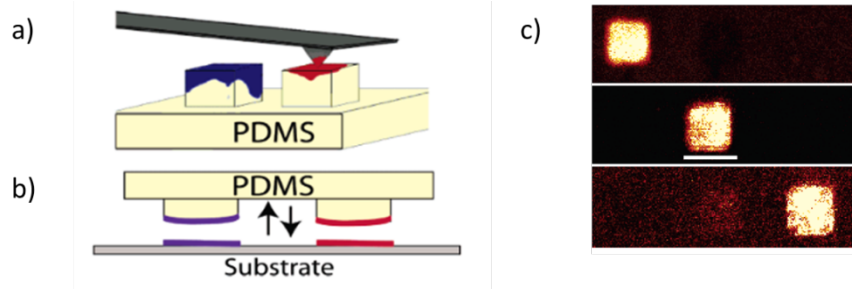

Figure 30 Schematic illustrating the SFINKS method. a) The AFM tip deposits ink onto individual features of the PDMS stamp. b) The stamp is brought in contact with the substrate to transfer the pattern. c) Fluorescence images of the printed pattern. The three images correspond to the same area scanned with different excitation wavelengths to detect the three different labelling fluorophores. The scale bar is 10 μm. Reproduced from reference 163.

Van Orden and co-workers inked three features of a PDMS stamp with three different DNA sequences and printed them on a glass slide, which was subsequently incubated in a solution containing the three complementary DNAs, each labelled with a different fluorophore. Fluorescence images confirmed that the printing was successful and the three patterns were visualised at three different excitation wavelengths (Fig. 30c). Both DPN and μCP proved to be successful techniques to pattern a wide range of biomolecules, including proteins and enzymes. Moreover, from the examples provided in the literature, it is clear that these techniques constitute an interesting approach to achieve multicomponent biomolecule immobilisation.

2.3.3. Thermochemical Nanolithography

Thermochemical nanolithography (TCNL) is a scanning probe lithography technique developed by Riedo's lab which employs a heated AMF tip to induce a chemical modification onto a surface in arbitrary micro- and nano-patterns.[164] A silicon AFM cantilever is resistively heated by a current flowing in the cantilever legs, which are highly

doped except for the region where the tip is positioned and the heat is used to trigger a nanoscale reaction on the surface.

Figure 31 Schematics of thermochemical nanolithography on a polymeric solid support. The heated AFM tip deprotects amine groups on the polymeric surface. The amine groups can be directly cross-linked to a biomolecule or undergo further modification to add a cross-linker suitable for further functionalization with different nano-objects. Reproduced from reference 165.

This technique has been employed on a variety of substrates, including graphene oxides, ceramics and polymers.[164-166] Riedo and co-workers showed that TCNL can be used to deprotect active amine groups on polymeric solid supports and the deprotected groups can be subsequently used to conjugate biomolecules.[165] They realised patterns of proteins and demonstrated that the proteins retained activity upon conjugation to the surface. Moreover, they presented a method to independently pattern arrays of different proteins in close proximity and with excellent control of the pattern geometry. Thanks to the high resolutions (up to 40 nm), high writing speed (up to millimetre per second) and the potential to be highly parallelised, this technique could be employed to realise large patterns of biomolecules with a wide range of applications in nanobiotechnology.

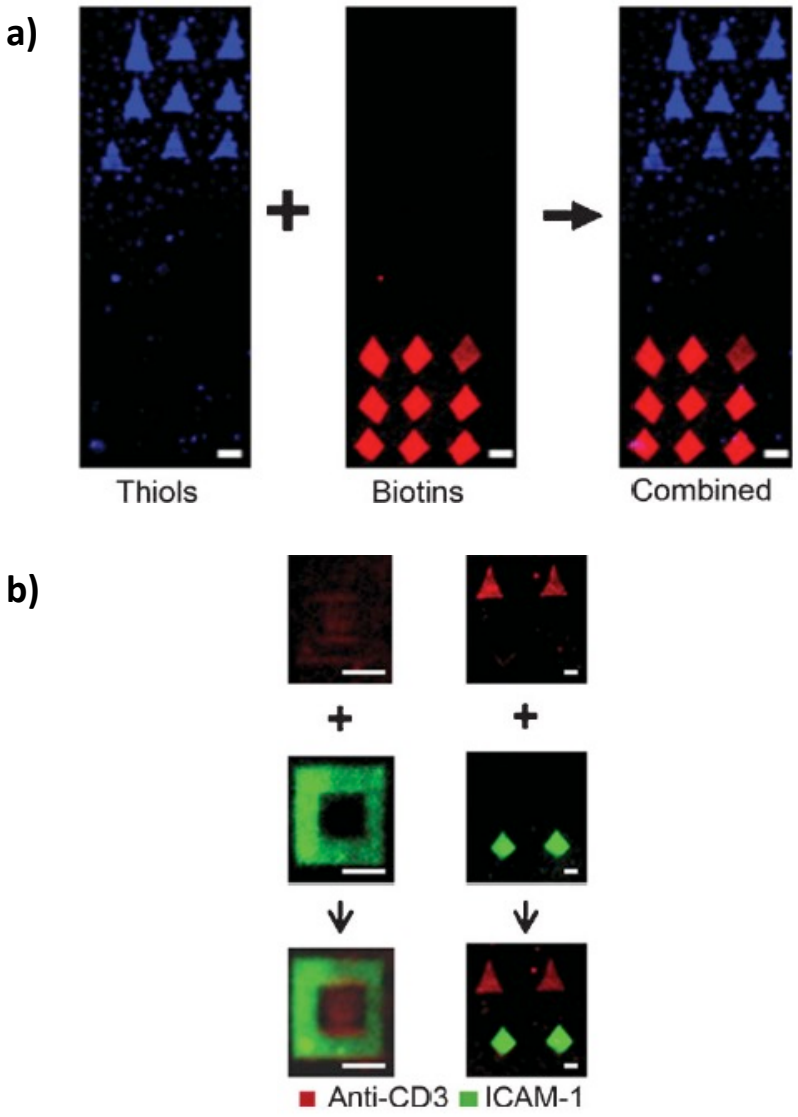

Figure 32 a) A co-pattern of thiols and biotins was fluorescently labelled by incubation of the surface first with a thiol-reactive dye (blue) and then with biotin reactive streptavidin conjugated to a red dye. The images show that the two dyes selectively bind to the thiol and biotin patterns, respectively. b) The cell signalling protein anti-CD3 is cross-linked to the amine pattern by means of NHS-biotin and streptavidin and the cell adhesion protein ICAM-1 is cross-linked to amines with glutarladeyde and they can be independently conjugated onto patterned substrates. The fluorescence images were obtained imaging the fluorophores separately with different set of filters and the images were then overlaid. Reproduced from reference 165.

2.4. Conclusions

In the past decades, there has been an increasing interest towards the properties and applications of hydro- and organogels formed by LMWGs, as proven by the exponential growth of the number of publications related to this topic.[15] This interest has been motivated by the number of existing and potential applications these materials may have, ranging from catalysis, to sensing and actuating, cosmetics, controlled release and drug delivery or tissue engineering.[21, 22, 23] Significant advances in this field occurred thanks to the identification of new LMWGs, which give a better understanding of the chemical basis for the formation of supramolecular gels and to the improvements in the techniques available for the characterisation of these materials.[15, 16, 25]

Amongst the variety of known LMWGs, peptides and peptide derivatives attracted particular attention thanks to the huge number of structures that can be achieved through the combination of different amino acid sequences. Peptide derivatives with very short peptide chains have been successfully employed as LMWGs. These materials can be easily produced at low cost and have shown a range of interesting properties, including the inherent possibility to provide a functional interface with biological materials.[167] Peptide-based molecular precursors have been shown to self-assemble into supramolecular structures either spontaneously or as a consequence of the application of different kinds of external stimuli, including temperature, mechanical triggers, pH and enzymes.[7-9]

Enzymatic hydrogelation as a route to design stimuli-responsive supramolecular hydrogels is drawing increasing attention. The combination of (bio-)catalysis and molecular self-assembly provides a powerful effective approach for developing smart biomaterials, allowing integration of processes from biological systems with the formation of hierarchical nanostructures. This approach has proved to be effective in the control of self-assembly of peptide-based LMWGs into hydrogels and to develop complex next-generation nanomaterials with possible applications in biology and medicine-related fields.

Peptide-based hydrogels are particularly attractive as scaffolds for regenerative medicine applications, thanks to their ability to mimic many properties of native tissues. Research in this field has made great progress; however, the development of innovative biomaterials for cell culture is still needed to design *in vitro* models that could better resemble the 3D

architecture of the native ECM as well as reproducing the physical and chemical stimuli cells experience in their natural environment.

Self-assembled peptide derivatives are powerful building blocks for the design of ECM mimics, thanks to their ability to self-assemble into highly organised fibrous networks. These materials present a number advantages compared to polymeric scaffold or naturally-derived materials: they have the appropriate nanoscale dimensions (fibre average diameter should be fairly smaller than the average cell dimension), they do not suffer the batch to batch compositional variation and impurity contamination typical of materials derived from biological molecules, their mechanical, topographical and chemical properties can be tuned to enhance the interaction between the scaffold and cells. Using enzymes to trigger the self-assembly (and subsequent gelation) of aromatic peptides amphiphiles can allow for a highly controlled process in which the assembly is localised in the vicinity of the enzyme. Moreover, with this approach a number of structurally diverse networks can be accessed, depending on the enzyme and pre-gelator selected.

3. Metastable Hydrogels from Aromatic Dipeptides *

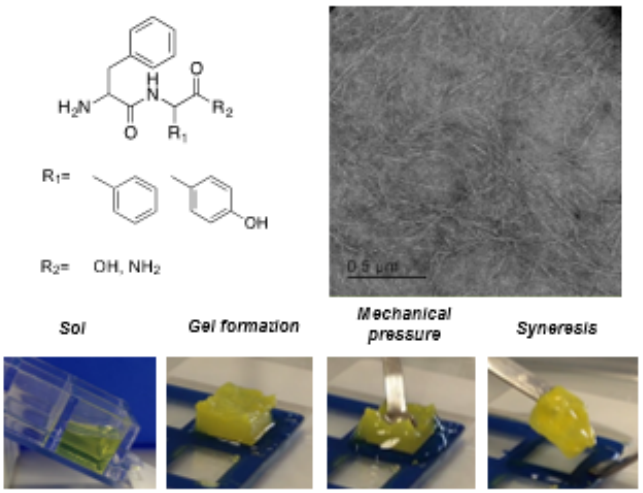

* The work in this Chapter has been published, in part, to Chemical Communications.[168]

Declaration of contribution to published article:

Any reproduced work from the aforementioned published article, including the written article itself, I was solely responsible for, together with the other authors of the article, unless otherwise stated.

3.1. Introduction

Supramolecular self-assembly provides an effective bottom-up approach for the fabrication of functional nanomaterials.[169, 170] Among the available molecular building blocks, peptides and peptide derivatives have attracted attention due to their chemical versatility and the inherent possibility to provide a functional interface with biological systems.[167, 171, 172] Very short peptides[6, 173, 174] and their derivatives[28] are of particular interest in this context due to their chemical simplicity, low cost and remarkable properties.[175]

The first example of nanostructure formation by self-assembly of dipeptides dates back to the early 2000s, when Gorbitz *et al.* observed the formation of supramolecular structures upon crystallisation of four dipeptides (dileucine (LL), leucine-phenylalanine (LF), phenylalanine-leucine (FL) and diphenylalanine (FF).[176] Among these four dipeptides FF, the key structural motif of Alzheimer's β-amyloid polypeptide, is probably the most well-known, thanks to pioneering work by Gazit and co-workers.[6, 177-180] They observed that this dipeptide self-assembles into hollow tubular nanostructures in aqueous solution, through a combination of hydrogen-bonding and π-π interactions.[6] Following this observation, unexpected properties not typically associated with biological matter have been reported for FF nanotubes. This includes demonstration that these nanostructures are stable in boiling water and organic solvent,[178] and that they are remarkably stiff, having a Young's modulus of ~ 20 GPa, which places them among the stiffest biological materials known.[181] Moreover, by varying assembly conditions FF-based building blocks have been shown to self-assemble into a variety of different structures, such as vesicles, ribbons and fibres.[182-184] Li et al. showed that FF may also act as an organo-gelator, forming organogels in chloroform or aromatic solvents.[185] So far, the only example of an (unmodified) dipeptide that is able to self-assemble to form a hydrogel is the isoleucine-phenylalanine (IF) reported by Ventura et al.[186] Other examples of dipeptide nanostructures include WF and FW nanoparticles[187] and VA and AV which self-assemble into different structural morphologies in various solvent media.[188] It is increasingly appreciated that in addition to the molecular structure of the building blocks, the self-assembly pathway is critical to properties of the supramolecular assemblies.[189]

In this Chapter, the formation of metastable FF (free acid and amide) hydrogels obtained upon sequential solvent switching and sonication of dipeptide solutions is reported. Once

formed, the gels show rapid syneresis upon mechanical stimulation (Fig. 33 and 36). Syneresis is the contraction of a gel accompanied by sudden release of the moisture initially contained within the gel network. This phenomenon has been mostly studied in polymer-based gels[190-192] and only a few reports exist about the syneresis of supramolecular hydrogels.[193-195] Adams and co-workers reported a few Fmoc-based peptide gels that show syneresis and recently they provided further insights into the origin of the process for a peptide-based gelator with an oligophenylene vinylene core.[196]

3.2. Results and Discussion

To form the hydrogels, 5 mg of FF or FF-NH_2 dipeptide is first dissolved in 80 µl of 1,1,1,3,3,3-hexafluoro-2-propanol (HFIP) and then diluted up to 1 mL in 100 mM sodium phosphate buffer pH 8 giving rise to a final molar concentration of 16 mM.[6] Upon sonication (5 to 10 ultrasound pulses of 10 s each) the colourless, transparent solution turns into a white opaque gel (Fig. 33). The critical gelation concentration (CGC) was determined by consecutive dilution with buffer and found to be ~ 8 mM for FF (~ 0.25 wt%) and ~ 4 mM for FF-NH_2 (~ 0.12 wt%).

Figure 33 Chemical structures of the dipeptides. (b) Schematic of the gelation process for FF and FF-NH_2. The opaque gel forms upon vortexing and sonication of the dipeptide solution. Mechanical touching with a spatula causes the rapid syneresis (seconds) of the gel which collapses to approximately 40% of its original volume. (c) Screenshots to illustrate the process.

Gels were formed exclusively when the combination of the two stimuli (ultrasound and solvent switch) is applied. Amorphous aggregates were observed when the dipeptides are dissolved in HFIP and buffer without sonication.

Sonication is commonly used in supramolecular chemistry to modulate self-assembly and gelation processes.[197-202] Ultrasound can assist the gelation process allowing conformational rearrangements and reorganisation to maximize non-covalent interactions.[197, 200] Both gels formed are stable at room temperature for several weeks when left undisturbed, but they exhibit rapid syneresis when they undergo mechanical stress (Fig. 33 and 36). This rapid expulsion of water is likely related to the extremely hydrophobic nature of the peptide fibres formed. To demonstrate the hydrophobicity of the fibres a fluorimetric assay based on 8-Anilino-1-naphthalenesulfonic acid (ANS) was employed. ANS is a fluorescent dye frequently employed in various fields of protein analysis as it binds to hydrophobic regions of proteins. Interactions of ANS with hydrophobic binding sites is accompanied by an increase in fluorescence and a blue shift of the peak maximum.[203] 5 mg of FF or FF-NH_2 dipeptide are first dissolved in 80 µl of HFIP and then diluted up to 1 mL in 100 µM ANS buffered solution (see section 3.4.9). The ANS buffered solution fluoresces around 540 nm (Figure 34). When the dye is mixed with the dipeptides, a significant increase in the fluorescence intensity emission is observed, accompanied by a blue shift of the maximum peak. This effect is even more evident when the peptide solutions are sonicated and the gel is formed. Upon mechanical disruption, the collapsed gel and the exuded liquid was separated and collected. The fluorescence emission confirms the hydrophobic nature of the

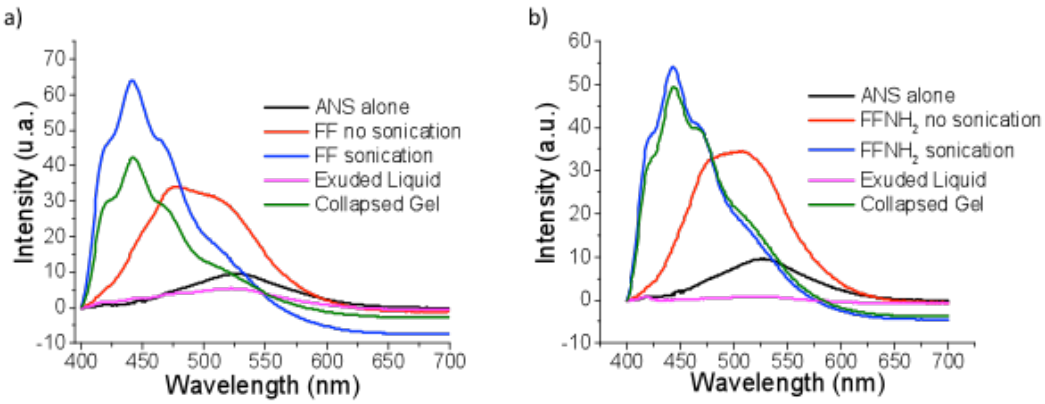

Figure 34 ANS binding fluorescence assay on FF (a) and FF-NH_2 (b) gels. For both systems, the assay shows a significant increase of fluorescence and a blue shift of the maximum, both before and after sonication. The assay also highlights the hydrophobic nature of the nanofiber network.

collapsed gel, whereas the spectrum of the exuded liquid does not show any significant peak (Figure 34).

Given the hydrophobic nature of the network and the rapid expulsion of the moisture observed upon mechanical disruption, hydrophobic compounds could show release or remained bound to the network of fibres. The hydrophobic dye thioflavin T (ThT), commonly used to stain β-sheet like fibres[204], was added to the peptide solutions, obtaining a bright yellow gel. Upon syneresis, a transparent liquid is exuded, in contrast to the collapsed gel that remains yellow, suggesting that the hydrophobic dye is retained into the supramolecular aggregates. A UV-Vis assay confirmed that more than 99% of the initial concentration of the dye is retained into the collapsed gel (Fig. 35 and 36).

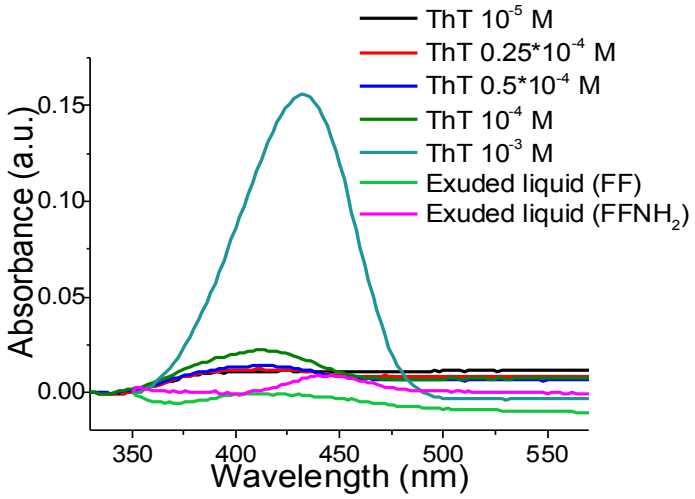

Figure 35 UV-Vis absorbance of ThT solutions and of the liquid exuded from the ThT containg gels. For both the liquid exuded from FF and FF-NH_2 gels upon syneresis, the characteristic ThT absorption peak around 415 nm is not visible.

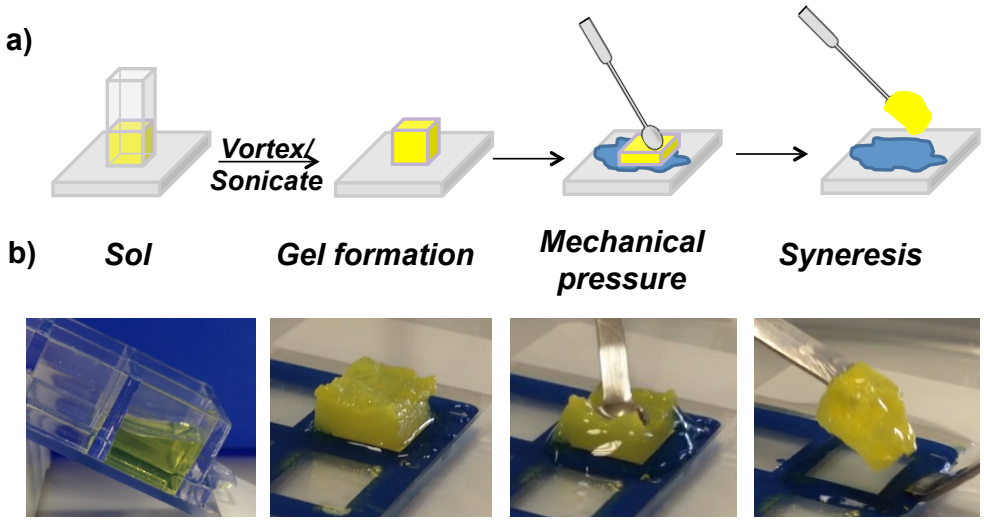

Figure 36 (a) Schematic of the gelation process for FF and FF-NH_2. The opaque gel forms upon vortexing and sonication of the dipeptide solution. A fluorescent dye (ThT) was added to help visualise the process and demonstrate that the nanofiber network effectively sequesters hydrophobic compounds, releasing uncoloured liquid upon syneresis. Mechanical touching with a spatula causes the rapid syneresis (seconds) of the gel which collapses to approximately 40% of its original volume. (b) Screenshots to illustrate the process.

The collapsed structures obtained upon syneresis remain intact and can still be handled and characterised. Due to the immediate collapse upon handling, the following characterisation was carried out on the collapsed structures.

Transmission and scanning electron microscopy (TEM and SEM) were used to gain insight into the nanoscale morphology of the dipeptide assemblies. Before sonication, the TEM images of both FF-NH_2 and FF (Fig. 37a and 37c, insets) show the presence of tubular structures of several micrometres of length and hundreds of nanometres of diameter, as previously reported.[6, 182]

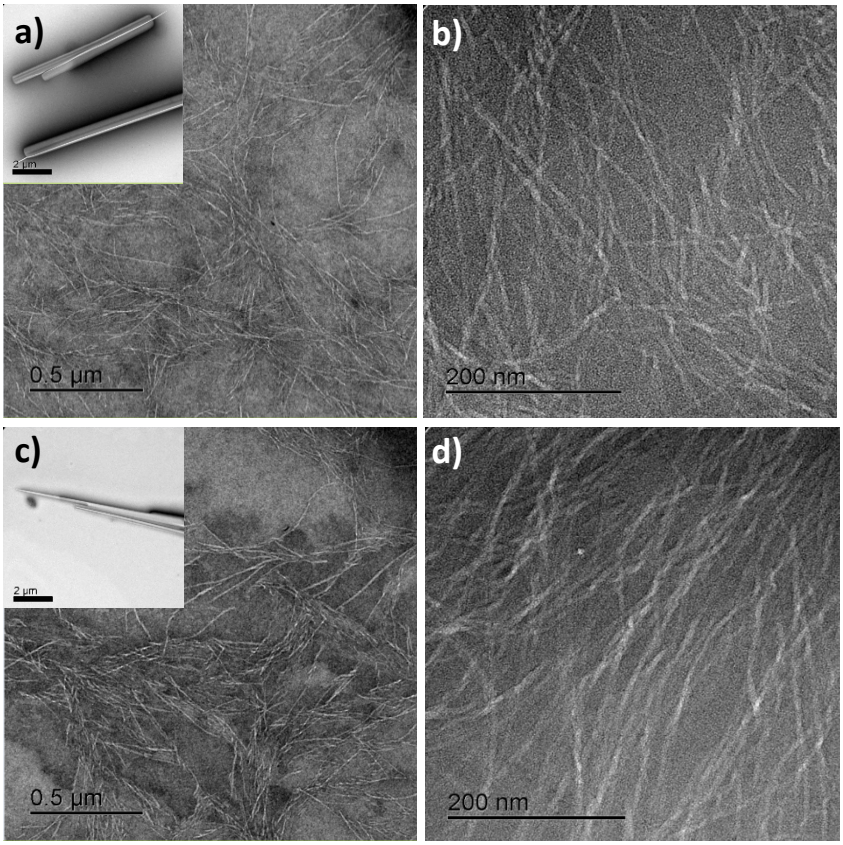

Figure 37 TEM images of FF-NH_2 (a and b) and FF (c and d). Before sonication both FF-NH_2 (a, inset) and FF (c, inset) form tubular nanostructures. After sonication, smaller nanofibers are observed for both samples.

Upon sonication, in addition to remaining nanotubes, much smaller fibres were observed, with a length of hundreds of nanometres and a diameter of approximately 10 nm (Fig. 37).

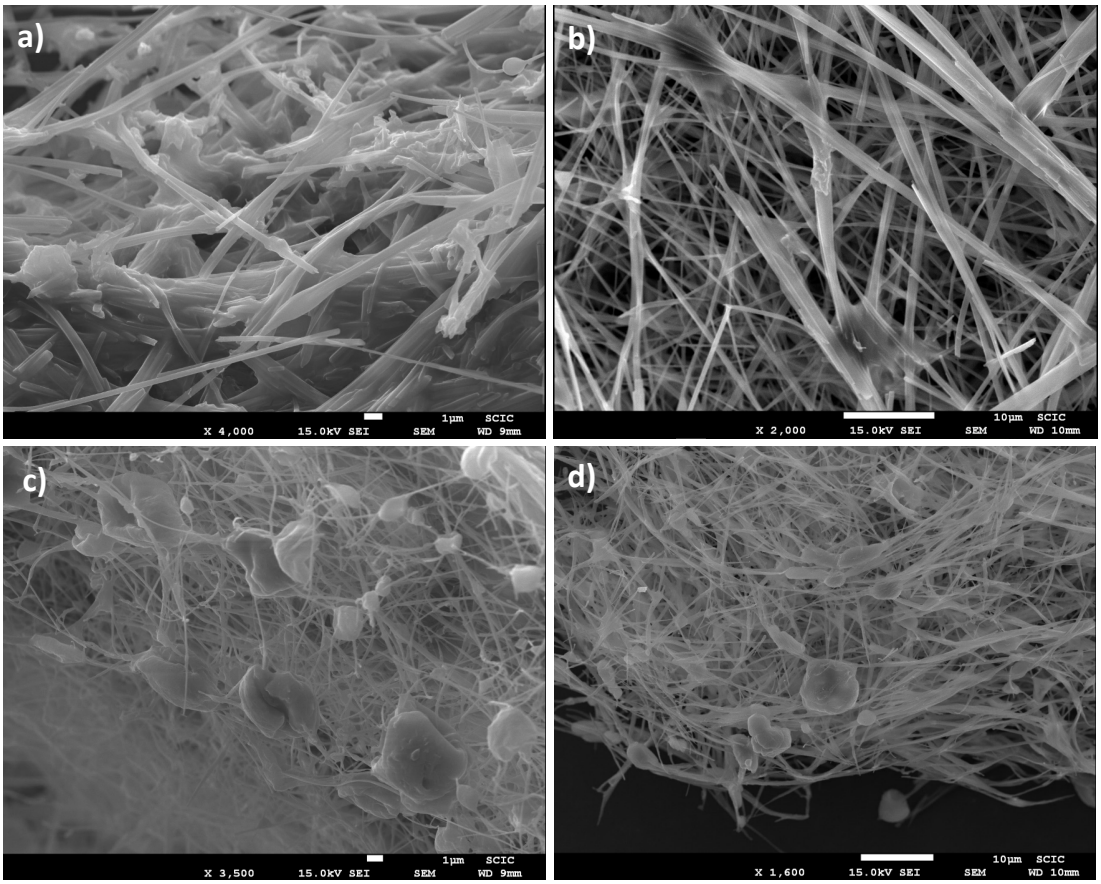

Figure 38 SEM images of the gels before and after syneresis. a) FF gel before syneresis; b) FF gel after syneresis; c) FF-NH_2 gel before syneresis; d) FF-NH_2 gel after syneresis. For both FF and FF-NH_2 gels, the morphology of the fibrous network does not change upon syneresis.

Diphenylalanine has been previously reported to self-assemble into nanofibrils in organic solvents,[184, 185] but to our knowledge this is the first report of diphenylalanine self-assembly into nanofibers in predominantly aqueous environment. The SEM pictures of both FF-NH_2 and FF confirmed the presence of an extended network of fibres and tubes (Fig. 38). As a control, the dipeptide phenylalanine-tyrosine (FY) did not form any observable aggregate or gel upon sonication demonstrating that the FF sequence is critical to the observed behaviour. TEM images of the reference sample FY showed that this dipeptide forms spherical aggregates and that the structure of the aggregates is not altered upon sonication (Fig. 39).

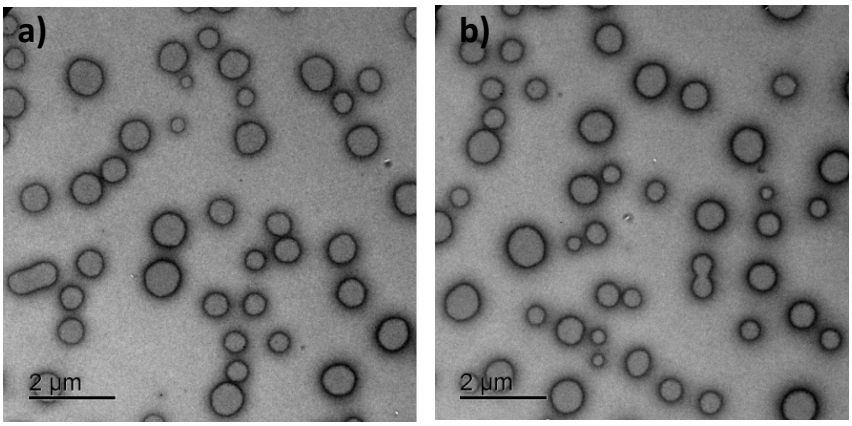

Figure 39 TEM images of the reference dipeptide FY before (a) and after (sonication). Sonication does not affect the molecular organisation of this sample as opposed to the effect on the dipeptides FF and FF-NH_2.

Gazit *et al.* hypothesised that FF molecules dissolved in HFIP arrange in a 2D extended β-sheet which with time should close along an axis to give a stable nanotubular structure.[205] However, upon sonication, the transition of dissolved dipeptide molecules from HFIP to buffer may induce rapid change in solubility assisting the formation of several nucleation sites. This could favour the supramolecular organisation of the FF molecules in kinetically trapped nanofibers, possibly preventing the extended 2D β-sheets (and subsequent larger tubes) to form. To investigate this, the gels formed upon sonication of the dipeptide solutions were taken through several heat/cool cycles in order to unlock kinetic aggregates. In the TEM images of the heated/cooled samples (Fig. 40) the only morphology observed is the nanotubes, confirming that this is the most stable form of aggregation and that the nanofibrous gels represent a metastable, kinetic trapped state.

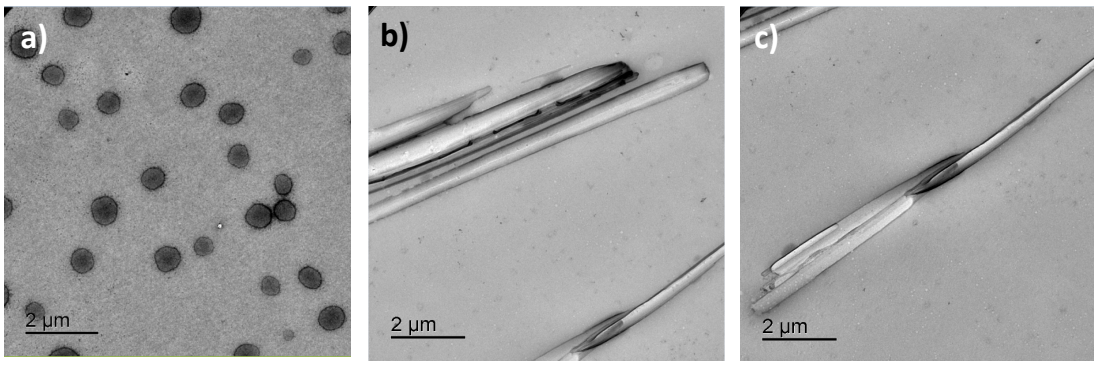

Figure 40 TEM images of FY (a), FF (b) and FF-NH_2 (c) after several heat/cool cycles. Upon annealing both FF and FF-NH_2 samples show exclusively the presence of tubular structures, confirming that this is the most thermodynamically stable state, whereas the reference sample FY is not affected by the heat/cool process.

Dynamic frequency sweep experiments were carried out to assess the mechanical properties of the collapsed material. For both FF and FF-NH_2 the rheology revealed a gel-like behaviour, providing an elastic modulus G' of 1.78 kPa for FF and 30.1 kPa for FF-NH_2 (Fig. 41) which is in the range of values previously reported for other peptide-based hydrogels.[206]

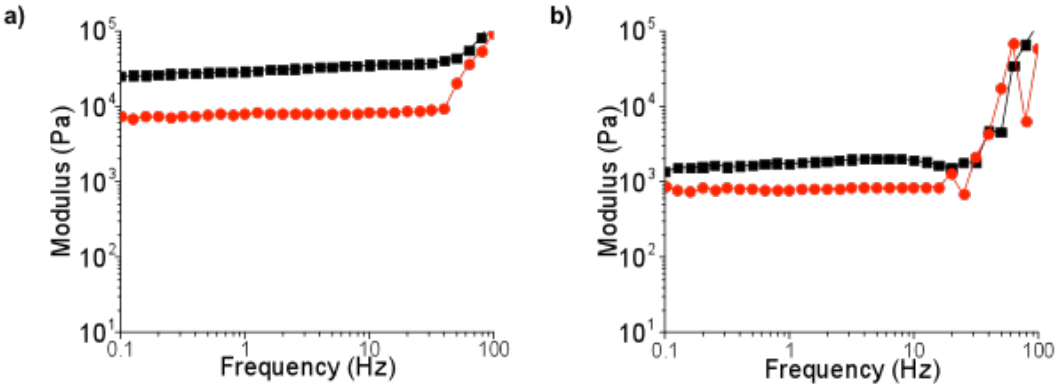

Figure 41 Linear viscoelastic diagrams of FF-NH_2 (a) and FF (b) gels. For both sample the storage modulus G' (black line) is greater than the loss modulus G" (red line), indicating a gel like-behaviour.

Fourier transform infrared (FTIR) spectroscopy is a valuable tool to analyse the secondary structure content of proteins, specifically in the amide I region (1600-1700 cm^{-1}). The enhancement of the signal in this region of the spectra is due to coupling of hydrogen bonds between amide groups. The absorption associated with the amide I band for protein solution is typically observed around 1650-1655 cm^{-1}.[173] In β-sheet-based supramolecular structures the presence of hydrogen bonds between the amide groups causes this band to shift towards lower frequencies. In the FTIR spectrum of FF-NH_2 gel (Fig. 42) the presence of a dominant absorption peak at 1625 cm^{-1} confirms a β-sheet-like arrangement of the amide groups.[173] The absorption around 1650 cm^{-1} is normally associated with a "random coil" conformation in proteins. For short peptides, this peak can be assigned to imperfect stacking of amide groups.[173, 207] The peak around 1585 cm^{-1} can be assigned to the free amine group at the N-terminus. A shoulder is visible around 1610 cm^{-1}, which could correspond to the peak visible in the solvent spectrum or to a different amide group environment in the stack (Fig. 42a and 42b, black line). The FTIR spectrum of FF gel is quite different and shows a peak around 1570 cm^{-1} due to the free carboxylic acid group and a peak around 1670 cm^{-1} which confirms the presence of H-bonding between the dipeptide

molecules suggesting a well ordered structure.[173] For the reference sample FY, no peaks were observed in the amide region and no difference was observed between the spectra measured before and after sonication, indicating a lack of organised amide bonds (Fig. 43). The observed CD spectrum for both FF-NH_2 and FF shows a positive signal around 218 nm (Fig. 42c and 42d). This signal is also visible for the dipeptides in solution, consistent with previously reported results[178] and the intensity of the peak decreases after sonication. For FF, upon sonication an additional (negative) peak around 232 nm (Fig. 42d) indicates an additional chiral component for the stacking of the phenylalanine residues.[185, 208, 209]

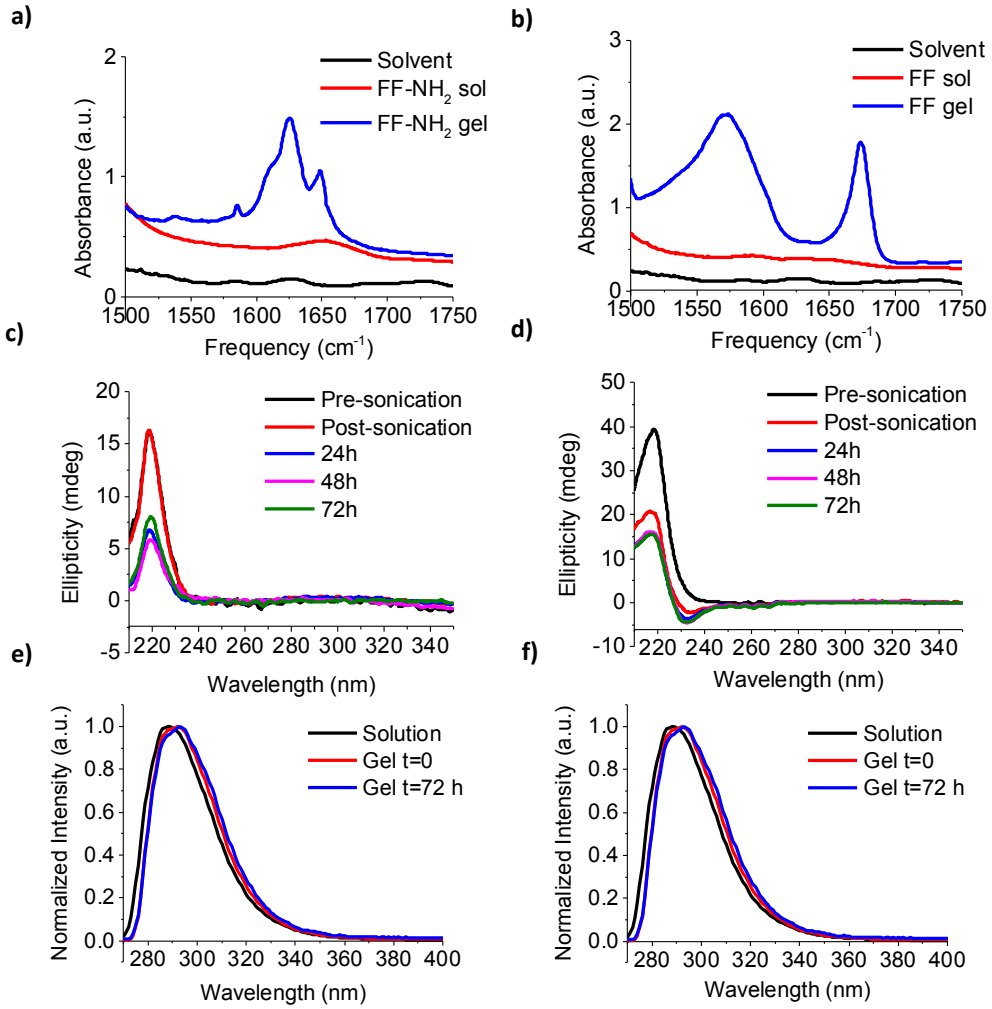

Figure 42 Spectroscopic analysis of dipeptides in solution and in gel state. FTIR spectra of FF-NH_2 (a) and FF (b). The spectra of the solvent (8% HFIP in pH8 buffer) is reported in black, the spectra of the dipeptides solution in red and the spectra of the gel upon sonication in blue. CD spectra of FF-NH_2 (c) and FF (d). The spectra are recorded before sonication and after sonication at t=0, 24, 48 and 72 h. Fluorescence emission (λexcitation= 260 nm) of FF-NH_2 (e) and FF (f) solutions (black line) and gels formed upon sonication at t=0 and 72 h (red and blue lines respectively).

Fluorescence spectroscopy was used to measure the emission spectra of the dipeptides in solution and of the gels formed upon sonication. For the dipeptide solutions the emission peak of the phenyl groups is observed around 285 nm. For both FF and FF-NH_2 the fluorescence emission is red-shifted upon sonication and gel formation (~ 6 nm for FF and ~ 5 nm for FF-NH_2, Fig. 42e and 42f). This suggests a more efficient π-π stacking of the phenyl groups upon sonication as previously reported for proteins [210] and self-assembled amyloid fibres.[185, 211] The above observations suggest that sonication reorganises the molecules, giving rise to enhanced π-π stacking between the aromatic groups and the intermolecular hydrogen bonding providing the driving force to form extended supramolecular aggregates.

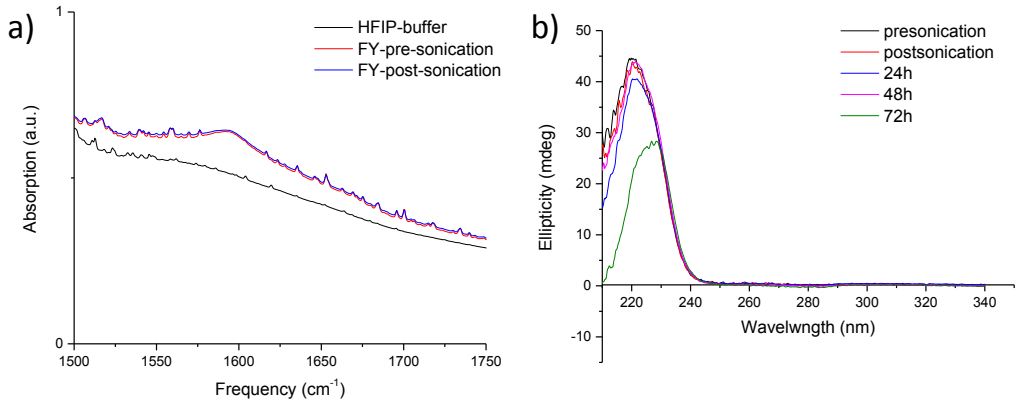

Figure 43 FTIR spectra of the reference dipeptide FY. The spectrum of the solvent (8% HFIP in pH8 buffer) is provided in black, the spectra of the FY solution before and after sonication are reported in red and blue respectively. No difference is observed in the spectrum upon sonication and no peaks associated with a H-bonded network are shown in the spectrum. CD spectra of the reference peptide FY. This molecule is chiral giving rise to a peak around 220nm but no substantial difference is observed upon sonication. After 72 h the intensity of the spectrum decreases, probably because of the formation of aggregates in the sample.

3.3. Conclusions

In summary, the formation of metastable hydrogels by the diphenylalanine dipeptide and its amidated derivative was observed. Unstable kinetically trapped hydrogels were achieved by sonication. The gels exhibit extreme syneresis upon mechanical stimulation but the collapsed structures still behave as a gel-like material. Thanks to their sensitivity to external mechanical stimuli and the rapid supramolecular collapse and the highly hydrophobic nature of the fibres formed, materials of this type might find applications as pressure

sensors or as selective scavengers for small hydrophobic molecules. Spectroscopic analysis of the dipeptide solutions and of the gels suggests that sonication induces a reorganisation of hydrogen bonding and an enhancement of π-π stacking, allowing the formation of an extended network of supramolecular aggregates.

3.4. Experimental

All reagents, including the peptides, were purchased from commercial sources (e.g. Sigma Aldrich, Bachem) at the highest purity and were used as supplied, unless stated otherwise in the experimental procedures. All solvents were used as supplied (analytical or HPLC grade) without further purification. All the experiments were performed at room temperature unless stated otherwise in the experimental procedures. Room temperature in the laboratory may have varied between 20 and 25 °C.

3.4.1. Preparation of the Samples

The samples were prepared by dissolving 5mg of dipeptide (FF-NH_2, FF-OH or FY-OH) into 80 µl of HFIP and then adding 920 µl of sodium phosphate buffer (pH ranging from 5 to 9). The samples were briefly vortexed and then sonicated several times for 10 s (VWR ultrasonic cleaner, 45 Hz). To prepare the free-standing gels, the peptide solutions were transferred into a 8-well chamber slide (Lab Tek) prior to sonication. The chamber slides were wrapped in Parafilm ® to avoid water infiltration into the wells during sonication.

3.4.2. Transmission Electron Microscopy (TEM)

Gels were prepared according to the procedure described in section 3.4.1 and left overnight. TEM images were captured using a FEI Tecnai T20 transmission electron microscope operating at 200 kV. Carbon-coated copper grids (200 mesh) were glow discharged in air for 30 s. The support film was touched onto the gel surface for 3 s and blotted down using filter paper. Negative stain (20 µL, 1 % aq. Methylamine vanadate obtained from Nanovan, Nanoprobes) was applied and the mixture blotted again with filter paper to remove excess. Each sample was allowed to dry afterwards for 2-3 minutes in a dust-free environment prior to TEM imaging. The dried grids with the samples were then imaged and the images were saved using Gatan Digital Micrograph software.

3.4.3. Scanning Electron Microscopy (SEM)

Gels were prepared according to the procedure described in section 3.4.1 and left overnight. The samples were freeze dried before (Fig. 38 a and c) or after syneresis (Fig. 38 b and d) and placed on top of an aluminium specimen mount stub and sputtered with Pt

before imaging. The samples were imaged with a JEOL 7001F microscope equipped with a digital camera.

3.4.4. UV-Vis Absorption Spectroscopy

UV-Vis absorption spectra were recorded in Jasco V-660 spectrophotometer. Samples for the measurement were prepared in PMMA UV-grade cuvettes (Fisher Scientific). The spectra were measured with a bandwidth of 5 nm, with a medium response and a scan speed of 40 nm/min

3.4.5. Infrared Spectroscopy (IR)

The gels were prepared according to the procedure described in section 3.4.1, but using deuterated buffers and left overnight. Samples were transferred in a standard IR transmission cell (Harrick Scientific) between two 2 mm CaF_2 windows, separated by a polytetrafluoroethylene (PFTE) spacer of 50 µm thickness. Spectra were recorded on a Bruker Vertex 70 spectrometer by averaging 25 scans at a spectral resolution of 1 cm^{-1}. Spectra were corrected for absorption from the buffer with a blank sample 8% HFIP in phosphate buffer.

3.4.6. Circular Dichroism (CD)

Samples were monitored by CD spectroscopy on a Jasco J-810 spectrometer equipped with a temperature control; spectra were recorded at 25 °C. Samples were prepared dissolving 1.25 mg of FF-NH_2 or 2.5 mg of FF in 80 µl of HFIP and then adding 920 µl of buffer. The samples were vortexed and sonicated and immediately loaded into a 0.2 mm quartz cover slip cuvette before gelation occurred. The spectra were measured at 50 $nmmin^{-1}$ with a 0.5 nm step size and a 1.0 nm bandwidth, between 200 and 350 nm. The measurements were repeated after 24, 48 and 72 h.

3.4.7. Rheology

Dynamic frequency sweep experiments were carried out on a strain-controlled rheometer (Kinexus rotational rheometer from Malvern) using a parallel-plate geometry (20 mm) with a 1 mm gap. An integrated temperature controller was used to maintain the temperature

of the sample stage at 25°C. To ensure the measurements were made in the linear viscoelastic regime, an amplitude sweep was performed and the results showed no variation in elastic modulus (G') and viscous modulus (G") up to a strain of 0.06%. The gels were prepared according to the procedure previously described. The dynamic modulus of the gels was measured as a frequency function, where the frequency sweeps were carried out between 1 and 100 Hz. The measurements were repeated at least three times to ensure reproducibility.

3.4.8. Fluorescence

PMMA UV grade cells with a path length of 10 mm were used for the study. Fluorescence emission spectra were measured on a Jasco FP-6500 spectrofluorimeter with light measured orthogonally to the excitation light, at a scanning speed of 500 nm min^{-1}. The excitation wavelength was 255 nm, and the spectra were measured between 265 and 500nm, with a bandwidth of 5 nm, a medium sensitivity and 0.5 nm data pitch.

3.4.9. ANS Binding

8-Anilino-1-naphthalenesulfonic acid (ANS) (Sigma Aldrich, UK) was dissolved in pH 8 100 mM sodium phosphate buffer to a final concentration of 100 μM. 2.5 mg of the dipeptides FF or FF-NH_2 were dissolved in 80 μl of HFIP and then diluited up to 1 ml with the ASN buffered solution. Two set of samples were prepared. The first set was not sonicated. The second set was sonicated inducing the gelation of the samples. Fluorescence emission was measured for all the samples as prepared and then after 24, 48 and 72 h. Fluorescence was monitored for the ANS buffered solution as well. Fluorescence emission spectra were measured on a Jasco FP-6500 spectrofluorimeter with light measured orthogonally to the excitation light, at a scanning speed of 500 nm min^{-1}. The excitation wavelength was 365 nm, and the spectra were measured between 400 and 700 nm, with a bandwidth of 5 nm, a low sensitivity and 0.5 nm data pitch.

3.4.10. Thioflavin T (ThT) retention in the gels

UV-Vis spectroscopy was employed to monitor the release/ retention of ThT by the gels upon syneresis. Reference solutions at different ThT concentration were prepared dissolving ThT in pH8 100 mM sodium phosphate buffer. The UV-Vis absorption of the ThT

buffered solutions was measured for ThT concentrations ranging between 10^{-3} and 10^{-5} M (lowest detectable concentration with the instrument). The dipeptide gels containing ThT were formed dissolving 5 mg of FF or FF-NH_2 in 80 µl of HFIP and then diluiting up to 1 ml with the buffered ThT solution 10^{-3} M. The samples were vortexed and sonicated and syneresis of the gels was triggered by mechanical compression of the gels. The exuded liquid was collected and the UV-Vis absorption was measured. No absorbance peak was detected for the liquids exuded both from FF and FF-NH_2 gels, indicating that the exuded liquids contain less than 10^{-5} M ThT. More than 99% of the fluorophore is hence retained in the collapsed gel. The absorption of the collapsed gel or of the gel before syneresis cannot be evaluated since absorbance values increase significantly upon ThT interaction with the fibres overcoming the saturation limit of the instrument.

4. Biocatalytic Self-Assembly Using Reversible and Irreversible Enzyme Immobilisation *

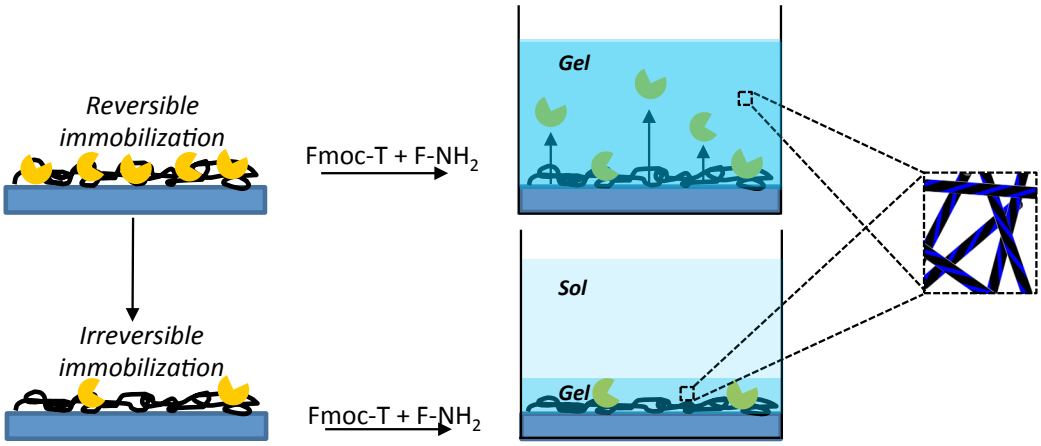

* The work in this Chapter has been published, in part, to Applied Materials and Interfaces.[212]

Declaration of contribution to published article:

Any reproduced work from the aforementioned published article, including the written article itself, I was solely responsible for, together with the other authors of the article, unless otherwise stated.

4.1. Introduction

As previously mentioned in Chapter 2, biocatalytic control of molecular self-assembly provides an effective approach for developing smart biomaterials. A number of enzymes have been utilised in this context, including phosphatases, esterases and proteases.[61, 72, 213] These catalysts are typically dissolved and mixed with self-assembly precursors to enable structure formation over time. The action of surface immobilised enzymes has also been explored. Williams *et al.* first reported on the immobilisation (using glutaraldehyde) of thermolysin on an amine functionalised glass surface to enable self-assembly of Fmoc-protected peptides on a surface.[79] This was subsequently followed by the use of a polydopamine coating for enzyme immobilisation, which resulted in the formation of a bulk gel in the container that the surface was immersed in.[214] More recently, Vigier-Carriere *et al.* employed alkaline phosphatase non-covalently immobilised in a polyelectrolyte multilayer to trigger the self-assembly and gelation of a Fmoc-protected tripeptide.[215]

Xu and co-workers exploited endogenously expressed enzymes that are either localised at cell surfaces or in specific subcellular spaces. Depending on the location of the enzymes overexpressed in disease-causing cells, self-assembly and gelation of peptide derivatives could be triggered in the intracellular or pericellular space, subsequently inducing cell apoptosis.[96, 98] In a similar approach, Pires *et al.* employed cell surface bound alkaline phosphatase (ALP) to convert a simple carbohydrate derivative into a hydrogelator that assembles into a localised nanofibrous mesh around the cells. In this work, it was found that cell surface bound network formation and consequent apoptosis is induced only by membrane-bound, and not secreted, ALP[216] , suggesting that the location of the enzyme has a substantial impact on the assembly process. In a recent paper, Xu *at al*. also exploited localised endogenous ALP activity on a peptide derivative that self-assembles upon de-phosphorylation and generates fluorescence, allowing profiling of ALP activity in live cells.[217] Locally secreted endogenous enzymes (matrix metalloproteases, MMPs) can trigger the reconfiguration of peptide micelles loaded with doxorubicin to localise formation of fibrous structure and confine the release of the drug payload at the site of enzyme overexpression, providing a means to achieving site-specific anti-tumoral therapies.[218]

Clearly, there are a number of examples of biocatalytic self-assembly where enzymes are variously exploited as freely dissolved, compartmentalised, or surface-attached species. In

particular, the aforementioned examples in biologically interfacing systems and in nanofabrication highlight the potential of using localised bio-catalytic self-assembly to enable complex (biological) function, by generating specific structural configurations through spatially selective nucleation and structure growth. Therefore, there is scope for further investigating the strategy of enzyme immobilisation for achieving spatially selective self-assembly. In this Chapter, a simple procedure to control the "reversibility" of enzyme immobilisation and hence control the level of spatial localisation of the self-assembly process is described.

4.2. Results and Discussion

Polydopamine and the novel polyphenol coatings were identified as constituting a mild and versatile aqueous approach to surface immobilisation that may be applied across diverse materials with minimal modification to the processing protocols.[115, 219, 220] While polydopamine coatings have been widely used to immobilise various proteins,[219] herein the first demonstration of immobilising enzymes using a polyphenol coating is reported. Dopamine (Fig. 44) spontaneously polymerises in aqueous solutions under mildly oxidising conditions to form thin polymeric films that are able to adhere to many types of surfaces without surface preparation and on substrates with complex geometries. The catechol (dihydroxyphenyl) groups of the polydopamine film confer a latent activity towards nucleophiles, that can be exploited for the conjugation of amine-containing biomolecules.[117, 221, 222] Recently the Messersmith group investigated a similar approach using plant polyphenols for the deposition of thin surface coatings on a variety of substrates.[220] Polyphenols are a large family of compounds that include epicatechin gallate (ECG), epigallocatechin (EGC), and tannic acid (TA), and the range of potential coating precursors holds promise for an expansive range of properties. In contrast to polydopamine, polyphenol coatings may be deposited at and around neutral pH and have good transparency at visible wavelengths. The constituent phenolic units, including catechol and trihydroxyphenyl (galloyl) groups, are proposed to participate in reactions similar to those contributing to polydopamine formation, and should allow for the conjugation of biomolecules on polyphenol coated surfaces.[223] For this study, three different building blocks have been investigated to compare the efficacy of using

polydopamine and polyphenol coatings for enzyme immobilisation: dopamine (**4**), pyrogallol (**5**) and tannic acid (**6**) (Fig. 44).

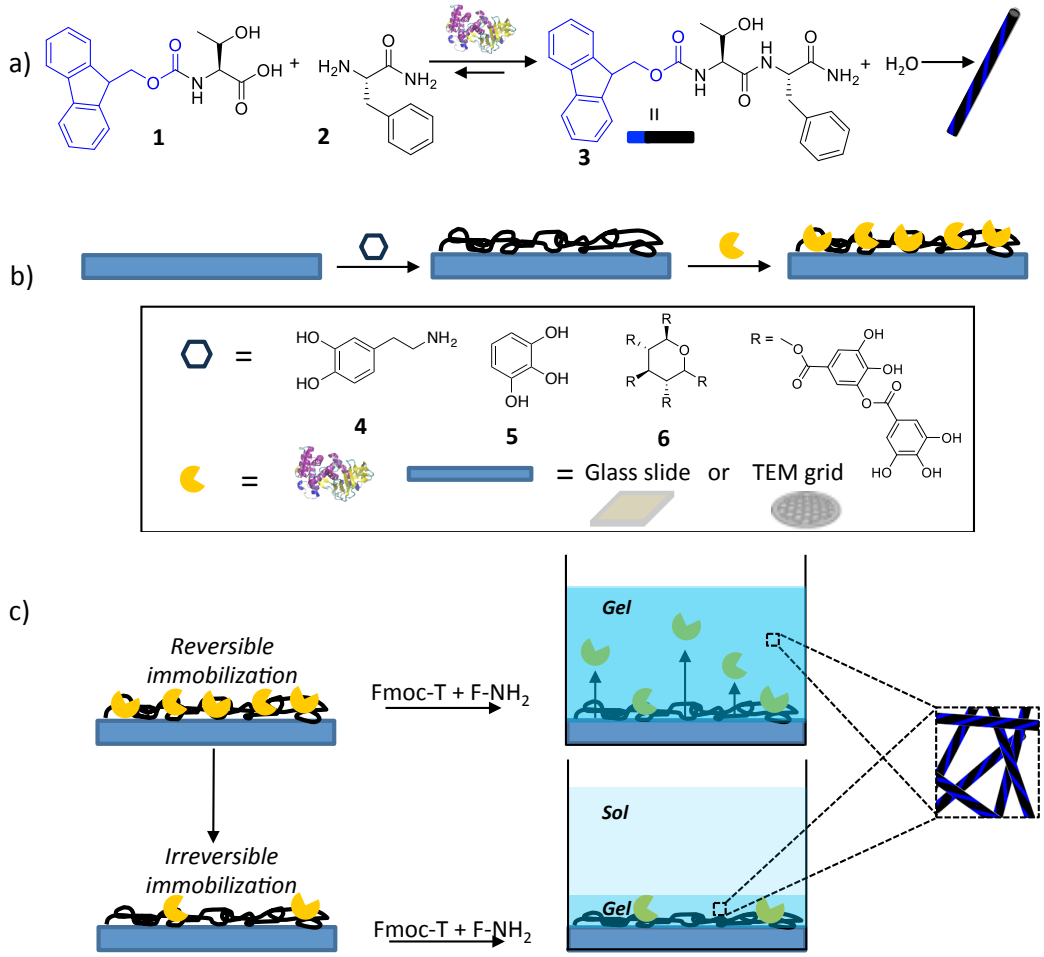

Figure 44 (a) Conversion of the pre-gelators Fmoc-T (1) and F-NH_2 (2) into the gelator Fmoc-TF-NH_2 (3) catalysed by thermolysin. (b) Surface modification with polydopamine or polyphenols and subsequent enzyme immobilisation (In the box: structure of dopamine (4), pyrogallol (5) and tannic acid (6) and the structure of thermolysin). The number of galloyl moieties per tannic acid can range from 2 to 12 depending on the plant source. We show penta-m-digalloyl-glucose from oak gall nuts. (c) Reversible and irreversible enzyme immobilisation on modified surfaces for bio-catalytic self-assembly. The enzymes reversibly bound to the surface catalyse the coupling of the pre-gelators Fmoc-T (1) and F-NH_2 (2) and the formation of a bulk gel. The enzymes irreversibly bound to the surface retain activity after the additional washing procedure and are able to catalyse the conversion of the pre-gelators only at the surface and enable subsequent localised self-assembly of the gelator Fmoc-TF-NH_2 into nanofibers.

To demonstrate that the findings translate across different surface types, and to facilitate the characterization of nanofiber self-assembly, glass cover slips and TEM carbon-coated copper grids were chosen as the support materials. The polydopamine and polyphenol coatings were deposited by simple immersion of the solid supports into a precursor solution for 2 h at room temperature (see section 4.4.1). The modified solid supports were subsequently dipped in a 1 mg/mL thermolysin solution overnight to allow for enzyme immobilisation.

The solid supports with immobilised thermolysin were used to control the location of the self-assembly of peptide amphiphiles. The modified amino acids Fmoc-T (**1**) and F-NH_2 (**2**) were employed as non-assembling precursors, which couple to form the gelator Fmoc-TF-NH_2 (**3**) upon thermolysin action (Fig. 44a). Fmoc-TF-NH_2 forms in high yield and self-assembles into fibrous structures, which in turn entangle to form supramolecular hydrogels.[224, 225]

After thermolysin immobilisation, the solid supports were treated using two different rinsing procedures (a milder or a more thorough wash, see section 4.4.2 and 4.4.4) and subsequently immersed in the pre-gelator solution.

Macroscopically different results were observed depending on the surface rinsing. When the surfaces were treated with the milder wash, all three immobilising agents were effective in producing enzyme functionalised surfaces that catalysed the condensation of the pre-gelators and subsequent gelation in the bulk phase, as demonstrated by standard tube inversion test and by reversed-phase HPLC analysis[226] (Fig. 45). Similar results were obtained whether glass cover slips or TEM grids were used as the solid support (see Fig. 46).

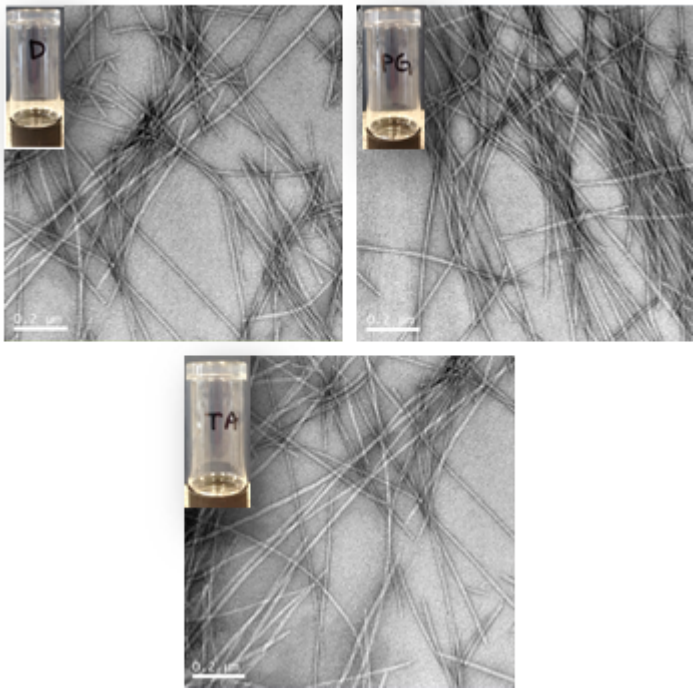

Figure 45 TEM images of the fibre network in the gels formed following the enzyme release from the surface coatings on glass cover slips. Surfaces produced by all three immobilising agents (dopamine, pyrogallol and tannic acid) were effective in catalysing condensation and gelation of the pre-gelator solution.

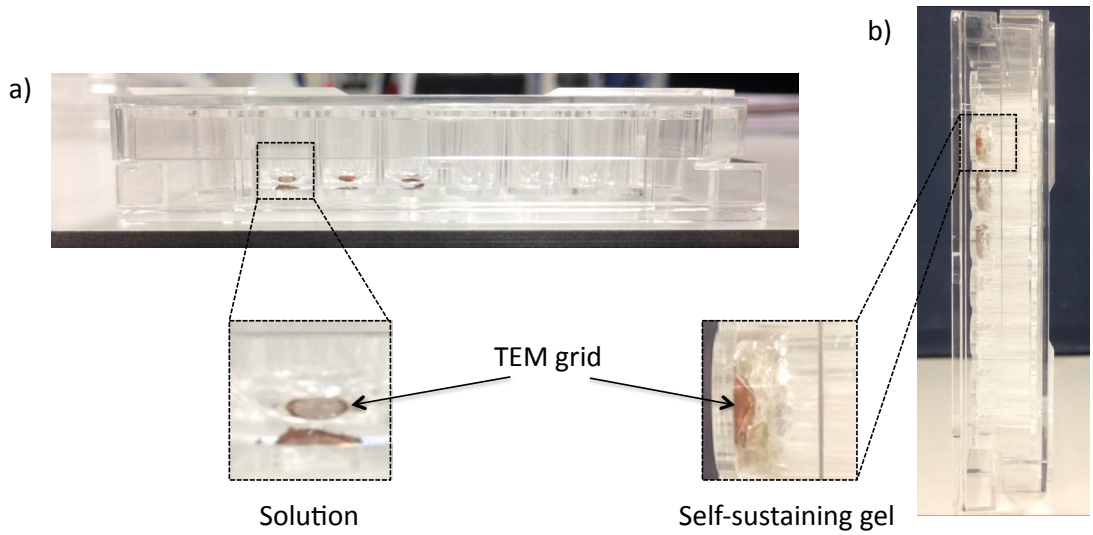

Figure 46 a) TEM grids modified with polydopamine, pyrogallol and tannic acid (from left to right). The modified TEM grids were placed in the wells of a 96 cell culture well plate and dipped in a solution of the pre-gelators Fmoc-T and FNH_2. After 4 days, gelation occurred (b).

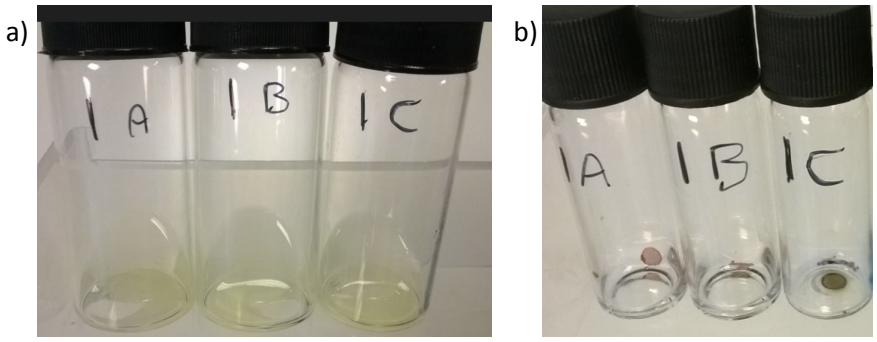

Figure 47 a) Glass coverslips coated with polydopamine, tannic acid and pyrogallol (from left to right) and immersed in a solution containing the pregelators (FmocT and FNH_2). b) TEM grids coated with polydopamine, tannic acid and pyrogallol (from left to right) and immersed in a solution containing the pregelators (FmocT and FNH_2). In both cases the surfaces where exposed to the solution for several weeks and no gelation was observed. The photos shown were taken after approximately one month of exposure.

Bulk gelation was observed within 3 to 4 days for all samples and HPLC analysis showed that the yield of pre-gelator conversion into the assembling species after gelation was similar in each case (~30%). In comparison, thermolysin dissolved in a bulk pre-gelator solution at a (typically high) concentration of 1 mg/mL catalyses gelation faster, reaching ~80% conversion after 4 h.[224, 225] It is likely that the longer gelation times and the lower conversion obtained from the immobilised enzyme are due to the lower overall amount of

enzymes available (see enzyme assay below). The similar yields of conversion obtained when using glass cover slips or TEM grids suggest that the total amount of immobilised enzymes may be similar for the two supports.

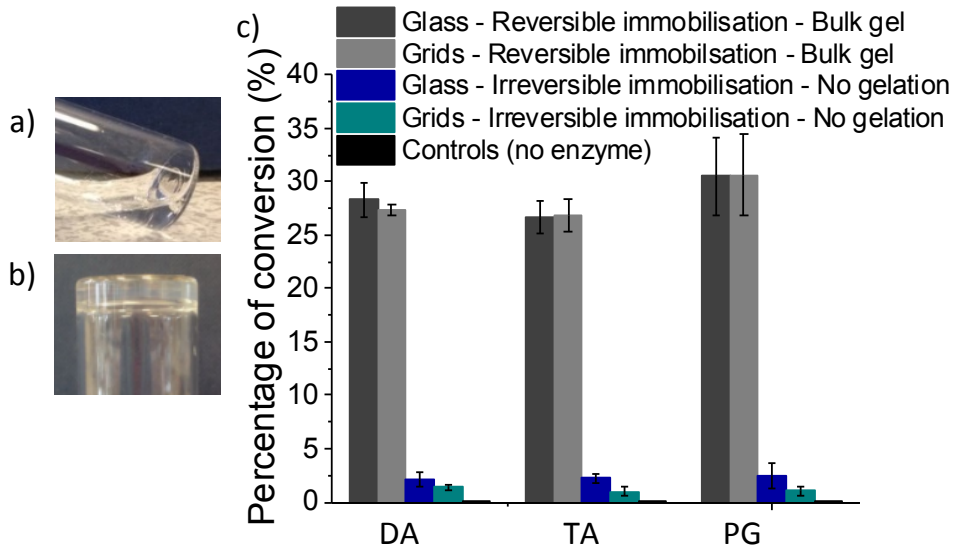

Figure 48 a) A glass cover slip with immobilised thermolysin is placed in a vial (immobilised enzyme side up) and dipped in a solution of pre-gelators. b) Formation of a hydrogel on top of the slide with the immobilised enzyme. c) Conversion values obtained through HPLC analysis of the gels formed on top of both the modified glass cover slips and TEM grids after 4 days indicates the conversion of the pre-gelators 1 and 2 to 3. Using a mild rinsing procedure, bulk gelation was observed on samples functionalised with all three immobilising agents (4, 5 and 6). When a more thorough wash was employed, bulk gelation was not observed and less than 3% conversion of the gel precursors was detected in the supernatant for all samples.

In contrast to these results, when the surfaces with the immobilised enzymes were treated with further rinsing before reaction with the pre-gelators, no bulk gelation was observed (see FRET assay below). HPLC analysis of the supernatant confirmed that less than 3% of the amino acid precursors were converted within the bulk liquid phase (Figures 48 and 49).

Similar results were obtained when the surface modification and enzyme immobilisation were performed directly on TEM grids.

These results indicated that depending on the surface treatment upon enzyme immobilisation two different results could be achieved: a semi-reversible enzyme immobilisation (which triggers the bulk gelation of the pre-gelators when enzymes desorb

from the surface), or irreversible enzyme immobilisation where no bulk gelation was observed. We were therefore interested in probing the enzyme release from the polymeric surface coatings and further investigating the surface effects in the case of irreversibly immobilised enzymes.

A Förster resonance energy transfer (FRET) fluorescence assay was employed to sensitively and directly probe the proteolytic activity of thermolysin during sequential washing steps.

The custom-made peptide E(EDANS)-GT↓LGK(DABCYL) was employed as the enzyme substrate. Fluorescence of the EDANS donor at the N-terminus is initially quenched via FRET by the DABCYL acceptor at the C-terminus. EDANS fluorescence is restored upon enzymatic cleavage at the T↓L position of the peptide to separate EDANS from the DABCYL acceptor. Proteolytic activity can hence be monitored by recording the fluorescence intensity *vs* time (measurement at the EDANS maximum emission wavelength: 510 nm).[227]

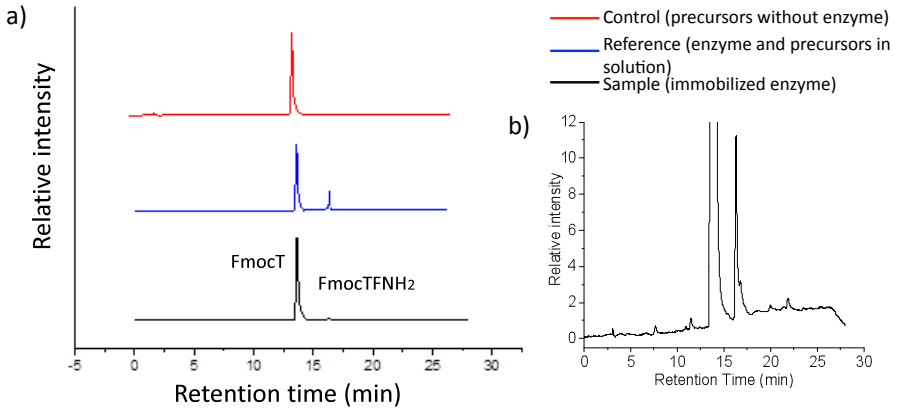

Figure 49 HPLC chromatograms. a) The presence of a peak corresponding to Fmoc-TF-NH_2 (black line) confirms the conversion of the precursors Fmoc-T and F-NH_2, catalysed by immobilized thermolysin. The chromatogram of a reference sample is reported to show the position of the peaks (blue line). b) Magnified view of the HPLC trace of the sample (black line) to better show the peak corresponding to the formation of FmocTF-NH_2.

After enzyme immobilisation, the routine "milder" wash mentioned above was initially applied, in which the solid supports were individually rinsed three times in ultrapure water. The samples were then immersed in 100 mM pH 8 phosphate buffer and placed on an orbital shaker for 30 min to aid the solubilisation of any physically adsorbed enzyme. This procedure was repeated until no activity was observed in the wash solution. Figure 50 shows that the first additional buffer immersion was able to release a significant amount of

enzymes from the functionalised surface, while only a very small amount of enzymes was released in a second immersion. The solution from the first immersion produced a rapid increase in fluorescence before reaching a plateau after 20 min, indicating the presence of desorbed enzymes that were able to convert of all the substrate present within 15 min. Similar results were obtained for the surfaces modified with tannic acid and pyrogallol (Fig. 51). Quantitative analysis of the fluorescence kinetics shows a thermolysin concentration of 8.3 x 10^{-3} mg/ml (see Fig. 52). In contrast, the solution obtained after the second buffer immersion was able to produce only a negligible increase in the fluorescence signal that was detected only when the emission data was recorded overnight (Fig. 50b), corresponding to a thermolysin concentration of 6.6 x 10^{-7} mg/ml, 4 orders of magnitude lower than in the first immersion/wash solution. The control (substrate solution without addition of any wash solution or solid sample) showed no activity overnight.

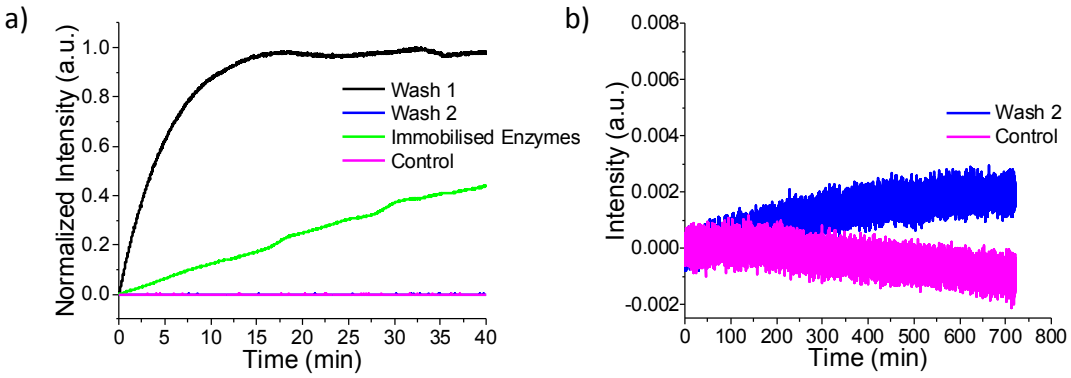

Figure 50 a) FRET assay to detect thermolysin activity in the wash solution and for the enzyme immobilised on the surface of a glass cover slip modified with polydopamine. In the first wash solution (black) the fluorescence intensity rapidly increased over time, reaching a plateau when the enzyme had converted all the substrate. In the second wash solution (blue), the recorded data did not show any significant change in the fluorescence intensity overnight. The "glass surface" data shows the fluorescence detected when a sample subjected to the two washes was placed in a FRET substrate solution, thus measuring the irreversibly immobilised enzyme activity (green). The control samples (magenta) include the FRET substrate in the absence of enzyme. b) Magnified view of the second wash and control data.

The FRET assay was also performed on the functionalised glass cover slip that had been subjected to the two stages of buffer immersion, by placing the glass sample directly in the fluorescence measurement chamber filled with a solution containing the substrate (see section 4.4.7.2). In contrast to the wash solutions and the control, a steady increase in fluorescence was observed (Fig. 50a: "glass surface" data). This indicates that enzymes must be immobilised on the functionalised glass surface after the various washing steps, and the converted EDANS enzyme product could diffuse from the surface into the bulk solution to be detected.

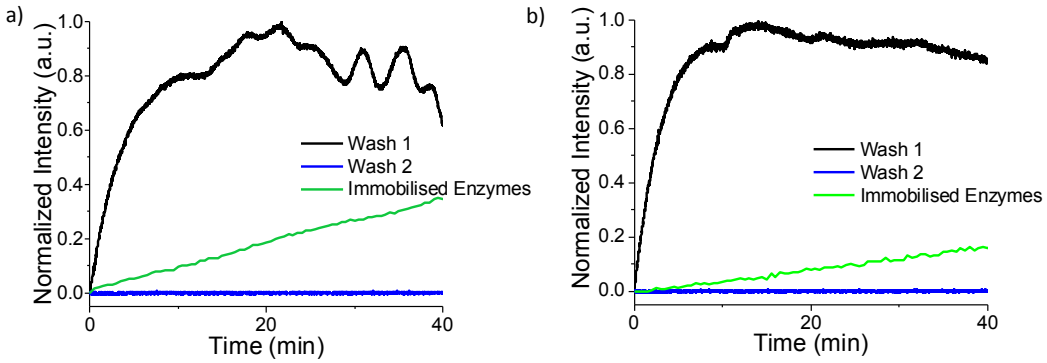

Figure 51 FRET assay to detect thermolysin activity in the wash solution and for the enzyme immobilized on the surface of a glass cover slip modified with tannic acid (a) and pyrogallol (b). In the first wash solution (black) the fluorescence intensity rapidly increased over time, reaching a plateau when the enzyme had converted all the substrate. In the second wash solution (blue), the recorded data did not show any significant change in the fluorescence intensity overnight. The "glass surface" data shows the fluorescence detected when a sample subjected to the more thorough procedure (i.e. after Wash 2) was placed in a FRET substrate solution, thus measuring the irreversibly immobilized enzyme activity (green).

Overall, the FRET experiment showed that there were two initial populations of enzymes on the functionalised surface after the "milder" routine rinse - reversibly and irreversibly attached - that could be differentiated simply using the additional buffer immersion procedure. These results are also in agreement with our hypothesis that the formation of a bulk hydrogel is due to the reversibly-bound enzymes released from the polyphenol/polydopamine coatings. It is assumed that the enzymes detected in the wash solutions were initially physisorbed on the surface. The majority of these reversibly attached enzymes could be desorbed during the first 30 min wash and in the second wash

only a negligible amount of enzyme was released from the surface. After this 2-step washing/immersion procedure, a significant amount of irreversibly immobilised enzymes remained on the surface. The fluorescence kinetics show substantial surface activity equivalent to what would be observed for a dissolved enzyme concentration of 2.7 x 10^{-5} mg/ml. Given a spectrometer cuvette volume of 1 mL and a sample surface area of 0.66 cm^2, the measured activity indicates an active immobilised thermolysin surface concentration of 40 ng/cm^2. In comparison, a monolayer of thermolysin corresponds to 98 ng/cm^2 (Fig. 53).

a)

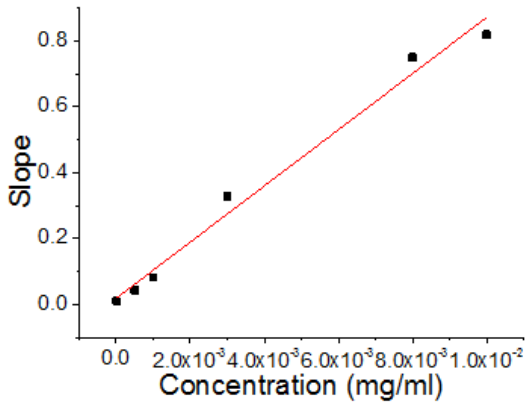

b)

$$y = mx + q$$
$$m = 85.2334$$
$$q = 0.01884$$

c)

	Slope (y)	Concentration (x) (µg/ml)
Wash1	0.72212	8.25
Wash2	0.0189	$6.57*10^{-4}$

Figure 52 a) Calibration curve for the calculation of the enzyme concentration in wash solutions. b) Linear equation of the calibration curve. c) Calculated values of the enzyme concentration in the wash solutions.

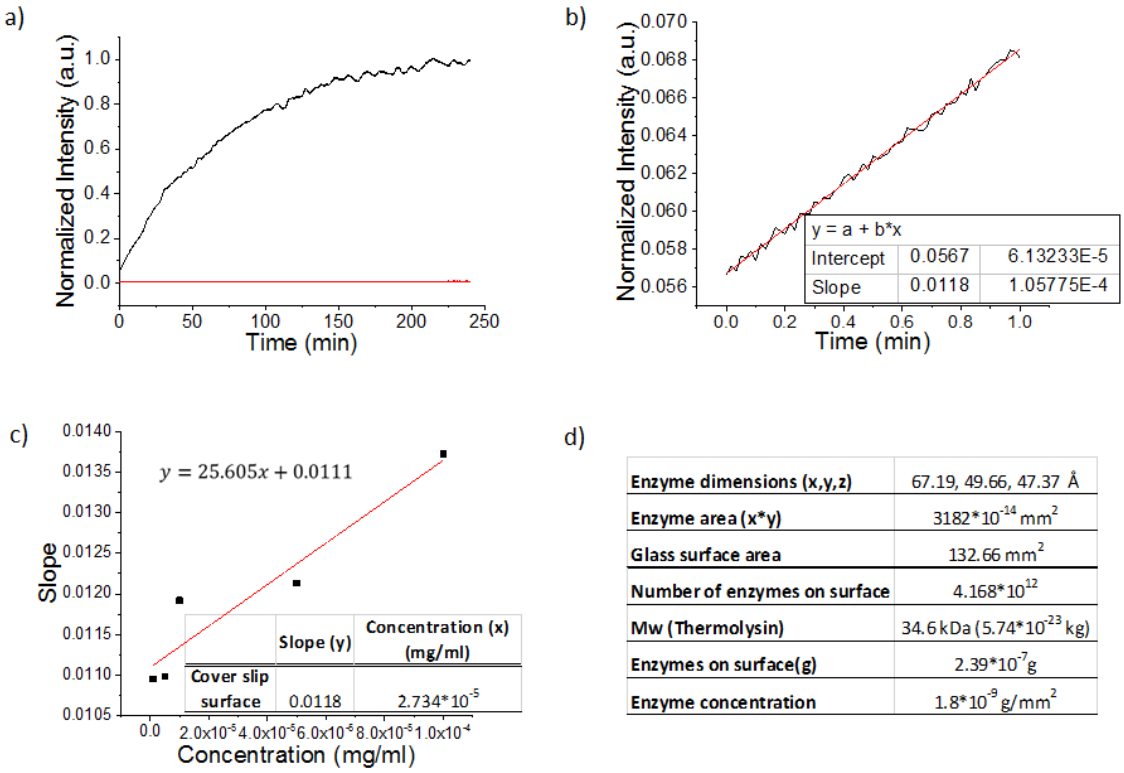

Figure 53 (a) Time course measurement of the fluorescent emission. The glass cover slip with the immobilised enzyme (13 mm of diameter) was cut in half to fit in the cuvette and dipped in a buffer solution containing the FRET substrate. The intensity of fluorescence was increasing over time, reaching a plateau when all the substrate molecules are converted. b) Linear fitting of the first 60 s of the time course. c) Calibration curve for the calculation of the enzyme immobilised on the surface. d) Table with the calculations of the theoretical enzyme concentration on the surface of the glass cover slip.

Taking advantage of having the enzymes immobilised on TEM grids, electron microscopy was employed to visualise the formation of any surface structures enabled by bio-catalytic self-assembly. 10 µl of Fmoc-T and F-NH_2 solution was pipetted on top of the grids and left overnight. Negative stain was applied and the samples were dried before TEM imaging. The images (Fig. 54) revealed the presence of a network of fibers on the grid surface, confirming that the immobilised enzymes were able to catalyse the conversion of the precursors into Fmoc-TF-NH_2, which then enabled their subsequent localised self-assembly into a thin mesh of nanofibrous structures. The control samples with polydopamine or polyphenol coated TEM grids exposed to the precursor solution with no enzyme immobilised on the surface did not show any nanostructure formation.

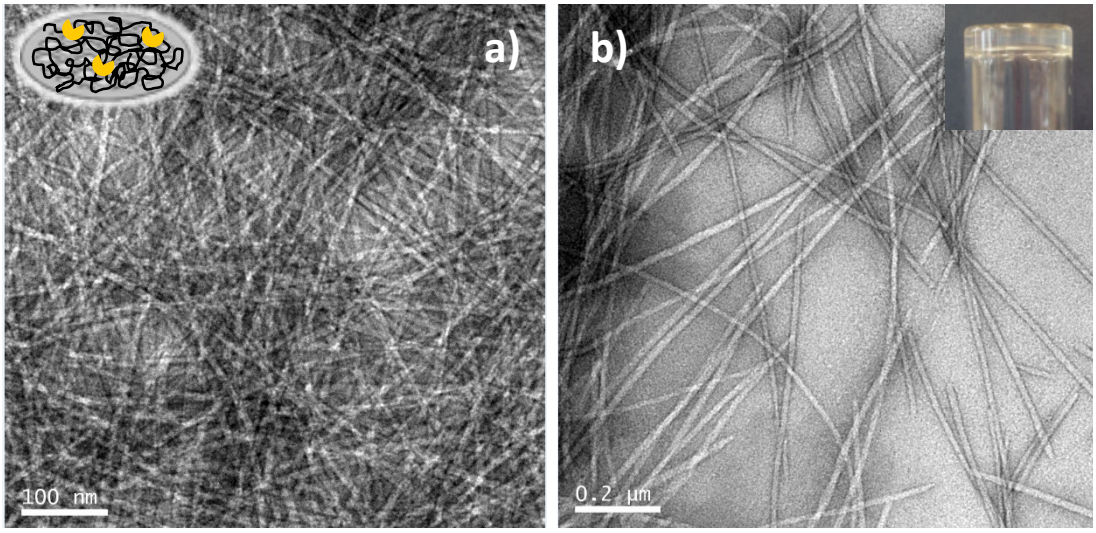

Figure 54 a) TEM images of fibers of Fmoc-TF-NH_2 grown on top of the carbon-coated copper TEM grids with immobilised thermolysin on polydopamine. b) Control: TEM image of fibers taken from a reference bulk gel formed from the same Fmoc-T and F-NH_2 pre-gelators using thermolysin dissolved in 1 mg/mL solution.

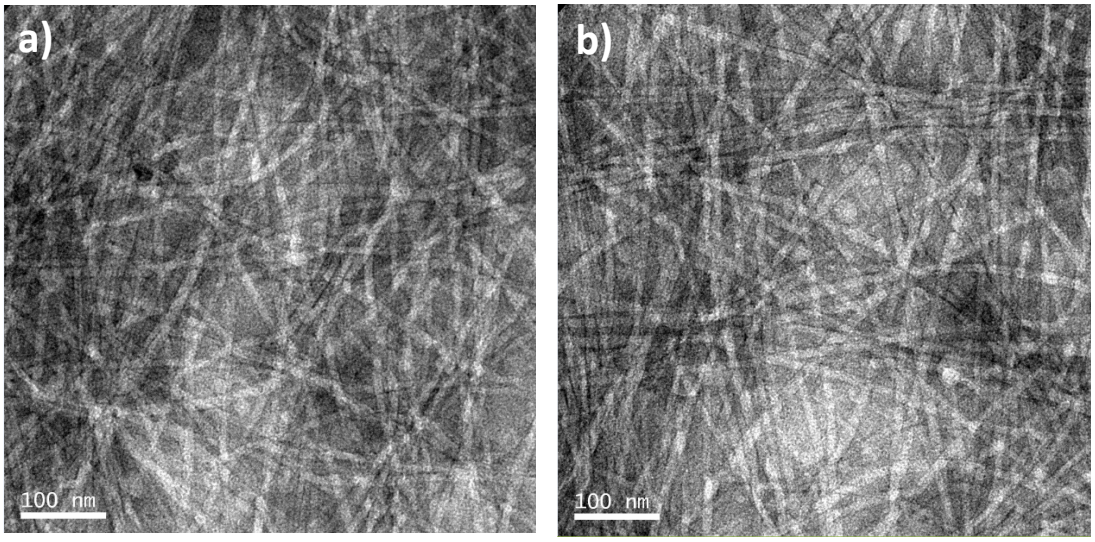

Figure 55 TEM images of fibers of Fmoc-TF-NH_2 grown on top of the carbon-coated copper TEM grids with immobilized thermolysin on tannic acid (a) and pyrogallol (b).

4.3. Conclusions

In this Chapter, novel polyphenol surface coatings for the immobilisation of thermolysin are described and are shown to be as effective as polydopamine coatings. Evidence is provided to show that surface-mediated bulk gelation is not due to enzymes immobilised on the

surface as previously suggested for a related system,[214] but is due to enzymes released into a pre-gelator solution. It was demonstrated that enzymes may be reversibly and irreversibly immobilised on a surface and that the relative amounts of these populations may be controlled by the sample surface treatment. Although protein desorption (i.e. reversible immobilisation) is a common phenomenon on the surfaces of a range of polymers, metals and metal oxides, there is no general rule on whether the conformation and activity of the released enzymes are preserved. On the other hand, common surface functionalisation techniques using silanes, thiols, or bifunctional linkers are designed to efficiently attach proteins through irreversible covalent bonds and significant desorption/release of proteins is not expected. Reactions of polydopamine and polyphenols are relatively slow,[220] allowing these coatings to be exploited for (eventual) irreversible covalent binding as well as protein release. In the system described in this Chapter, when the polyphenol/polydopamine coated samples undergo a mild washing procedure, reversibly bound thermolysin remaining on the surface can be released to catalyse the formation of the gelator Fmoc-TF-NH_2 in the solution covering the surface and enable formation of a bulk gel. When the samples undergo a more extensive washing procedure to ensure that loosely bound enzymes were removed, the remaining, irreversibly bound enzymes were still able to catalyse the conversion of the pre-gelators but only in close proximity to the surface. These results indicate that this procedure led to the immobilisation of half a monolayer of active enzymes, which enabled the localised formation of self-assembled nanofibers but no bulk gelation. This shows that enzyme (surface) localisation provides a means to achieve spatial control of self-assembly as previously demonstrated for non-enzymatic catalysts,[228] and provides opportunities for the use of biocatalytic self-assembly for the formation of patterned nanostructures.

4.4. Experimental

All reagents, including the peptides, were purchased from commercial sources (*e.g.* Sigma Aldrich, Bachem) at the highest purity and were used as supplied, unless stated otherwise in the experimental procedures. All solvents were used as supplied (analytical or HPLC grade) without further purification. All the experiments were performed at room temperature unless stated otherwise in the experimental procedures. Room temperature in the laboratory may have varied between 20 and 25 °C.

4.4.1. Polydopamine or Polyphenol Coating on Glass Cover Slips or Carbon-Coated Copper Grids

The glass cover slips were cleaned by sonication for 10 min in a surfactant solution (2% HellmanexTM, Sigma Aldrich, UK), rinsed with ultrapure water. The carbon-coated copper grids were used as provided from the supplier (Agar Scientific, UK). The solid supports were immersed in a solution of Dopamine hydrochloride (Sigma Aldrich, UK) at a concentration of 2.5 mg/ml in 10mM TRIS buffer pH 8.5. The deposition of polyphenol coatings occurs in similar conditions, immersing the supports in a solution of tannic acid or pyrogallol at a concentration of 2.5mg/ml in 0.1M Bicine/0.6M NaCl pH7.8 buffer. The solid supports were slowly shaken for 2 h by means of an orbital shaker to ensure a uniform coating was forming on the surface. Subsequently, they were rinsed in ultrapure water and dried with a nitrogen flow.

4.4.2. Thermolysin Immobilisation on Polydopamine or Polyphenol Coated Supports for Enzyme Release (Semi-Reversible Immobilisation)

Immediately following the polydopamine/polyphenol coating, thermolysin was immobilised by immersion of the solid supports in an enzyme solution at a concentration of 1 mg/ml in 100 mM pH 8 phosphate buffer overnight. After this step, each sample was individually rinsed three times in ultrapure water.

4.4.3. Pre-Gelators Conversion and Bulk Gelation Catalysed by Released Enzymes

A solution containing the non-assembling pre-gelators Fmoc-T (Sigma Aldrich) and F-NH_2 (Bachem) (0.01 M and 0.04 M respectively, in 100 mM pH 8 phosphate buffer) was prepared. 1 mL of this mixture were poured on top of the glass cover slips with immobilised thermolysin and 100 µL were put on top of the TEM grids with immobilised thermolysin and left overnight. The conversion of the pre-gelators was monitored by HPLC analysis.

4.4.4. Thermolysin Immobilisation on Polydopamine or Polyphenol Coated Substrates for Localised Self-Assembly (Irreversible Immobilisation)

Immediately following the polydopamine/polyphenol coating, thermolysin was immobilised by immersion of the solid supports in an enzyme solution at a concentration of 1 mg/ml in 100 mM pH 8 phosphate buffer overnight. After this step, each sample was individually rinsed three times in ultrapure water and then immersed in 3 ml of 100 mM pH 8 phosphate buffer. The samples were placed on an orbital shaker to aid the solubilisation of any physically adsorbed enzyme and after 30 min the solution was removed and replaced with clean buffer. This procedure was repeated until no enzyme activity was revealed in the wash solutions by the FRET assay.

4.4.5. Pre-Gelators Conversion and Localised Self-Assembly Catalysed by Immobilised Enzymes

A solution containing the non-assembling pre-gelators Fmoc-T (Sigma Aldrich) and F-NH_2 (Bachem) (0.01 M and 0.04 M respectively, in 100 mM pH8 phosphate buffer) was prepared. 100 µL of this mixture were poured on top of the glass slide and 10 µL on top of the TEM grids with immobilised thermolysin and left overnight. The conversion of the pre-gelators was monitored by HPLC analysis and the localised formation of fibers was visualised by TEM.

4.4.6. FRET Assay for Thermolysin Detection

The FRET substrate, E(EDANS)-GT↓LGK-(DABCYL), was purchased from China Peptides and dissolved in DMSO to a final concentration of 0.5mM. PMMA UV grade cells with a path length of 10 mm were used for the study. Fluorescence emission spectra were measured on a Jasco FP-6500 spectrofluorimeter with light measured orthogonally to the excitation light, at a scanning speed of 500 nm min^{-1}. The excitation wavelength was 340 nm, and the spectra were measured between 355 and 650 nm, with a bandwidth of 5 nm, a medium sensitivity and 0.5 nm data pitch. The glass cover slips were washed following the modified procedure as described in section 4 and the wash solutions were collected. 6 µl of the FRET solution were added to 1 ml of wash solution. Fluorescence emission spectra were recorded for the wash solutions until no enzyme activity was revealed in the last wash. The emission data were recorded in a time course mode for 8 h to verify that there was no activity increasing over time. The excitation wavelength was 340 nm, and the emission was recorded every 60 s at the maximum emission wavelength (510 nm), with a bandwidth of 5 nm and a medium sensitivity.

The FRET assay was also employed to measure the activity of the enzyme immobilised on the slide. To this end, the glass cover slip with the immobilised enzyme was washed following the modified procedure as described in section 4 until no activity was detected in the wash solutions. The cover slip (13 mm of diameter) was then cut in half with a glass cutter to fit in the PMMA UV grade cell and was placed in the cuvette with the back side leaning on one of the walls and dipped in 1 ml of 100 mM pH8 phosphate buffer. 6 µl of FRET substrate solution were then added and the fluorescence signal recorded with the beam of excitation light passing through the surface of the cover slip. The emission spectrum was measured and then the emission data were recorded for 4 h, with the same parameters employed for the wash solutions. As in the case of the first wash solution, the intensity of fluorescence was increasing over time, reaching a plateau when the enzyme had converted all the substrate molecules in solution (Fig. 50).

4.4.7. FRET Assay for Quantitative Measurements

4.4.7.1. Enzyme Concentration in Wash Solution

Six reference samples of known enzyme concentration were prepared, in a range between 10^{-5} and 10^{-2} mg/ml. 6 µl of FRET solution were added to 1 ml of each reference sample. For each sample, a time course experiment was carried out recording the fluorescence intensity at the maximum emission wavelength (510 nm) as a function of time over two hours. The fluorescence emission was measured on a Jasco FP-6500 spectrofluorimeter at an excitation wavelength of 340 nm, with light measured orthogonally to the excitation light, with a bandwidth of 5 nm and a medium sensitivity. PMMA UV grade cells with a path length of 10 mm were used for the study. A linear fitting was applied to the first 60 s of the time course measurements, to determine the slope of the initial part of the curve. The values of the slope were plotted as a function of the concentration to build a calibration curve.

To estimate the enzyme concentration in the washes, the glass cover slips with the immobilised enzymes were washed following the modified procedure as described in section 4.4.4. 6 µl of FRET solution were added to 1ml of wash solution and a time course experiment was carried out for the first and the second wash, with the same conditions as for the reference samples. Also in this case, the slope of the curve was calculated applying a linear fitting to the first 60 s of the time course measurements. The value of the enzyme concentration in the washes was calculated introducing the values of the slope in the linear equation of the calibration curve (Fig. 52). These calculations shown that the first and the second wash solutions contained respectively ~8.25×10^{-3} mg/ml and ~6.57×10^{-7} mg/ml of enzyme (Fig. 52c).

4.4.7.2. Enzyme Concentration on the Glass Cover Slip

Firstly, the theoretical enzyme concentration for a fully covered surface was calculated. The enzyme dimensions were taken from the Protein Data Bank and the amount of enzyme on the surface for the formation of a monolayer was calculated dividing the surface area of the glass slide by the calculated area of the enzyme. In order to build a new calibration curve, reference samples were prepared in a concentration range that included the theoretical enzyme concentration on the cover slip (between 10^{-6} and 10^{-4} mg/ml). For each sample a

linear fit was applied to the first 60 s of the time course measurement to determine the slope of the initial part of the curve. The values of the slope were reported as a function of the concentration to build a calibration curve.

To estimate the enzyme concentration on the surface of the glass cover slip, a time course experiment was carried out as described in section 4.4.7.1. Also in this case, the slope of the curve was calculated applying a linear fitting to the first 60 s of the time course measurements. The value of the enzyme concentration on the glass cover slip was calculated introducing the values of the slope in the linear equation of the calibration curve (Fig. 52).

The calculated value for the enzyme concentration on the slide was ~2.73×10^{-5} mg/ml. This is equivalent to an active immobilised amount of 0.4×10^{-9} g/mm^2 (given a spectrometer cuvette volume of 1 mL and a sample size of 0.66 cm^2). In comparison, a monolayer of thermolysin corresponds to ~ 0.98×10^{-9} g/mm^2. This value was obtained multiplying the theoretical enzyme concentration for a fully covered surface (~ 1.80×10^{-9} g/mm^2) by the correction factor 0.547 as for the RSA model jamming limit 2D[229], giving a final value of ~ 0.98×10^{-9} g/mm^2 (Fig 53d).

4.4.8. Transmission Electron Microscopy (TEM)

4.4.8.1. TEM on Bulk Gels

Gels were prepared according to the procedure described in section 3. TEM images were captured using a FEI Tecnai T20 transmission electron microscope operating at 200kV. Carbon-coated copper grids (200 mesh) were glow discharged in air for 30 s. The support film was touched onto the gel surface for 3 seconds and blotted down using filter paper. Negative stain (20 µL, 1 % aq. Methylamine vanadate obtained from Nanovan, Nanoprobes) was applied and the mixture blotted again with filter paper to remove excess. Each sample was allowed to dry afterwards for 2-3 minutes in a dust-free environment prior to TEM imaging. The dried grids with the samples were then imaged and the images were saved using Gatan Digital Micrograph software.

4.4.8.2. TEM for Visualisation of Localised Self-Assembly

The TEM grids were prepared as described in section 5 and left overnight. Negative stain (20 µL, 1 % aq. Methylamine vanadate obtained from Nanovan, Nanoprobes) was applied and the mixture blotted again with filter paper to remove excess. Each sample was allowed to dry afterwards for 2-3 minutes in a dust-free environment prior to TEM imaging. The dried grids with the samples were then imaged and the images were saved using Gatan Digital Micrograph software.

4.4.9. Reversed-phase High Performance Liquid Chromatography (HPLC)

HPLC analysis was carried out to measure the enzymatic conversion of the precursors (Fmoc-T and F-NH_2 to Fmoc-TF-NH_2). To monitor the conversion in bulk gels, 20 µl of gel were diluted up to 1 ml in a solution of acetonitrile/water (50:50 v/v mixture) containing 0.1% trifluoroacetic acid (TFA). To monitor the conversion of the samples with localised surface self-assembly on the surface, the samples were prepared as described in section 5. The samples were then rinsed with 2 ml of ultrapure water and 20 µl of wash solution were diluted up to 1ml in a solution of acetonitrile/water (50:50 v/v mixture) containing 0.1% trifluoroacetic acid. A Dionex P680 HPLC system was used to analyse the mixtures of peptide derivatives. Aliquots of 30 µL were injected with a flow rate of 1 mL min^{-1} into a Macherey-Nagel C-18 column (250 mm of length and 4.6 mm of internal diameter) containing silica particles (diameter: 5 µm, pores diameter: 10 nm). The gradient used was a linear exchange between water/acetonitrile (80:20, 0.1% TFA) at 4 min to water/acetonitrile (20:80, 0.1% TFA) at 35 min. This concentration was kept constant until 40 min when the gradient was decreased to 20% (v/v) acetonitrile in water at 42 min. The intensity of each identified peak was determined by UV detection at 280 nm. The percentage yields were calculated from HPLC integrated peak areas.

5. Spatially Controlled Biocatalytic Self-Assembly on Magnetic Nanoparticles *

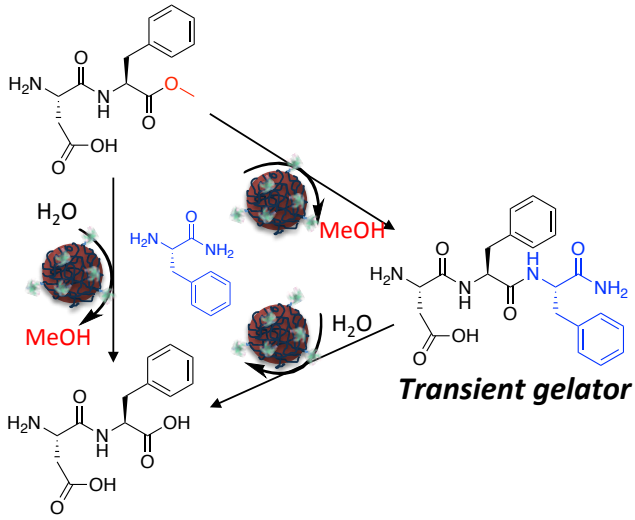

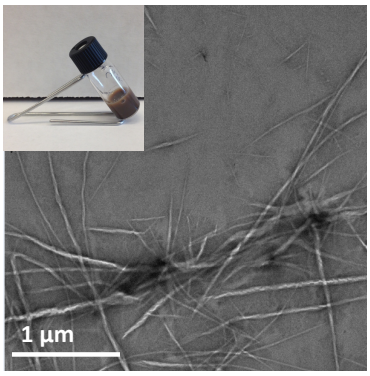

* The work in this Chapter has been submitted, in part, to ACS Applied Materials and Interfaces for publication.

Declaration of contribution to published article:

Any reproduced work from the aforementioned submitted article, including the written article itself, I was solely responsible for, together with the other authors of the article, unless otherwise stated.

5.1. Introduction

In the previous Chapters (Chapters 2 and 4), the potential of using bio-catalytic self-assembly for processing of supramolecular materials was highlighted and various enzymes that are employed in this context either freely dissolved in solution or as surface attached species were described. Specifically, in Chapter 4 the potential of using localised bio-catalytic self-assembly to generate organised structural configurations through spatially selective nucleation and structure growth was highlighted.

Numerous applications of bio-catalytic self-assembly in biologically interfacing systems and in nanofabrication have recently emerged and a number of examples that employ confined or patterned catalysts to trigger localised reactions are available in the literature,[79, 142] but to our knowledge there are no reports that specifically show the effect of the enzyme location on the nucleation and growth of biocatalytic systems and to prove that the self-assembly initiates in proximity of the enzymes as expected. In this Chapter, enzymes immobilised on nanoparticles are employed to control and visualise the localisation of the self-assembly. In order to generalise our results, both a system at equilibrium and a non-equilibrium one are investigated. The possibility to employ biocatalytic self-assembly towards producing non-equilibrium structures has attracted significant interest, since these systems may display features that are not normally associated with synthetic systems but are commonly features of naturally occurring catalytic self-assembling systems. These systems maybe dynamic, reconfigurable and self-healing and may find use in adaptive nanotechnologies.[213, 230] Ulijn and co-workers recently demonstrated the formation of non-equilibrium nanostructures by competing enzyme-induced assembly and disassembly of aromatic peptide amphiphiles,[213] and more recently of a purely peptidic system.[230] In one of the systems investigated in this Chapter, the non-equilibrium system, controlled localised self-assembly of peptide derivatives and the formation of transient nanostructures are combined.

5.2. Results and Discussion

Two different systems that are known to self-assemble upon enzyme action are investigated. The first system (System 1, Fig. 56b) employs the enzyme thermolysin to catalyse the amide bond formation between the non-assembling precursors Fmoc-T and F-

NH_2, the same system described in Chapter 4. The self-assembling product Fmoc-TF-NH_2 forms stable hydrogels. In the second system (System 2, Fig. 56c), chymotrypsin is used to catalyse peptide formation by transacylation. The precursors employed are the dipeptide methyl ester aspartame (DF-OMe) and the amidated peptide F-NH_2. In the presence of chymotrypsin, the tripeptide gelator DFF-NH_2 is formed turning the solution into a hydrogel. In a competing reaction, the tripeptide is subsequently hydrolysed to give DF and F-NH_2. As a result of these competing processes, the gel is transiently formed and the gel-to-sol transition occurs in approximately 24 h.[230]

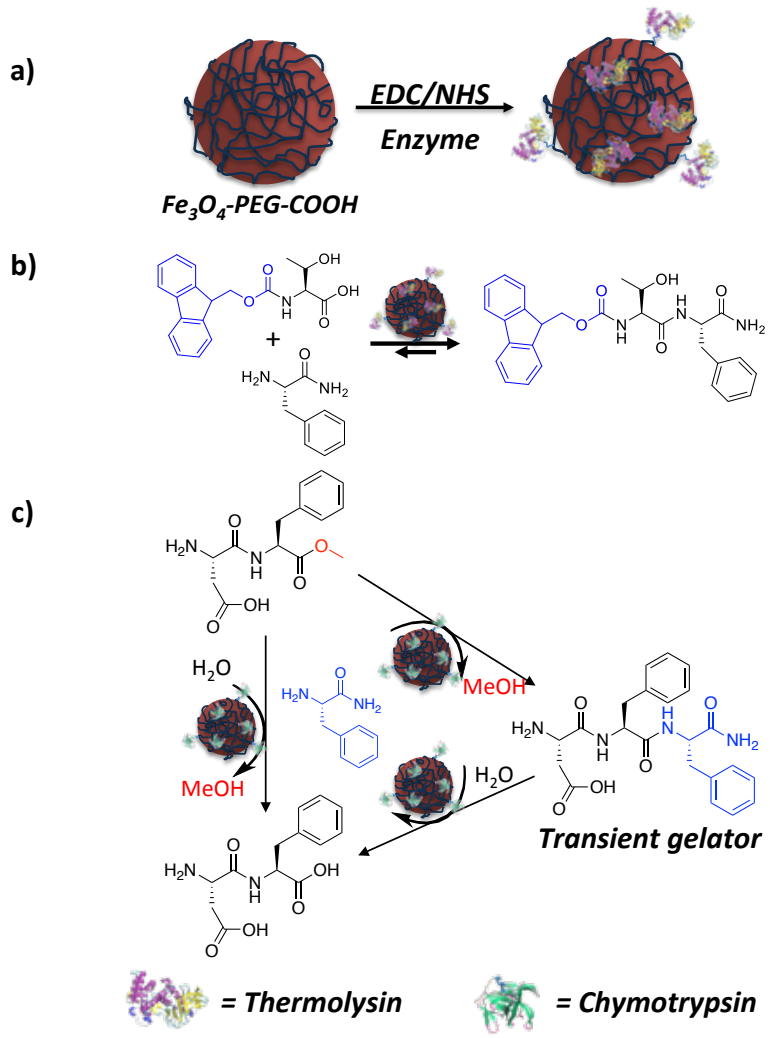

Figure 56 a) Schematics of the enzyme immobilization on PEG-COOH modified nanoparticles by EDC/NHS coupling. b) Reaction of the precursors FmocT and FNH_2 with thermolysin-nanoparticles conjugates to give the gelator $FmocTFNH_2$. c) Reaction of the precursors DFOMe and FNH_2 with chymotrypsin-nanoparticles conjugates to give the transient gelator $DFFNH_2$ and following hydrolysis to give the dipeptide DF. Thermolysin and chymotrypsin from PDB.

In order to study the above biocatalytic self-assembly processes using magnetic nanoparticle-immobilized catalysts, thermolysin and chymotrypsin were immobilised on carboxylic acid terminated nanoparticles by means of EDC/NHS coupling (section 5.4.1 and Fig 56a). In order to remove any unbound enzyme, the nanoparticle-enzyme conjugates were washed multiple times. 500 nm polyethylenglycol(PEG)-COOH modified nanoparticles were employed as this size allows for easy separation of the nanoparticles with a magnetic separation rack.

Fluorescence spectroscopy was employed to monitor the activity of thermolysin and chymotrypsin *via* the Förster resonance energy transfer (FRET) assay, similar to the approach described in Chapter 4. The FRET assay was employed to measure the enzymatic activity in the wash solutions collected after the enzyme conjugation to the nanoparticles (section 5.4.2 and Fig. 57). When no activity is detected in the wash, the nanoparticle-enzyme conjugates are collected and added to the precursor solution. With this procedure it is possible to ensure that any catalytic activity is due to the enzymes immobilised on the nanoparticles and not to free enzymes in solution.

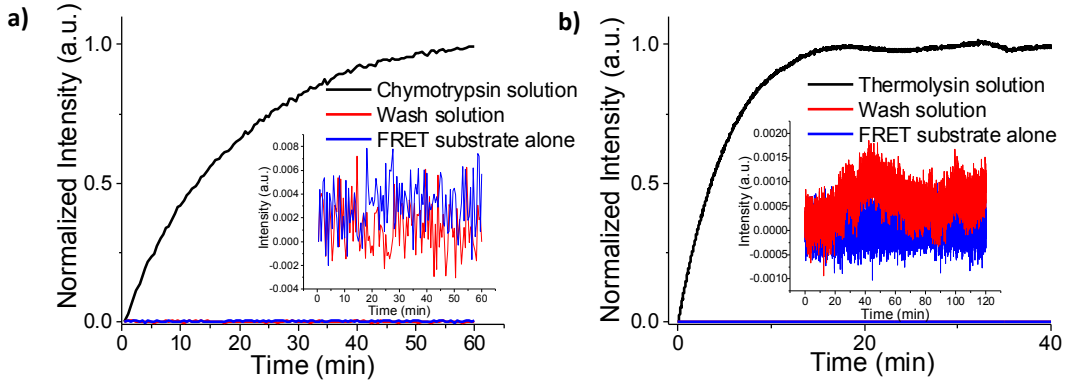

Figure 57 FRET assay to detect enzymatic activity. a) Assay for the chymotrypsin-nanoparticle conjugates. b) Assay for the thermolysin-nanoparticles conjugates. For both systems reference samples with the free enzymes and the FRET substrate were prepared (black line). A control sample with the FRET substrate alone in buffer was analysed as well (blue line). The final washes (red line) show no enzymatic activity, meaning that the all the unbound enzymes have been removed.

The thermolysin-nanoparticle conjugates are added to the precursors Fmoc-T (20 mM) and F-NH_2 (80 mM) (System 1). The chymotrypsin-nanoparticle conjugates are added to the

precursors DF-OMe (20 mM) and F-NH_2 (40 mM) (System 2). The mixtures are briefly vortexed and left to equilibrate and for both systems the conversion of the precursors is followed by HPLC analysis (Fig. 58). In System 1, the solution turns into a transparent light brown gel over approximately 4 days, as the thermolysin-nanoparticle conjugates slowly precipitate towards the bottom of the glass vial (Fig. 60). The conversion of the precursors into the final products slowly increases over time, reaching a plateau at less than 6% after approximately 12 days. This relatively low yield can be explained considering the geometry of the system. First of all, the overall amount of enzymes is much lower compared to the previously studied reaction with free enzyme in solution (see Chapter 4, Section 4.2) because, although the initial concentration of enzyme is the same in the two cases, only a fraction of enzyme is retained upon washing in the nanoparticle-enzyme conjugates. A similar situation was observed in the semi-reversible immobilization described in Chapter 4, where the conversion yield reached values up to ~ 30% due to the enzymes released in the pre-gelator solution. On the contrary, in the case of the irreversible enzyme immobilization described in Chapter 4, where the enzymes were confined to the surface, the percentage of conversion was only around 3%. The results described in this Chapter are hence in agreement with the data reported in the previous Chapter. In Chapter 4, the enzymes (irreversibly) immobilised on a flat solid support were able to catalyse the conversion of the pre-gelators and subsequently the self-assembly only in the vicinity of the surface, but not the bulk gelation of the solution. Here, the presence of the nanoparticle-enzyme conjugates dispersed in solution compared to a flat surface allows for catalyst mobility in solution and for a more homogeneous nucleation and growth of self-assembled nanostructures throughout the pre-gelator solution. This results in turn in the gelation of the solution.

In System 2, the reaction is much quicker than in System 1 and an opaque dark brown gel is formed in approximately 30 min (Fig. 57). The HPLC analysis confirms that the conversion into the transient tripeptide gelator DFF-NH_2 is complete within approximately 6 h (Fig. 58). When DF-OMe and F-NH_2 are mixed with the free chymotrypsin, the gel formed is stable for approximately 24 h, then the tripeptide is hydrolysed and the gel-to-sol transition occurs.[230] The gel formed with the chymotrypsin-nanoparticle conjugate is stable for several weeks and the hydrolysis reaction of the tripeptide gelator DFF-NH_2 to DF-OH proceeds at a much slower rate, with a percentage of DFF-NH_2 in the mixture as high as 80% after one month (Fig. 58). The chirality of the self-assembled structure was monitored with circular dichroism (CD) spectroscopy (Fig. 59). The nanoparticles-enzyme conjugates were analysed

before addition to the precursors solution, to ensure no CD signal could be due to the conjugates (Fig. 59, black line). The precursors (Fmoc-T and DF-OMe) were analysed as well and no CD signal could be associated to them either (Fig. 59, red line). For System 1, the CD spectrum at t=0 showed the appearance of a small positive peak was observed around 220-230 nm. Upon gel formation, a clear positive peak around 220 nm is visible and corresponds to the peak observed for the gel formed with free enzyme. For System 2, the positive peak around 220 nm is clearly visible at t=0, since the reaction is much faster than the reaction in System 1. For both systems, the peaks around 220 correspond to the peaks observed for the gels formed with free enzyme and suggest the formation of β-sheet-like arrangements as previously reported in the literature for similar systems.[208, 231]

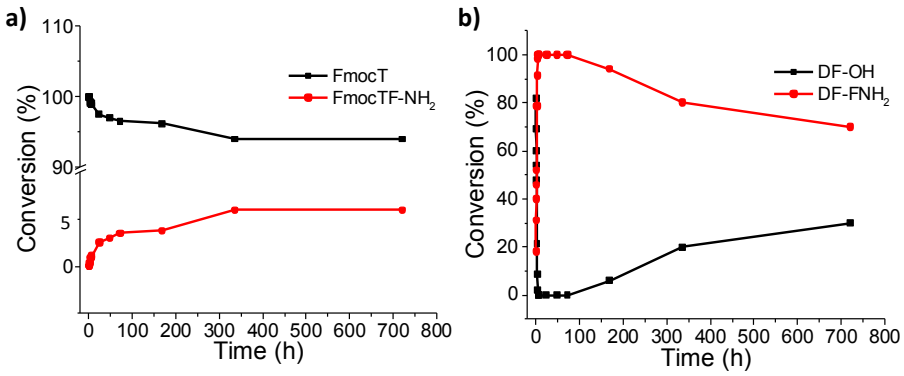

Figure 58 HPLC conversion. The conversion of the precursors into the final products reaches almost 6% after approximately 12 days for System 1 (a). For System 2 (b) the conversion into the transient tripeptide gelator DFF-NH_2 is complete within approximately 6 h.

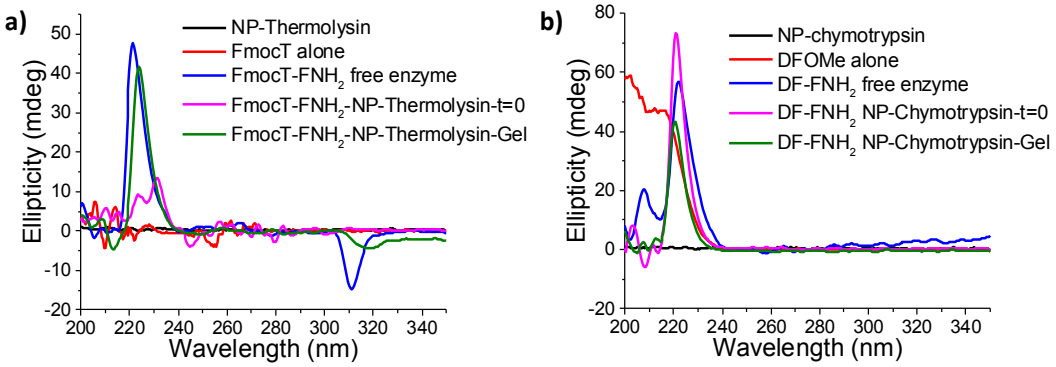

Figure 59 CD spectra. The observed CD spectra for both systems show a positive signal around 220 nm, which suggests the formation of β-sheet-like arrangements.

Transmission electron microscopy was employed to visualise the morphology of the self-assembled structures. For both gels, the images reveal how the growth of the self-assembled fibres initiates from the enzyme-nanoparticle conjugates (Fig. 60). In system 1 many micellar aggregates are also visible, which can be attributed to the presence of the precursor Fmoc-T, given the low percentage of conversion into the final products. For both systems, the morphology of the self-assembled nanostructures is similar to what was previously reported in the literature.[224, 230]

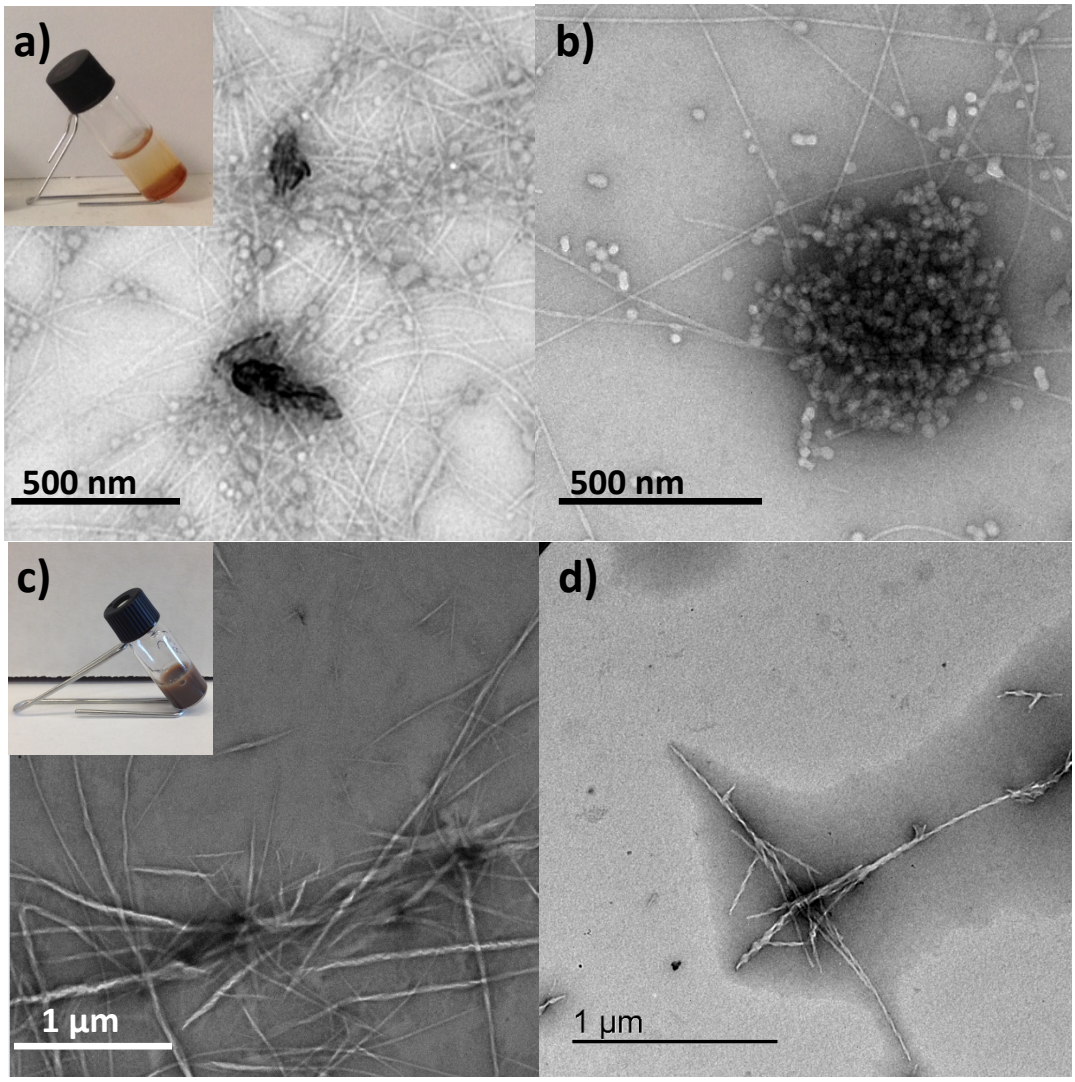

Figure 60 TEM images of the nanostructure formation catalysed by the enzymes immobilized on the nanoparticles. Both for System 1 (a and b) and for System 2 (c and d) it is possible to observe the nucelation and growth of the nanofibers starting from the surface of the nanoparticles. In the inset: gels formed for system 1 (a) and system 2 (b).

Rheology was employed to study the mechanical properties of the gels and to compare them with those of the same gels formed with free enzymes in solution (section 5.4.7). For System 1, the presence of the nanoparticles has little effect on the mechanical properties of the gel, with the storage modulus G' increasing from $35.5*10^3$ Pa for the gel formed with free thermolysin to $51.5*10^3$ Pa for the gel formed with the enzyme-nanoparticles conjugates.

The effect of the nanoparticles incorporation is dramatically evident in System 2, where G' increases by almost one order of magnitude, from $1.89*10^3$ Pa for the gel obtained with free chymotrypsin to $15.42*10^3$ Pa for the gel obtained with the enzyme-nanoparticle conjugates. This is due to the slower rate of hydrolysis of the transient gelator DFF-NH_2 when chymotrypsin is immobilised on the nanoparticles (Fig. 61). For both systems, the results obtained from the rheological measurements are remarkable because they show that the gels have similar (System 1) or even better (System 2) mechanical properties compared to the corresponding systems obtained with the free enzyme in solution, even though the conversion of the precursors to the self-assembling products is much lower.

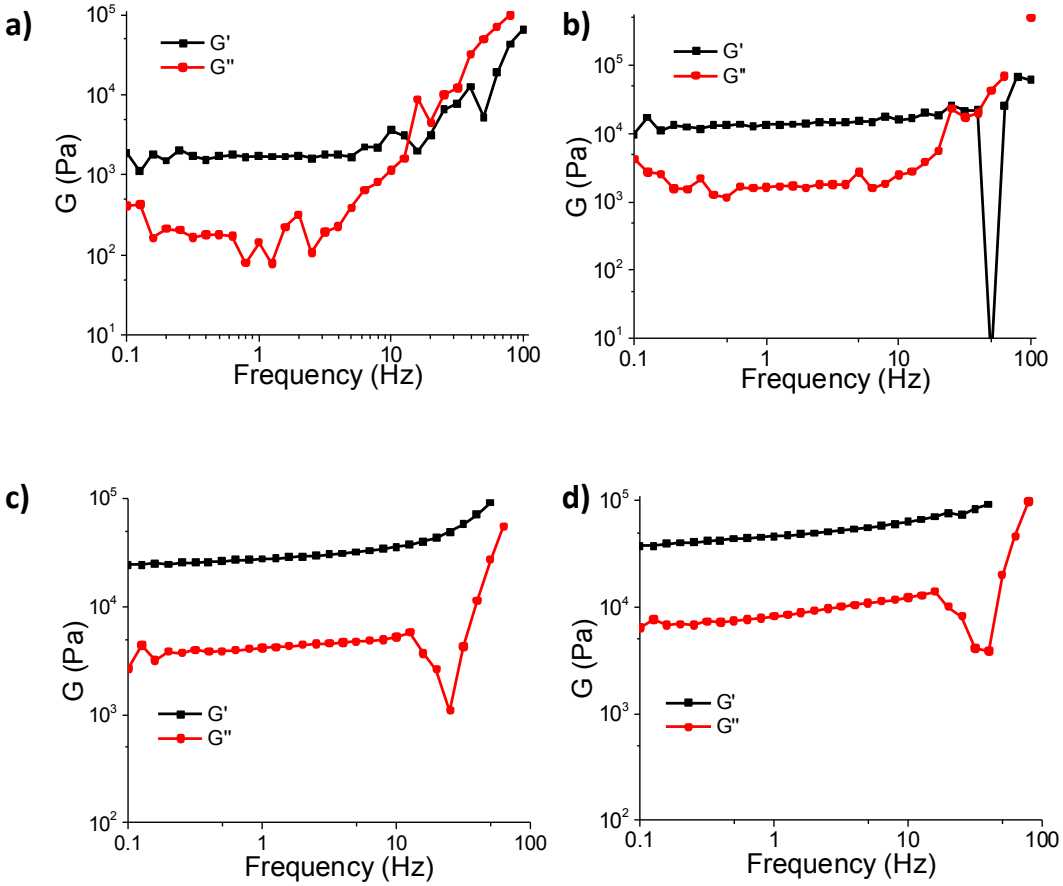

Figure 61 Dynamic frequency sweep experiments. a) DFF-NH_2 gels prepared with free chymotrypsin. G'= 1.89*10^3 Pa. b) DFF-NH_2 gels prepared with the chymotrypsin-nanoparticles conjugates. G'= 15.42*10^3 Pa. c) FmocTF-NH_2 gels prepared with free thermolysin. G'= 35.5*10^3 Pa. d) FmocTF-NH_2 gels prepared with thermolysin-nanoparticles conjugate. G'= 51.5*10^3 Pa.

Permanent magnets were employed to investigate the effect of a magnetic field on the formation of the self-assembled structures (section 5.4.8). Given the long time required for System 1 to gel, these experiments were carried out only for System 2. 100 µl of the mixture of chymotryspin-nanoparticles conjugates and precursors were placed in a well of a 96-well cell culture plate. The magnet was placed at three different positions relative to the well: Position 1 (on top of the well), 2 (1.2 cm from the well) and 3 (2.4 cm from the well) (Fig. 62) and the system was left to equilibrate. When the magnet was placed in Position 1, the nanoparticles quickly migrated to the surface and no gelation was observed. When the magnet was placed in Position 2, the nanoparticles slowly migrated towards the magnet, giving rise to the formation of a gel with a gradient of colour. When the magnet was in

position 3, no macroscopic effect on the gel appearance was observed, but the gelation occurred more slowly, suggesting that the nanoparticles are displaced by the magnet to some extent.

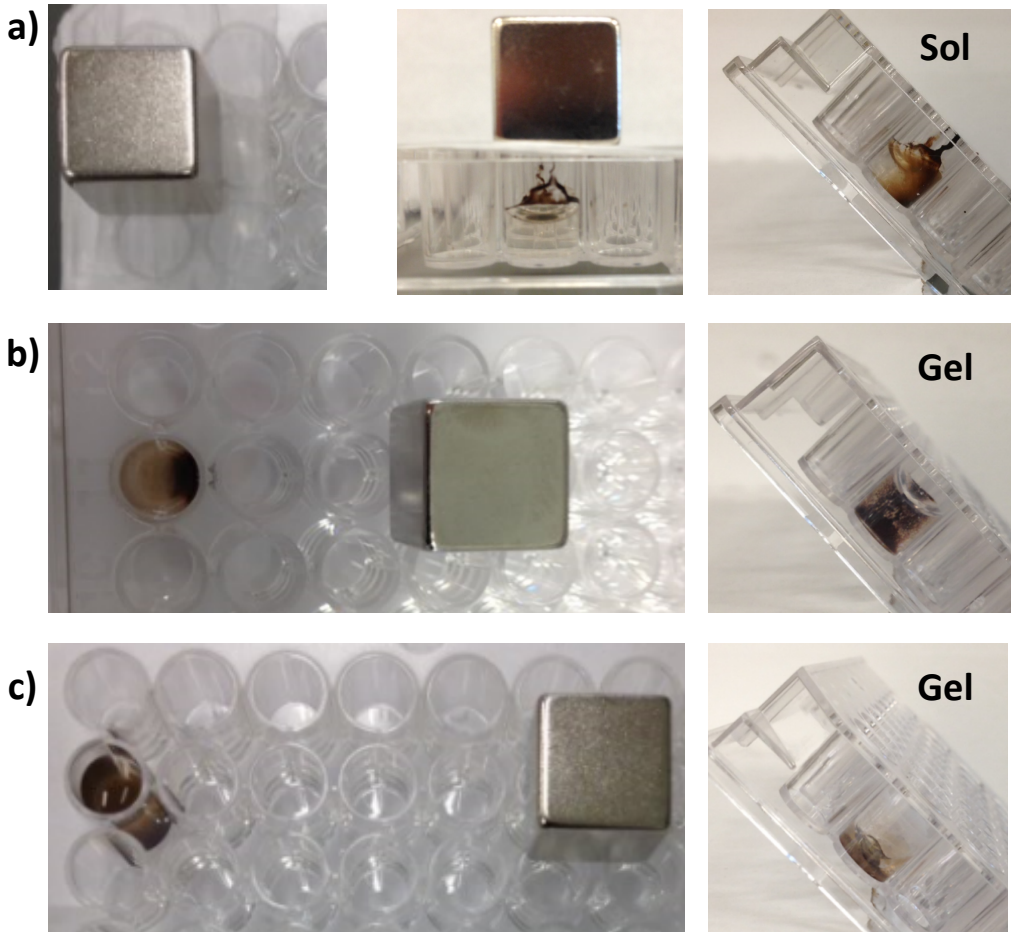

Figure 62 a) Magnetic cube in position 1 (on top of the well). The nanoparticles quickly migrate to the surface and the sample does not form a gel. b) Magnetic cube in Position 2. The particles migrate to some extent towards the cube. The sample formed a gel overnight. A gradient of colour is visible in the gel. c) Magnetic cube in Position 3. The sample forms a gel within 3 h. No gradient of colour is visible in the gel.

To investigate the effect of a magnetic field after the gel has formed, the magnetic cube was placed next to the vial containing the gel (Fig. 63). The gel slowly started to shrink, finally reaching 15% of its original volume after approximately one month. The change in the shape of the gel induced by the magnet is permanent, since if the magnet is removed, the gel does not relax to its original shape. The HPLC chromatograms show that in the transparent supernatant the percentage of conversion is less than 20%, whereas in the

shrunken gel it is still as high as 70%. TEM pictures show that very few fibres are present in the supernatant, whereas a high density of fibres is observed in the shrunken gel (Fig. 64). One of the possible outcomes of exposing the gels to a magnetic field could have been the removal of the nanoparticle-enzyme conjugates and the resulting nanoparticle-free gels. The results furhter show instead that the self-assembled nanofibres are nucleated from and have strong interactions with the nanoparticles-enzyme conjugates, because the gel is separated together with the conjugates to leave the liquid supernatant. The external magnetic field consequently influences the shape of the gels, providing a means to externally control and manipulate the whole system.

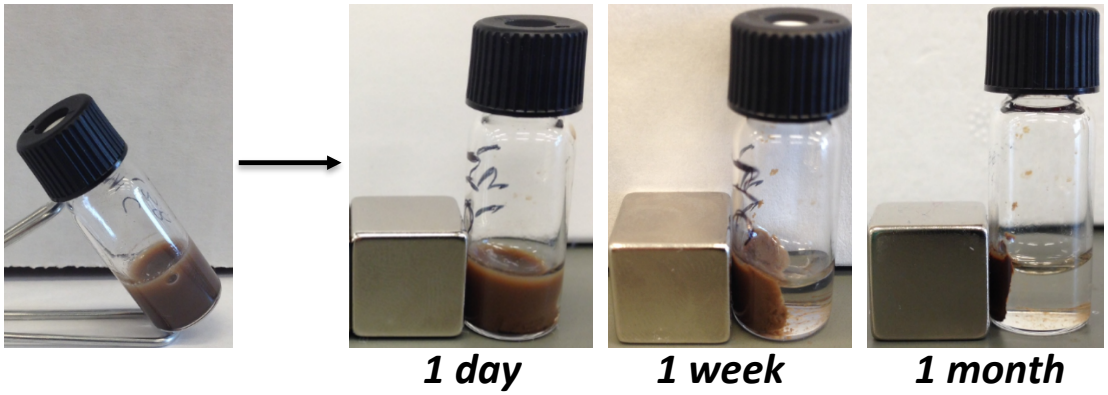

Figure 63 Images to show the effect of a magnetic field on the DF-FNH$_2$ gel formed with the chymotrypsin-nanoparticles. The gel progressively shrinks over time under the effect of the magnetic field reaching approximately 15% of its initial volume after 1 month.

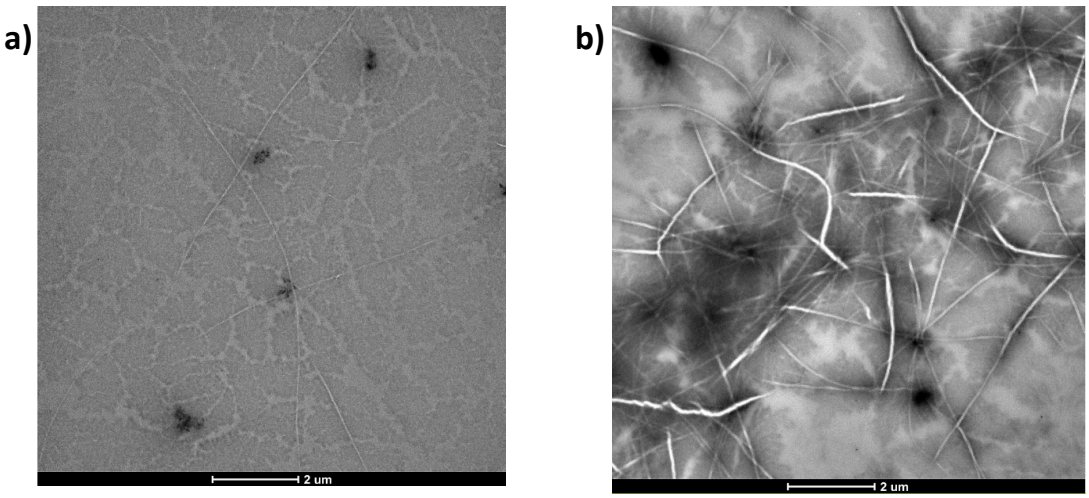

Figure 64 TEM images of transparent supernatant collected upon separation with the magnetic cube (a) and of the shrunk gel (b).

5.3. Conclusions

Enzymes immobilised on magnetic nanoparticles were employed for the first time to prove the effect of the catalyst location on the spatial control of nucleation and growth of biocatalytic self-assembled systems. This was generalised for an equilibrium (System 1) and a non-equilibrium system (System 2). For both gels, electron microscopy images show how the growth of the self-assembled structures initiates from the enzyme-nanoparticle conjugates. The incorporation of the nanoparticles in the gels was shown to affect the final mechanical properties, as shown by the rheology measurements. This is particularly evident in System 2, where G' increases by almost one order of magnitude compared to the gel obtained with free chymotrypsin. Exploiting the magnetic properties of the nanoparticles, the shape of the gel could be manipulated with an external magnetic field, inducing an externally-controlled reduction of volume over time. This introduces an additional level of control to modify the final properties of the gel.

5.4. Experimental

All reagents, including the peptides, were purchased from commercial sources (*e.g.* Sigma Aldrich, Bachem) at the highest purity and were used as supplied, unless stated otherwise in the experimental procedures. All solvents were used as supplied (analytical or HPLC grade) without further purification. All the experiments were performed at room temperature unless stated otherwise in the experimental procedures. Room temperature in the laboratory may have varied between 20 and 25 °C.

5.4.1. Enzyme Immobilisation on Magnetic Nanoparticles

The magnetic nanoparticles were purchased form Micromod (nanomag®-D, 500 nm, 10 mg/ml suspension in water, Fe_3O_4 nanoparticles with PEG-COOH surface groups). N-(3-Dimethylaminopropyl)-N′-ethylcarbodiimide hydrochloride (EDC, Sigma Aldrich) and N-Hydroxysulfosuccinimide sodium salt (sulfo-NHS, Sigma Aldrich) were dissolved separately in MES monohydrate buffer (Sigma Aldrich) 0.5 M pH 5.5 to a final concentration of 200 mM. 200 µL of nanoparticles were mixed to 500 µL of EDC solution and 500 µL of sulfo-NHS solution and left for 30 min in an Eppendorf tube rotator to activate the carboxylic acid. The nanoparticles were separated from the supernatant by means of a magnetic separation rack and redispersed in MES buffer. This procedure was repeated twice with MES buffer and twice with sodium phosphate buffer 100 mM pH 7.4 to remove any excess of EDC and sulfo-NHS. Chymotrypsin (α-Chymotrypsin from Bovine pancreas, ≥ 40 U/mg, Sigma Aldrich) and Thermolysin (Thermolysin from Bacillus thermoproteolyticus, 10200 U/mg, Calbiochem) were dissolved in sodium phosphate buffer 100 mM pH 7.4 to a final concentration of 1 mg/ml and 0.1 mg/mL respectively. The magnetic nanoparticles were separated from the supernatant by means of a magnetic separation rack and redispersed in 1 mL of enzyme solution. The mixture was left in an Eppendorf tube rotator for two hours. The nanoparticles were then washed multiple times with phosphate buffer 100 mM pH 7.4 (separating the nanoparticles from the supernatant with the magnetic separation rack) and the washing solution were collected to detect the presence of enzyme by FRET assay.

5.4.2. Forster Resonance Energy Transfer (FRET) Assay for Protease Detection

The FRET substrate E(EDANS)-G-T-L-G-K(DABCYL) was purchased from China Peptides and it was dissolved in dimethyl sulfoxide (DMSO) to a final concentration of 500 μM. 6 μL of the FRET substrate were added to 1 mL of wash solution. PMMA UV grade cells with a path length of 10 mm were used for the study. Fluorescence emission spectra were measured on a Jasco FP-6500 spectrofluorimeter with light measured orthogonally to the excitation light, at a scanning speed of 500 nm min^{-1}. The excitation wavelength was 340 nm, and the spectra were measured between 355 and 650nm, with a bandwidth of 5 nm, a medium sensitivity and 0.5 nm data pitch. Time course measurements were recorded with an excitation wavelength of 340 nm and fluorescence emission was detected at 510 nm. The measurements were repeated until no activity was detected in the wash solutions. An average of 15 washes were needed for the thermolysin-nanoparticles conjugates and 5 washes for the chymotrypsin-nanoparticles conjugates. The nanoparticles-enzyme conjugates were hence redispersed in 200 μL of phosphate buffer 100 mM pH 7.4.

5.4.3. Gels Preparation

The nanoparticles-enzyme conjugates were separated from the supernatant with a magnetic separation rack. The supernatant was removed and the nanoparticles-enzyme conjugates were redispered in 1 mL of peptide solution. The peptide solutions were prepared in phosphate buffer 100 mM pH 7.4 (DF-OMe 20 mM, F-NH_2 40 mM for the nanoparticles-chymotrypsin conjugates and FmocT 20 mM, F-NH_2 80 mM for the nanoparticles-thermolysin conjugates). The mixture was briefly vortexed and sonicated. Gelation was observed within 30 min for the system with nanoparticles-chymotrypsin conjugates (System 2) and after approximately 4 days for the system with nanoparticles-thermolysin conjugates (System 1).

The gels with the free enzymes were prepared with the same concentration of precursors and with 0.1 mg/ml of thermolysin for System 1 and 1 mg/ml of chymotrypsin for System 2.

5.4.4. Transmission Electron Microscopy (TEM)

TEM was employed to visualise the morphology of the bare nanoparticles, the nanoparticles-enzyme conjugates and the gels. Gels were prepared according to the procedure described in section 5.4.3. TEM images were captured using a FEI Tecnai T20 transmission electron microscope operating at 200 kV. Carbon-coated copper grids (200 mesh) were glow discharged in air for 30 s. 5 μL of the nanoparticles or the nanoparticles-enzyme conjugate solutions were deposited on the glow discharged grids, left for 30 s and then blotted down using filter paper. For the gel samples, the glow-discharged grids were touched onto the gel surface for 3 seconds and blotted down using filter paper. Negative stain (20 μL, 1 % aq. Methylamine vanadate obtained from Nanovan, Nanoprobes) was applied and the mixture blotted again with filter paper to remove excess. Each sample was allowed to dry afterwards for 2-3 minutes in a dust-free environment prior to TEM imaging. The dried grids with the samples were then imaged and the images were saved using Gatan Digital Micrograph software.

5.4.5. Circular Dichroism (CD)

Samples were monitored by CD spectroscopy on a Jasco J-810 spectrometer equipped with a temperature control; spectra were recorded at 25 °C. Gels were prepared according to the procedure described in section 5.4.3. 100 μL of gel were loaded between two quartz cover slips. The spectra were measured at 50 nm min^{-1} with a 0.5 nm step size and a 1.0 nm bandwidth, between 200 and 350 nm.

5.4.6. Reversed Phase High Performance Liquid Chromatography (HPLC)

HPLC analysis was carried out to measure the enzymatic conversion of the precursors (Fmoc-T and F-NH_2 to Fmoc-TF-NH_2, DF-OMe and F-NH_2 to DFF-NH_2). The gel samples were prepared according to the procedure described in section 5.4.3 and 20μl of gel were diluited up to 1ml in a solution of acetonitrile/water (50:50 v/v mixture) containing 0.1% trifluoroacetic acid. These samples were analysed with HPLC to confirm enzymatic conversion of the precursors.

A Dionex P680 HPLC system was used to analyse the mixtures of peptide derivatives. Aliquots of 30 µL were injected with a flow rate of 1 mL min^{-1} into a Macherey-Nagel C-18 column (250 mm of length and 4.6 mm of internal diameter) containing silica particles (diameter: 5 µm, pores diameter: 10 nm). The gradient used was a linear exchange between water/acetonitrile (80:20, 0.1% TFA) at 4 min to water/acetonitrile (20:80, 0.1% TFA) at 35 min. This concentration was kept constant until 40 min when the gradient was decreased to 20% (v/v) acetonitrile in water at 42 min. The intensity of each identified peak was determined by UV detection at 280 nm. The percentage yields were calculated from HPLC integrated peak areas.

5.4.7. Rheology

Dynamic frequency sweep experiments were carried out on a strain-controlled rheometer (Kinexus rotational rheometer from Malvern) using a parallel-plate geometry (20 mm) with a 1 mm gap. An integrated temperature controller was used to maintain the temperature of the sample stage at 25°C. To ensure the measurements were made in the linear viscoelastic regime, an amplitude sweep was performed and the results showed no variation in elastic modulus (G′) and viscous modulus (G″) up to a strain of 0.06%. The gels were prepared according to the procedure previously described in section 5.4.3. The dynamic modulus of the gels was measured as a frequency function, where the frequency sweeps were carried out between 1 and 100 Hz. The measurements were repeated at least three times to ensure reproducibility.

5.4.8. Effect of a Magnetic Field on the Gel Formation

Magcraft® Rare-Earth Cube Magnets (12.7mm long x 12.7mm wide x 12.7mm thick) with an individual pull force of approximately 10 Kg were employed for these experiments. DFF-NH_2 gels were prepared with chymotrypsin-nanoparticles conjugates as described in section 3. 100 µl of the mixture were pipetted in a well of a 96-wells cell culture plate. The magnetic cubes were then placed at different distances from the sample. The magnet was placed at three different positions relative to the well: Position 1 (on top of the well), 2 (1.2 cm from the well) and 3 (2.4 cm from the well) and the system was left to equilibrate. Only the samples with the magnetic cube in position 2 and 3 formed a gel.

5.4.9. Effect of a Magnetic Field upon Gel Formation

Magcraft® Rare-Earth Cube Magnets (12.7mm long x 12.7mm wide x 12.7mm thick) with an individual pull force of approximately 10 Kg were employed for these experiments. DFF-NH_2 gels were prepared with chymotrypsin-nanoparticles conjugates as described in section 3. 500 µl of the mixture were pipetted into a glass vial and left to equilibrate. When the gel was formed, a magnetic cube was placed next to the vial. The gel slowly started to shrink finally reaching 15% of its original volume after approximately one month. The HPLC chromatograms show that in the transparent supernatant the percentage of conversion is less than 20%, whereas in the shrunk gel it is still as high as 80%. TEM pictures show that a very few fibres are present in the supernatant.

6. Localised Self-Assembly of Aromatic Peptide Amphiphiles by Patterned Enzymes

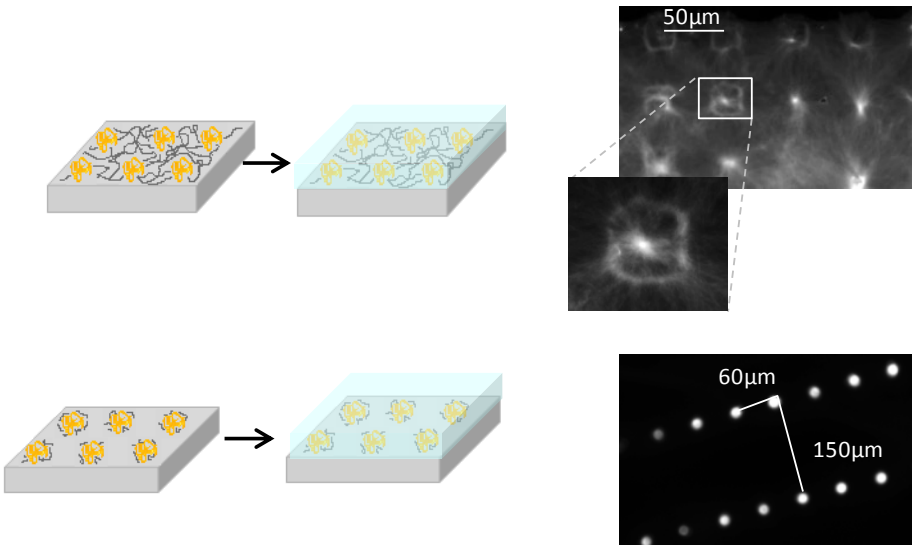

6.1. Introduction

In Chapter 4, polydopamine coated glass coverslips were employed to immobilise thermolysin and the results obtained showed that the enzyme is both strongly bound to the surface and retains its activity upon immobilisation. In Chapter 5, the importance of the enzyme location for the spatial control of nucleation and growth of biocatalytic self-assembled structures was highlighted. The possibility to realise a controlled pattern of enzymes or other biomolecules with micro- and nanometre resolution on solid surfaces is of great interest for a number of technological applications, as mentioned in the Literature Review (Chapter 2).[139, 140] Following the results described in the previous Chapters (Chapters 4 and 5), we moved from enzyme immobilisation on the whole surface to a pattern of enzymes to achieve localised biocatalytic self-assembly. In this Chapter, microcontact printing is employed to create patterns of enzymes on a polydopamine coated surface, subsequently used to catalyse the localised self-assembly of aromatic peptide amphiphiles.

6.2. Results and Discussion

Microcontact printing (μCP) is a soft lithographic technique that uses the relief patterns on an elastomeric stamp to form patterns of "ink" on the surface of a substrate through conformal contact.[150, 232, 233] The elastomeric stamp is the key element of soft lithography, it is prepared by pouring a liquid polymer precursor onto a suitable master; after the polymerisation of the precursor is complete, the stamp can be peeled off. The subsequent stamp is be the negative of the master, which is typically created from silicon using traditional photolithography techniques. A number of polymers are available as possible materials for the fabrication of the stamp, but the most commonly used is poly(dimethylsiloxane) (PDMS). This silicon elastomer is inert to many chemicals, it is physically tough but flexible (allowing for conformal contact between the stamp and the substrate) and has a low surface energy, which facilitates the transfer of the ink from the stamp to the substrate.[233] This technique was developed in the late 1990s by G. Whitesides and co-workers to print self-assembled monolayers (SAMs) of thiols on gold surfaces.[150, 232]

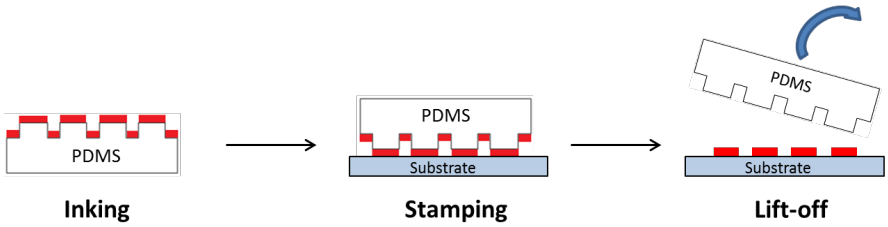

Figure 65 Schematics representing the key steps in microcontact printing. The PDMS stamp is first inked with a solution of the molecules to be transferred on the substrate. The stamp is then brought in contact with the substrate and hence lifted off it. Modified from [150].

This technique has been employed to print a variety of different "inks" on a number of solid supports.[233] For this study, polydopamine-coated glass coverslips prepared as previously described in Chapter 4 (see section 4.4.1) were employed as solid supports. PDMS stamps were prepared as described in section 6.4.1, inked with a solution of the protein to print and brought in contact with the polydopamine-coated substrate. Prior to printing thermolysin, fluorescein isothiocyanate labelled bovine serum albumin (FITC-BSA) was printed onto the slides, according to the procedure described in Section 6.4.2. This fluorescent model protein was chosen since the optical properties of FITC (excitation at 494 nm and emission at 518 nm) allows for the immediate visualisation of the patterned proteins by fluorescence microscopy (Fig. 66).

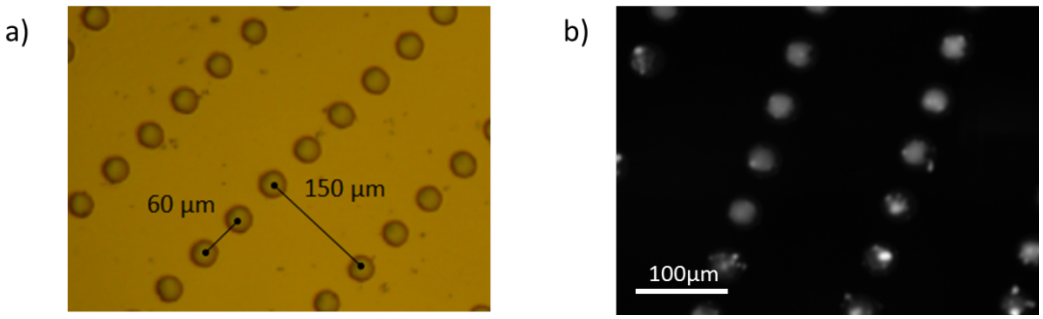

Figure 66 a) Bright field image of the PDMS stamp used to print FITC-BSA. b) Fluorescence microscopy image showing the pattern of FITC-BSA on a polydopamine coated glass slide. The pattern consists of arrays of pillars 60µ x 150µ, imaged with a 20x objective.

The fluorescence images clearly showed the pattern of proteins was successfully transferred from the PDMS stamp to the polydopamine coated glass slide (Fig. 66b).

Following these results, microcontact printing was employed for thermolysin. Two different approaches were investigated, in the first case (two-step procedure), the polydopamine coating was applied to the glass slides prior to the printing. The PDMS stamp was inked with thermolysin, brought in contact with the surface and left overnight (Fig. 67a). A one-step procedure was also investigated, in this case, the PDMS stamp was directly inked with a solution of both dopamine and thermolysin, brought in contact with a clean glass slide and left overnight (Fig. 67b). This approach was found to be more convenient for the sequential printing of different enzymes.

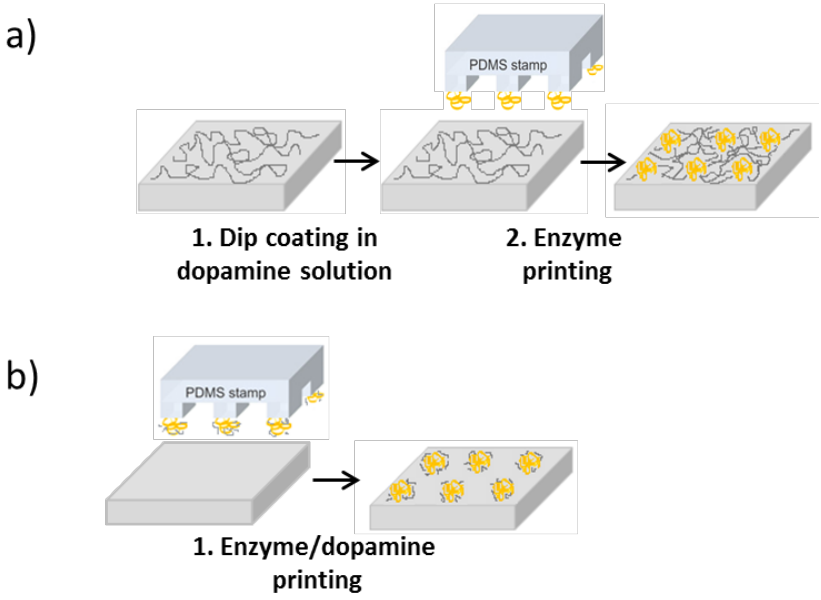

Figure 67 a) Two-step procedure for the enzyme patterning by microcontact printing. Firstly, the polydopamine coating is formed on the glass slide by dip coating. The pattern of enzymes is then transferred onto the surface by bringing the PDMS stamp inked with the enzyme solution in conformal contact with the surface. b) One-step procedure for the enzyme patterning by microcontact printing. The PDMS stamp is inked with a solution of dopamine and enzyme and is then brought in contact with a clean glass slide.

Both the samples created with the two-step procedure and those prepared with the one-step procedure were used to verify the possibility of catalysing the localised formation of self-assembled structures with the immobilised enzymes; Fmoc-T and F-NH_2 were again used as precursors for this study.

Williams *et al.* partially functionalised a glass slide with enzymes, cross-linking thermolysin to an amine-terminated surface and proved that the formation of the self-assembled

structures occurred exclusively on the side of the slide where the enzyme was present.[79] The aim of the study described in this Chapter is to design a pattern of enzymes on the glass substrate. It is expected that the localised formation of self-assembled structures occurs only in proximity of the spots where the enzymes are immobilised due to the low solubility of the assembled material. In order to prove this, a solution containing the non-assembling precursors Fmoc-T and F-NH_2 was prepared and the dye Thioflavin T (ThT) was added to the solution. The shift in the fluorescence emission maximum of ThT and an increase in the fluorescence signal can be exploited to detect the presence of β-sheet structures by fluorescence microscopy (section 6.4.3). The precursor/ThT solution was poured on top of the slides (both those prepared with the two-step procedure and those prepared with the one-step procedure) and left overnight. The slides were then gently rinsed and the images of ThT stained fibres were acquired using fluorescence microscopy. The fluorescence images in Fig. 68 and 69 show for both samples the formation of bright fluorescence spots indicating the presence of β-sheet structures corresponding to the patterned enzymes. The samples prepared with the one-step procedure clearly show bright circular spots and a uniform dark background where the dopamine/enzyme solution was not printed (Fig. 69). The samples prepared with the two-step procedure show a characteristically brighter ring around the spots where the enzymes were immobilised (Fig. 68d, 68e, 68f). This could be due to an uneven pressure applied to the stamp during the printing or to drying effects (coffee stain effect). In these images, it can be clearly seen how bundles of fibres grow radially starting from the centre of the patterns. The self-assembled structures are then likely adhering to the polydopamine coating, even upon rinsing. Moreover, the polydopamine coating itself gives a slightly worse contrast compared to the bare glass.

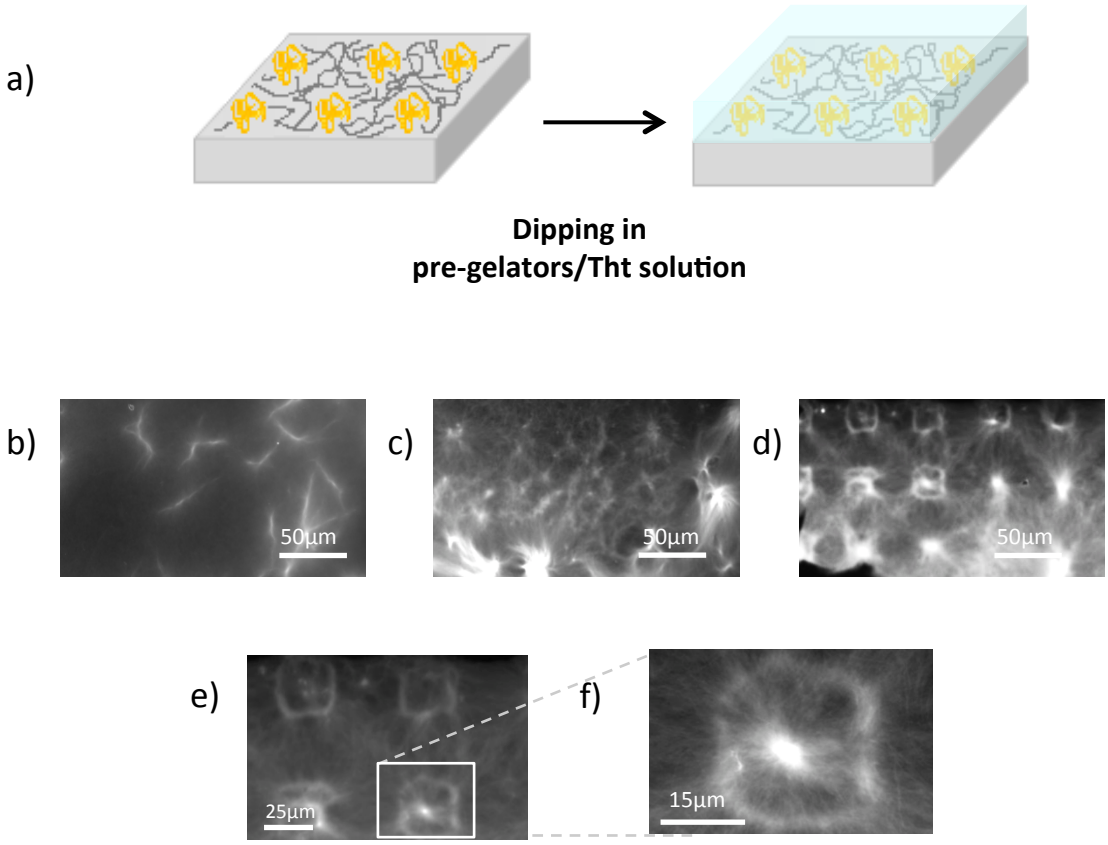

Figure 68 a) After the two-step enzyme immobilisation, the slides are dipped in a solution containing the pre-gelators. ThT was used to stain amyloid-like fibres. b) Fluorescence image of the sample before the rinsing step. Before rinsing, the images show a bright fluorescence signal on the whole surface and no pattern can be observed. c), d) Fluorescence images of the sample after the first (c) and the second (d) rinsing step (10x magnification). Upon rinsing, the pattern becomes clearer and the images show the localised formation of fibres growing from the immobilised enzymes. e), f) Fluorescence images of the sample after the second rinsing step, at higher magnifications (20x and 50x).

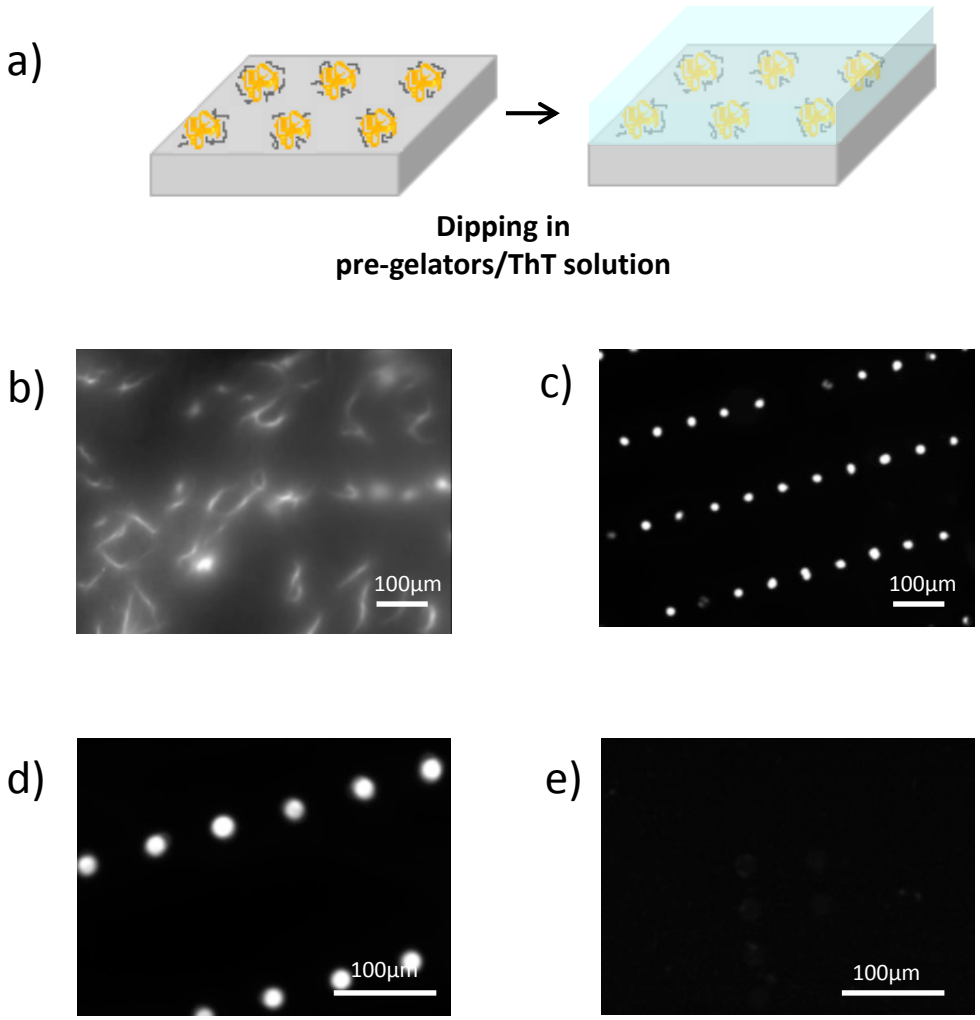

Figure 69 After the one-step enzyme immobilisation, the slides are dipped in a solution containing the pre-gelators. ThT was used to stain β-sheets. b) Fluorescence image of the sample before the rinsing step. Before rinsing, the images show a bright fluorescence signal on the whole surface and no pattern can be observed. c), d) Fluorescence images of the sample after the first rinsing step, at two different magnifications (10x and 20x). Upon rinsing, the pattern becomes clearer and the images show bright fluorescence spots indicating β-sheets formation corresponding to the immobilised enzymes. e) Control sample prepared staining with ThT the printed enzymes.

6.3. Conclusions

A soft-lithographic technique (microcontact printing) was used to pattern thermolysin on a substrate. A PDMS stamp was prepared from a silicon wafer and subsequently used to transfer a pattern of enzymes on the substrate. Two different approaches were investigated. In the two-step approach, thermolysin was patterned on a polydopamine coated glass slide. In the one-step approach, a solution containing dopamine and

thermolysin was directly printed on a clean glass slide. In both cases, the surfaces with the patterned thermolysin were used to trigger the formation and subsequent self-assembly of Fmoc-TF-NH_2 into a fibrous structure. The formation of β-sheet fibres was detected by fluorescence microscopy by staining the self-assembled structures with ThT. The fluorescence images confirmed the localised formation of fibres, corresponding to the spots where the enzymes were immobilised. Although fluorescence microscopy was successfully employed to obtain images of the localised formation of self-assembled structures, a few reproducibility issues arose when visualising the samples. These problems were mainly due to the rinsing step that was performed prior to imaging the samples (see Section 6.4.5).

The results displayed in this Chapter are the best examples achieved with this procedure, but they were obtained following numerous attempts. A significant effort was made to keep the experimental conditions constant in order to try to reproduce these results. Slight modifications to the rinsing procedure (such as precisely timing the rising step, employing a controlled flow of water instead of dipping the samples in water or even eliminating the rinsing step) were applied, trying to optimise the imaging step. This turned out to be particularly difficult to control manually and resulted in images showing either a too high or a too low fluorescence signal. It was then concluded that there is scope for improving this procedure, perhaps trying to employ devices that allow the automatisation of the washing procedure. As an alternative, different microscope set-ups could be employed, such as a water-immersion objective, which would allow to visualize the wet samples without any rinsing or drying steps required.

6.4. Experimental

All reagents, including the peptides, were purchased from commercial sources (*e.g.* Sigma Aldrich, Bachem) at the highest purity and were used as supplied, unless stated otherwise in the experimental procedures. All solvents were used as supplied (analytical or HPLC grade) without further purification. All the experiments were performed at room temperature unless stated otherwise in the experimental procedures. Room temperature in the laboratory may have varied between 20 and 25 °C.

6.4.1. Preparation of PDMS Stamps

The two-part silicon elastomer Sylgard® 184 (Dow Corning, dual cartridge kit) was used for the preparation of the stamps. The silicon wafers used as templates were provided by Dr. K. H. Aaron Lau. The pattern on the silicon wafers consists of arrays of holes of 25 µm of diameter and 30 µm of depth. This pattern is the negative image of the pattern transferred to the PDMS stamps, which will hence consist of arrays of pillars of 25 µm of diameter and 30µm of height. Different spacing between the holes in the silicon templates (25x25 µm, 50x50 µm, 100x100 µm, 50x80 µm, 60x150 µm) gave rise to different geometries on the PDMS stamps. The silicon wafers were cleaned by sonication in toluene (10 min) and in ethanol (10 min) and subsequently dried and placed in a plastic petri dish. The silicon elastomer was poured on top of the wafers with the aid of a manual applicator to ensure the two parts were mixed homogeneously and to maintain a 1:10 ratio between the two parts. The wafers were then placed into a vacuum oven, setting the temperature at 30 °C and left to cure overnight. The PDMS stamps were finally cut to the desired size.

6.4.2. Protein Patterning

- **Two-Step Procedure**

The PDMS stamps prepared according to the procedure described in section 6.4.1 were cleaned by sonication for 10 min in a surfactant solution (2% Hellmanex™ , Sigma Aldrich, UK), rinsed multiple times with ultrapure water and with ethanol and dried. The stamps were then cleaned in an oxygen plasma cleaner in order to improve the wettability of the surface by the enzyme aqueous solution. The stamps were treated in a plasma chamber (Electronic Diener Plasma Surface Technology) for 30 s with a power of 30W. Immediately

following, the protein solution (FITC-BSA or thermolysin, 0.1 mg/ml in 100 mM pH8 sodium phosphate buffer) was poured on top of the PDMS stamp. After 1 h, the excess of protein solution was removed with a nitrogen flow and the stamp was brought in conformal contact with the freshly prepared polydopamine coated glass slide and left overnight. The stamp was carefully lifted off the surface. The slide with immobilised FITC-BSA was gently rinsed in ultrapure water and dried with nitrogen flow. The slide with the immobilised thermolysin was dipped in 100 mM pH8 buffer and placed on an orbital shaker for 30min to aid the solubilisation of any loosely adsorbed enzyme. The slide was then rinsed with ultrapure water and gently dried with nitrogen flow.

- **One-Step Procedure**

The PDMS stamps prepared according to the procedure described in section 6.4.1 and cleaned as described in the previous section. A mixture of thermolysin (0.1 mg/ml in 100 mM pH8 sodium phosphate buffer) and dopamine (0.1 mg/ml in 10 mM pH8.5 TRIS buffer) was poured on top of the PDMS stamp. After 1h, the excess of solution was removed with a nitrogen flow and the stamp was brought in conformal contact with a glass slide and left overnight (the glass slide was previously cleaned with Hellmanex^{TM} as described in section 6.4.2). The stamp was carefully lifted off the surface. The slide with the immobilised thermolysin was dipped in 100 mM pH8 buffer and placed on an orbital shaker for 30 min to aid the solubilisation of any loosely adsorbed enzyme. The slide was then rinsed with ultrapure water and gently dried with nitrogen flow.

6.4.3. Localised Fibre Formation Catalysed by Patterned Enzymes

A solution containing the non-assembling precursors Fmoc-T (Sigma Aldrich) and F-NH_2 (Bachem) (10 mM and 40 mM respectively, in 100mM pH8 phosphate buffer) was prepared. Thioflavin T (ThT, Sigma) was dissolved in ultrapure water and added to the precursors solution to a final concentration of 1 µM. 100 µL of this mixture were poured on top of the glass slide with patterned thermolysin and left overnight. The slide was placed in a humidity chamber to avoid solvent evaporation.

6.4.4. General Procedure for the Preparation of a Fmoc-TF-NH_2 Gel

Samples of Fmoc-TF-NH_2 were prepared dissolving the precursors Fmoc-T (Sigma Aldrich) and F-NH_2 (Bachem) (0.01 M and 0.04 M respectively) in 100 mM pH8 phosphate buffer and adding to the mixture thermolysin to a final concentration of 1 mg/mL. The samples were vortexed and sonicated and left 30 min to equilibrate.

6.4.5. Optical Imaging

The samples prepared as described in Section 6.4.3 were gently washed by immersion into ultra pure water prior to optical imaging, to remove excess material. Images of ThT stained fibres were acquired using a fluorescence microscope (Nikon eclipse LV 100). Different objectives were used to visualise the samples at different magnifications (Nikon LU Plan Flour 10x/0.30 A, WD 15; Nikon LU Plan Fluor 20x/0.40 A, WD 13; Nikon LU Plan ELWD 50x/0.55 B WD 9.8).

A combination of three optical filters consisting of an excitation optical filter of 438/22 nm, a dichromatic mirror 458 nm and a filter for detection of the fluorescence at 483/32 nm were incorporated in a filter cube. The images were recorded with a black and white Photometric Coolsnap HQ camera.

7. Conclusions and Future Work

7.1. Conclusions

In this work, two different approaches to direct the self-assembly in peptide based systems have been presented, one based on mechanical response (Chapter 3) and the other on biocatalytic self-assembly triggered by immobilised enzymes (Chapters 4 to 6).

In Chapter 3, the first instance of the gelation in predominantly aqueous media by the well-known dipeptide diphenylalanine and its amidated derivative was reported. By sonication of the dipeptide solutions, unstable kinetically trapped hydrogels were produced. The gels exhibited extreme syneresis upon mechanical stimulation, despite this the collapsed structures maintained gel-like properties. Due to their rapid supramolecular collapse and the highly hydrophobic nature of the fibres formed, the gels were employed as selective scavengers for a small hydrophobic molecule.

The work carried out in Chapters 4 to 6 investigated different approaches to achieve localised self-assembly of peptide derivatives employing immobilised enzymes. In Chapter 4, polydopamine and novel polyphenol surface coatings were described for the immobilisation of thermolysin. Subsequently, it was demonstrated that surface-mediated bulk gelation is not due to enzymes immobilised on the surface, but rather enzymes released into a pre-gelator solution. It was shown that enzymes may be reversibly and irreversibly immobilised on a surface and that the relative amounts of these populations may be controlled by the sample surface treatment (rinsing).

The results obtained in Chapter 4 show that enzyme immobilization can allow for a highly controlled process in which the self-assembly is localised in the vicinity of the enzyme. Following these fundamental results, two methodologies were developed to achieve a new level of spatial control of nucleation and growth of biocatalytic self-assembling systems and to visualize the localized self-assembled nanostructures. In Chapter 5, this was achieved by employing, for the first time, enzymes immobilised on magnetic nanoparticles. This approach was generalised for an equilibrium (System 1) and a non-equilibrium system (System 2); in both systems, the self-assembly of the peptide-based gelators resulted in the

formation of stable hydrogels. In particular, this approach allowed for the stabilisation of the gelator formed in System 2, which is transient when formed with the free enzyme in solution but it is stable for several weeks when formed with the enzyme-nanoparticles conjugates. For both gels, electron microscopy images clearly demonstrated how the growth of the self-assembled structures were initiated by the enzyme-nanoparticle conjugates. Exploiting the magnetic properties of the nanoparticles, the shape of the gel was manipulated with an external magnetic filed, inducing an externally controlled reduction of volume over time, thus, introducing an additional level of control to modify the final properties of the gel.

Finally, in Chapter 6 a soft-lithographic technique (microcontact printing) was employed to pattern thermolysin onto a polydopamine coated substrate. Two different approaches were investigated. In the two-step approach, thermolysin was patterned on a polydopamine coated glass slide. In the one-step approach however, a solution containing dopamine and thermolysin was directly printed on a clean glass slide. In both cases, the thermolysin patterned surfaces were used to trigger the formation and subsequent the self-assembly of Fmoc-TF-NH_2 into a fibrous structure. Fluorescence microscopy was employed to confirm the localised formation of ThT-stained self-assembled nanostructures, but a few reproducibility issues arose when visualizing the samples, mainly due to the difficulty in keeping the experimental conditions constant. Improvements to the printing procedure were outlined, including the automation of some steps to ensure better reproducibility.

Overall, the findings provided in this thesis offer the next steps towards understanding fundamental principles in biocatalytic self-assembly of peptide-based systems, as well as a method to achieve control over the nucleation and growth of the self-assembled nanostructures and towards future applications in biocatalytic self-assembly driven nanotechnologies.

7.2. Future Work

Following the experimental Chapters of this Thesis, based on the development of different methodologies to direct the self-assembly of peptide amphiphiles and to achieve and visualize the localized enzyme responsive self-assembly of peptide, some questions remain unanswered and a few aspects could be further examined.

In Chapter 3 we described the formation of metastable hydrogels from the dipeptide FF and its amidated form, which exhibited extreme syneresis upon mechanical stimulus. Thanks to this property and to the highly hydrophobic nature of the fibres formed, the gels were employed as selective scavengers for a small hydrophobic molecule. In this thesis, this application was limited to thioflavin T, but with further investigation this property could be generalised for different types of hydrophobic molecules with potential application as a simple and fast procedure to separate organic contaminants from aqueous solutions.

In Chapters 4 and 5 we investigated the effect of enzyme localization on the self-assembly of peptide derivatives. In Chapter 4 we provided an important proof of concept towards understanding fundamental principles in biocatalytic self-assembly of peptide-based systems, which was the foundation for the research carried on in the following chapters. We demonstrated the localised formation of nanofibres triggered by surface-confined enzymes. These modified surfaces might find application as 2D substrates for cell culture, since the nanofibres on the surface could allow for better cell adhesion and spreading compared to conventional 2D substrates.

In Chapter 5 we employed enzyme immobilized on magnetic nanoparticles to trigger the self-assembly of peptide derivatives and subsequent hydrogelation. The magnetic properties of the nanoparticles were exploited to externally manipulate the gels. We demonstrated that the external magnetic field caused a significant reduction of the hydrogel volume and subsequent separation of the aqueous supernatant, with the magnetic nanoparticles trapped in the gel. With further functionalisation of the nanoparticles to target specific molecules, these systems could be applied for on-demand and selective entrapment and removal of unwanted substances on aqueous solutions.

In Chapter 6 we developed a method to visualize the localized enzyme-triggered nanostructure formation by exploiting a patterning technique. Although fluorescence

microscopy was successfully employed to obtain images of the localized formation of β-sheet structures, a few reproducibility issues arose when visualizing the samples. These problems were mainly due to the rinsing step that was performed prior to imaging the samples (see section 6.4.5). In order to address these issues, different experimental set-ups could be investigated. For example, a water immersion objective could be employed to visualize the β-sheet formation (Fig. 70). In this set-up, a solution containing the precursors and ThT could be poured on top of a glass slide with the patterned enzymes and the water immersion objective could be directly dipped in the solution, thus eliminating the rinsing step that may disturb the assembled structures. Moreover, dipping the objective in the precursor solution prior to the formation of the self-assembled structures might allow for the visualization of the early stages of β-sheet formation.

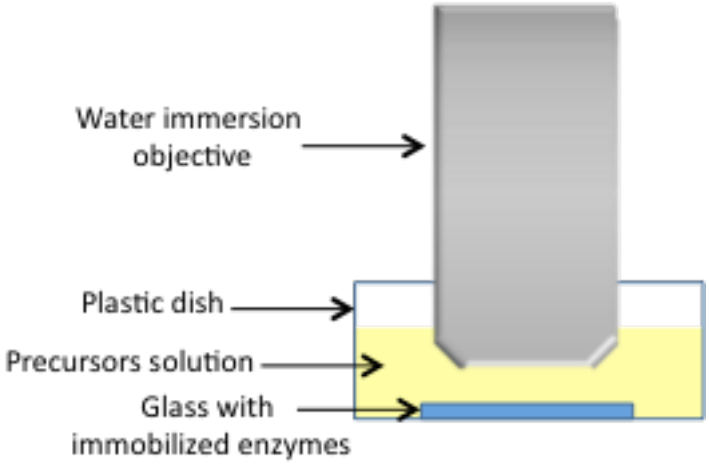

Figure 70 Proposed fluorescence microscope set-up. The glass slide is secured in a plastic dish and covered with a precursors solution. The water immersion objective is then directly dipped in the solution.

A way forward with these systems could be to move from micro-patterning of enzymes to nano-patterning and to employ high resolution microscopy and AMF techniques to visualise the nanostructure formation. Different techniques for patterning enzymes could be employed to achieve a better control and a higher resolution of the patterned areas. A promising option could be thermochemical nanolithography (TCNL). As we discussed in the Literature Review, this technique allows high resolution patterning of chemical functionalities on solid supports and has been previously employed to fabricate protein nano-arrays. [165]

While not discussed in this thesis, a preliminary study employing this technique for enzyme patterning was initiated and the results are the subject of further, ongoing research (in collaboration with Elisa Riedo's lab) (Fig. 71 and 72).

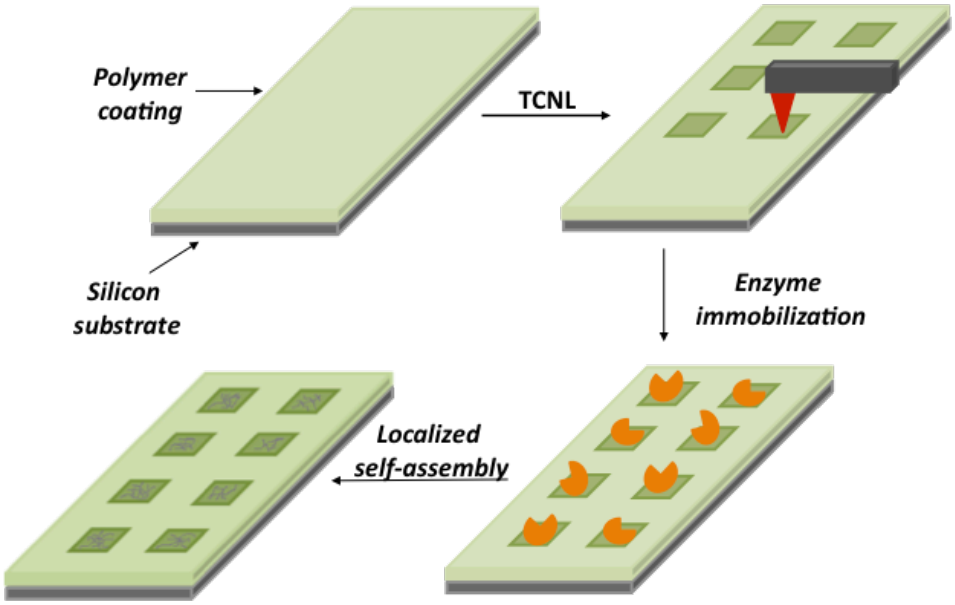

Figure 71 Schematics of TCNL for enzyme patterning and localised self-assembly. The heated AFM tip exposes patterns of reactive amines on the solid support. The enzymes are cross-linked to the amines and the solid support is covered with a solution containing the pregelators. The conversion of the pre-gelators and subsequent self-assembly is expected to be initiated by the patterned enzymes

Significant effort was required for the standardisation of the TCNL procedure, including AFM calibration and optimisation of the microscope layout, customisation of the software program to direct the patterning and optimisation of the voltage applied to realise the pattern. This standardisation procedure was necessary to achieve the optimal degree of chemical activation of the patterned areas of the solid support to allow for enzyme conjugation and to minimise non-specific absorption.

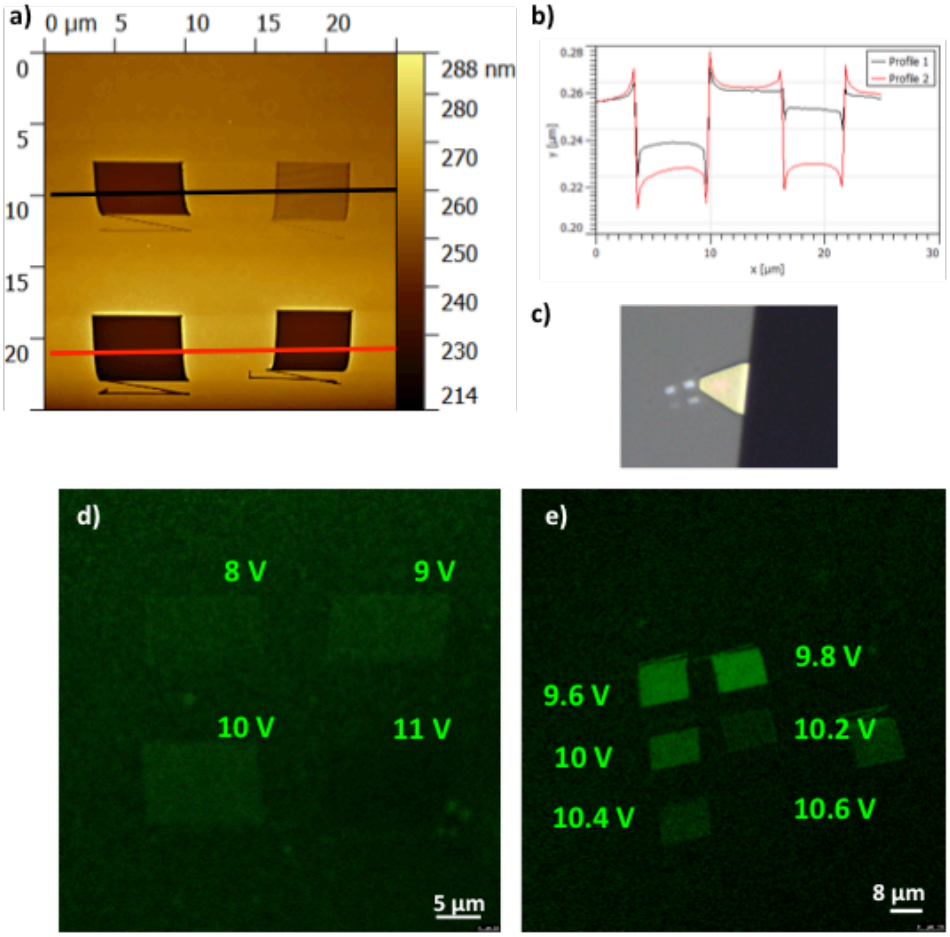

Figure 72 a) AFM topography image of the patterns of amines chemically exposed on the polymeric solid support. b) Dept profile of the patterns shown in figure a. c) Photographic image of the pattern and the AFM tip as seen from the camera integrated in the microscope set-up. d) and e) Fluorescence images obtained cross-linking the fluorophore Alexa-488-NHS to the deprotected amines on the surface. The different intensity of fluorescence illustrate the relation between deprotection efficiency and the applied voltage.

Following these preliminary studies, it would be interesting to employ TCNL for enzyme nano-patterning and to employ super-resolution fluorescence microscopy combined with AFM methods to characterise the enzyme-triggered nanostructure formation in real time. This approach would enable systematic investigation into fundamental aspects of bio-catalytic self-assembly at the nanoscale. Moreover, a further development of this technique could be the realisation of multi-enzymatic systems, which could produce highly complex structural assemblies. This approach could eventually enable the fabrication of multifunctional nanostructures with potential applications in nanotechnology and material science, and for the next generation synthetic mimics of catalytic self-assembly systems found in nature.

8. References

1. E. Mattia and S. Otto, *Nature Nanotechnology*, 2015, **10**, 111-119.

2. L. Pauling and R. B. Corey, *Proceedings of the National Academy of Sciences*, 1951, **37**, 251-256.

3. L. Pauling and R. B. Corey, *Nature*, 1953, **171**, 59-61.

4. J. D. Hartgerink, E. Beniash and S. I. Stupp, *Science*, 2001, **294**, 1684-1688.

5. R. Vegners, I. Shestakova, I. Kalvinsh, R. M. Ezzell and P. A. Janmey, *Journal of Peptide Science*, 1995, **1**, 371-378.

6. M. Reches and E. Gazit, *Science*, 2003, **300**, 625-627.

7. J. M. A. Carnall, C. A. Waudby, A. M. Belenguer, M. C. A. Stuart, J. J.-P. Peyralans and S. Otto, *Science*, 2010, **327**, 1502-1506.

8. M. Xiong, C. Wang, G. Zhang and D. Zhang, in *Functional Molecular Gels*, The Royal Society of Chemistry, 2014, DOI: 10.1039/9781849737371-00067, pp. 67-94.

9. G. O. Lloyd and J. W. Steed, *Nature chemistry*, 2009, **1**, 437-442.

10. Y. Liu, J. L. Terrell, C.-Y. Tsao, H.-C. Wu, V. Javvaji, E. Kim, Y. Cheng, Y. Wang, R. V. Ulijn, S. R. Raghavan, G. W. Rubloff, W. E. Bentley and G. F. Payne, *Advanced Functional Materials*, 2012, **22**, 3004-3012.

11. T. Graham, *Philosophical Transactions of the Royal Society of London*, 1861, **151**, 183-224.

12. P. J. Flory, *Faraday Discussions of the Chemical Society*, 1974, **57**, 7-18.

13. N. Zweep and J. H. van Esch, in *Functional Molecular Gels* Royal Society of Chemistry, 2013, DOI: 10.1039/9781849737371-00001, pp. 1-29.

14. N. M. Sangeetha and U. Maitra, *Chemical Society Reviews*, 2005, **34**, 821-836.

15. J. W. Steed, *Chemical communications*, 2011, **47**, 1379-1383.

16. P. Terech and R. G. Weiss, *Chemical Reviews*, 1997, **97**, 3133-3160.

17. V. J. a. R. V. Ulijn, in *Supramolecular Chemistry: From Molecules to Nanomaterials*, John Wiley and Sons, 2012.

18. Y. M. A.-H. a. R. V. Ulijn, in *Hydrogels in Cell-Based Therapies*, Royal Society of Chemistry, 2014.

19. G. M. Whitesides and B. Grzybowski, *Science*, 2002, **295**, 2418-2421.

20. J. M. Lehn, *Angew. Chem. Int. Ed. Engl.*, 1990, **29**.

21. K. Y. Lee and D. J. Mooney, *Chemical Reviews*, 2001, **101**, 1869-1880.

22. M. Guenther, Gerlach, G., in *Hydrogel Sensor and Actuators* Springer, 2009.

23. X. Zhao, F. Pan, H. Xu, M. Yaseen, H. Shan, C. A. Hauser, S. Zhang and J. R. Lu, *Chem Soc Rev*, 2010, **39**, 3480-3498.

24. M. O. Piepenbrock, G. O. Lloyd, N. Clarke and J. W. Steed, *Chem Rev*, 2010, **110**, 1960-2004.

25. L. A. Estroff and A. D. Hamilton, *Chemical Reviews*, 2004, **104**, 1201-1218.

26. M. Yamanaka, *Journal of Inclusion Phenomena and Macrocyclic Chemistry*, 2013, **77**, 33-48.

27. M. de Loos, B. L. Feringa and J. H. van Esch, *European Journal of Organic Chemistry*, 2005, **2005**, 3615-3631.

28. S. Fleming and R. V. Ulijn, *Chem Soc Rev*, 2014, DOI: 10.1039/c4cs00247d.

29. K. S. K. Hanabusa, K. Hirose, M. Kimura and H. Shirai, *Chemistry Letters*, 1996, **25**.

30. T. Brotin, R. Utermohlen, F. Fages, H. Bouas-Laurent and J.-P. Desvergne, *Journal of the Chemical Society, Chemical Communications*, 1991, DOI: 10.1039/C39910000416, 416-418.

31. H. Kobayashi, A. Friggeri, K. Koumoto, M. Amaike, S. Shinkai and D. N. Reinhoudt, *Organic Letters*, 2002, **4**, 1423-1426.

32. K. Köhler, G. Förster, A. Hauser, B. Dobner, U. F. Heiser, F. Ziethe, W. Richter, F. Steiniger, M. Drechsler, H. Stettin and A. Blume, *Angewandte Chemie International Edition*, 2004, **43**, 245-247.

33. X. Zhao, F. Pan, H. Xu, M. Yaseen, H. Shan, C. A. E. Hauser, S. Zhang and J. R. Lu, *Chemical Society Reviews*, 2010, **39**, 3480-3498.

34. R. V. Ulijn and A. M. Smith, *Chemical Society Reviews*, 2008, **37**, 664-675.

35. M. Hughes, Ph.D. , University of Strathclyde **2012**.

36. J. Jeremy M. Berg, L. Tymoczko, Lubert Stryer, *Biochemistry, 6th ed.*, **2007**.

37. C. A. Schalley, in *Analytical Methods in Supramolecular Chemistry*, Wiley-VCH, 2007.

38. D. D. Eric Anslyn, *Modern Physical Organic Chemistry*, University Science Book, **2006**.

39. C. L. Nesloney and J. W. Kelly, *Bioorganic & Medicinal Chemistry*, 1996, **4**, 739-766.

40. A. Langham, A. Waring and Y. Kaznessis, *BMC Biochemistry*, 2007, **8**, 11.

41. L. S. Birchall, S. Roy, V. Jayawarna, M. Hughes, E. Irvine, G. T. Okorogheye, N. Saudi, E. De Santis, T. Tuttle, A. A. Edwards and R. V. Ulijn, *Chemical Science*, 2011, **2**, 1349-1355.

42. S. A. S.-P. a. R. S. Hodges, *Biochemical and Biophysical Research Communications*, 1976, **72**.

43. D. Eisenberg, W. Wilcox, S. M. Eshita, P. M. Pryciak, S. P. Ho and W. F. Degrado, *Proteins: Structure, Function, and Bioinformatics*, 1986, **1**, 16-22.

44. L. R. W.F. DeGrado, and S.P. Ho, *Cold Spring Harb Symp Quant Biol* 1987, **52**.

45. S. P. Ho and W. F. DeGrado, *Journal of the American Chemical Society*, 1987, **109**, 6751-6758.

46. L. Regan and W. DeGrado, *Science*, 1988, **241**, 976-978.

47. M. R. Ghadiri, J. R. Granja, R. A. Milligan, D. E. McRee and N. Khazanovich, *Nature*, 1993, **366**, 324-327.

48. S. Zhang, T. Holmes, C. Lockshin and A. Rich, *Proceedings of the National Academy of Sciences*, 1993, **90**, 3334-3338.

49. A. Aggeli, M. Bell, N. Boden, J. N. Keen, P. F. Knowles, T. C. B. McLeish, M. Pitkeathly and S. E. Radford, *Nature*, 1997, **386**, 259-262.

50. J. P. Schneider, D. J. Pochan, B. Ozbas, K. Rajagopal, L. Pakstis and J. Kretsinger, *Journal of the American Chemical Society*, 2002, **124**, 15030-15037.

51. M. R. a. E. Gazit, *Physical Biology*, 2006, **3**.

52. W. J. M. FrederixPim, G. G. Scott, Y. M. Abul-Haija, D. Kalafatovic, C. G. Pappas, N. Javid, N. T. Hunt, R. V. Ulijn and T. Tuttle, *Nature chemistry*, 2015, **7**, 30-37.

53. J. D. Hartgerink, E. Beniash and S. I. Stupp, *Proceedings of the National Academy of Sciences of the United States of America*, 2002, **99**, 5133-5138.

54. F. Versluis, H. R. Marsden and A. Kros, *Chemical Society Reviews*, 2010, **39**, 3434-3444.

55. J. C. Stendahl, M. S. Rao, M. O. Guler and S. I. Stupp, *Advanced Functional Materials*, 2006, **16**, 499-508.

56. Y.-C. Yu, M. Tirrell and G. B. Fields, *Journal of the American Chemical Society*, 1998, **120**, 9979-9987.

57. P. Berndt, G. B. Fields and M. Tirrell, *Journal of the American Chemical Society*, 1995, **117**, 9515-9522.

58. H. Cui, M. J. Webber and S. I. Stupp, *Peptide Science*, 2010, **94**, 1-18.

59. A. M. Smith, R. J. Williams, C. Tang, P. Coppo, R. F. Collins, M. L. Turner, A. Saiani and R. V. Ulijn, *Advanced Materials*, 2008, **20**, 37-41.

60. E. K. Johnson, D. J. Adams and P. J. Cameron, *Journal of Materials Chemistry*, 2011, **21**, 2024-2027.

61. A. R. Hirst, S. Roy, M. Arora, A. K. Das, N. Hodson, P. Murray, S. Marshall, N. Javid, J. Sefcik, J. Boekhoven, J. H. van Esch, S. Santabarbara, N. T. Hunt and R. V. Ulijn, *Nature chemistry*, 2010, **2**, 1089-1094.

62. H. Wang, Z. Wang, D. Song, J. Wang, J. Gao, L. Wang, D. Kong and Z. Yang, *Nanotechnology*, 2010, **21**, 155602.

63. M. R. a. E. Gazit, *Israel Journal of Chemistry*, 2005, **45**.

64. Y. Zhang, H. Gu, Z. Yang and B. Xu, *Journal of the American Chemical Society*, 2003, **125**, 13680-13681.

65. T. J. D. Jørgensen, P. Roepstorff and A. J. R. Heck, *Analytical Chemistry*, 1998, **70**, 4427-4432.

66. V. Jayawarna, M. Ali, T. A. Jowitt, A. F. Miller, A. Saiani, J. E. Gough and R. V. Ulijn, *Advanced Materials*, 2006, **18**, 611-614.

67. S. Fleming, S. Debnath, P. W. J. M. Frederix, N. T. Hunt and R. V. Ulijn, *Biomacromolecules*, 2014, DOI: 10.1021/bm401720z.

68. Z. Yang and B. Xu, *Chemical communications*, 2004, DOI: 10.1039/B408897B, 2424-2425.

69. D. M. Ryan, S. B. Anderson, F. T. Senguen, R. E. Youngman and B. L. Nilsson, *Soft Matter*, 2010, **6**, 475-479.

70. H. Xu, A. K. Das, M. Horie, M. S. Shaik, A. M. Smith, Y. Luo, X. Lu, R. Collins, S. Y. Liem, A. Song, P. L. A. Popelier, M. L. Turner, P. Xiao, I. A. Kinloch and R. V. Ulijn, *Nanoscale*, 2010, **2**, 960-966.

71. X. Yang, G. Zhang and D. Zhang, *Journal of Materials Chemistry*, 2012, **22**, 38-50.

72. Z. Yang, H. Gu, D. Fu, P. Gao, J. K. Lam and B. Xu, *Advanced Materials*, 2004, **16**, 1440-1444.

73. B. M. B. a. F. Batista-Viera, in *Methods in Biotechnology: Immobilization of Enzymes and Cells*, ed. H. P. Inc., 2006.

74. D. N. Tran and K. J. Balkus, *ACS Catalysis*, 2011, **1**, 956-968.

75. R. J. Williams, R. J. Mart and R. V. Ulijn, *Peptide Science*, 2010, **94**, 107-117.

76. S. Debnath and R. V. Ulijn, in *Functional Molecular Gels*, The Royal Society of Chemistry, 2013, DOI: 10.1039/9781849737371-00095, ch. 4, pp. 95-116.

77. Z. Yang, H. Gu, Y. Zhang, L. Wang and B. Xu, *Chemical communications*, 2004, DOI: 10.1039/B310574A, 208-209.

78. S. Dos Santos, A. Chandravarkar, B. Mandal, R. Mimna, K. Murat, L. Saucède, P. Tella, G. Tuchscherer and M. Mutter, *Journal of the American Chemical Society*, 2005, **127**, 11888-11889.

79. R. J. Williams, A. M. Smith, R. Collins, N. Hodson, A. K. Das and R. V. Ulijn, *Nature nanotechnology*, 2009, **4**, 19-24.

80. A. K. Das, R. Collins and R. V. Ulijn, *Small*, 2008, **4**, 279-287.

81. Z. Yang, G. Liang and B. Xu, *Soft Matter*, 2007, **3**, 515.

82. K. Thornton, Smith, A. M., Merry C. L. R. and Ulijn, R. V., *Biochemical Society Transactions*, 2009, **37**.

83. S. J. Rowan, S. J. Cantrill, G. R. L. Cousins, J. K. M. Sanders and J. F. Stoddart, *Angewandte Chemie International Edition*, 2002, **41**, 898-952.

84. P. T. Corbett, J. Leclaire, L. Vial, K. R. West, J.-L. Wietor, J. K. M. Sanders and S. Otto, *Chemical Reviews*, 2006, **106**, 3652-3711.

85. S. K. M. Nalluri and R. V. Ulijn, *Chemical Science*, 2013, **4**, 3699.

86. C. G. Pappas, R. Shafi, I. R. Sasselli, H. Siccardi, T. Wang, V. Narang, R. Abzalimov, N. Wijerathne and R. V. Ulijn, *Nat Nano*, 2016, **11**, 960-967.

87. K. H. Smith, E. Tejeda-Montes, M. Poch and A. Mata, *Chemical Society Reviews*, 2011, **40**, 4563-4577.

88. M. Zelzer, S. J. Todd, A. R. Hirst, T. O. McDonald and R. V. Ulijn, *Biomaterials Science*, 2013, **1**, 11-39.

89. R. V. Ulijn, *Journal of Materials Chemistry*, 2006, **16**, 2217-2225.

90. H. S. Azevedo and I. Pashkuleva, *Advanced Drug Delivery Reviews*, 2015, **94**, 63-76.

91. E. A. Phelps, N. Landazuri, P. M. Thule, W. R. Taylor and A. J. Garcia, *Proceedings of the National Academy of Sciences of the United States of America*, 2010, **107**, 3323-3328.

92. J. Patterson and J. A. Hubbell, *Biomaterials*, 2010, **31**, 7836-7845.

93. T. R. Hoare and D. S. Kohane, *Polymer*, 2008, **49**, 1993-2007.

94. L. S. Birchall, R. V. Ulijn and S. J. Webb, *Chemical communications*, 2008, DOI: 10.1039/B805321A, 2861-2863.

95. Y. Gao, Y. Kuang, Z.-F. Guo, Z. Guo, I. J. Krauss and B. Xu, *Journal of the American Chemical Society*, 2009, **131**, 13576-13577.

96. Z. Yang, G. Liang, Z. Guo, Z. Guo and B. Xu, *Angewandte Chemie International Edition*, 2007, **46**, 8216-8219.

97. M. Hughes, S. Debnath, C. W. Knapp and R. V. Ulijn, *Biomaterials Science*, 2013, **1**, 1138-1142.

98. Y. Kuang, J. Shi, J. Li, D. Yuan, K. A. Alberti, Q. Xu and B. Xu, *Angewandte Chemie International Edition*, 2014, **53**, 8104-8107.

99. R. M. Capito, H. S. Azevedo, Y. S. Velichko, A. Mata and S. I. Stupp, *Science*, 2008, **319**, 1812-1816.

100. M. Zhou, A. M. Smith, A. K. Das, N. W. Hodson, R. F. Collins, R. V. Ulijn and J. E. Gough, *Biomaterials*, 2009, **30**, 2523-2530.

101. Enateri V. Alakpa, V. Jayawarna, A. Lampel, Karl V. Burgess, Christopher C. West, Sanne C. J. Bakker, S. Roy, N. Javid, S. Fleming, Dimitris A. Lamprou, J. Yang, A. Miller, Andrew J. Urquhart, Pim W. J. M. Frederix, Neil T. Hunt, B. Péault, Rein V. Ulijn and Matthew J. Dalby, *Chem*, **1**, 512.

102. R. A. Sheldon and S. van Pelt, *Chemical Society Reviews*, 2013, **42**, 6223-6235.

103. M. Hartmann and X. Kostrov, *Chemical Society Reviews*, 2013, **42**, 6277-6289.

104. E. Magner, *Chemical Society Reviews*, 2013, **42**, 6213-6222.

105. Z. Zhou and M. Hartmann, *Top Catal*, 2012, **55**, 1081-1100.

106. S. Datta, L. R. Christena and Y. R. S. Rajaram, *3 Biotech*, 2013, **3**, 1-9.

107. L. Cao, *Carrier-bound Immobilized Enzymes - Principles, Applications and Design*, WILEY-VCH **2005**.

108. J. M. Nelson and E. G. Griffin, *Journal of the American Chemical Society*, 1916, **38**, 1109-1115.

109. R. A. Sheldon, *Advanced Synthesis & Catalysis*, 2007, **349**, 1289-1307.

110. P. Wang, *Current Opinion in Biotechnology*, 2006, **17**, 574-579.

111. S. A. Ansari and Q. Husain, *Biotechnology Advances*, 2012, **30**, 512-523.

112. M. D. Trevan, in *New Protein Techniques*, ed. J. Walker, Humana Press, 1988, vol. 3, ch. 37, pp. 495-510.

113. C. Mateo, V. Grazu, J. M. Palomo, F. Lopez-Gallego, R. Fernandez-Lafuente and J. M. Guisan, *Nat. Protocols*, 2007, **2**, 1022-1033.

114. C. Mateo, O. Abian, M. Bernedo, E. Cuenca, M. Fuentes, G. Fernandez-Lorente, J. M. Palomo, V. Grazu, B. C. C. Pessela, C. Giacomini, G. Irazoqui, A. Villarino, K. Ovsejevi,

F. Batista-Viera, R. Fernandez-Lafuente and J. M. Guisán, *Enzyme and Microbial Technology*, 2005, **37**, 456-462.

115. H. Lee, S. M. Dellatore, W. M. Miller and P. B. Messersmith, *Science*, 2007, **318**, 426-430.

116. D. R. Dreyer, D. J. Miller, B. D. Freeman, D. R. Paul and C. W. Bielawski, *Langmuir : the ACS journal of surfaces and colloids*, 2012, **28**, 6428-6435.

117. J. Liebscher, R. Mrówczyński, H. A. Scheidt, C. Filip, N. D. Hădade, R. Turcu, A. Bende and S. Beck, *Langmuir : the ACS journal of surfaces and colloids*, 2013, **29**, 10539-10548.

118. J. G. Rivera and P. B. Messersmith, *Journal of Separation Science*, 2012, **35**, 1514-1520.

119. A. Ragheb, M. A. Brook and M. Hrynyk, *Chemical communications*, 2003, DOI: 10.1039/B306885D, 2314-2315.

120. H. Y. Wang, T. Kobayashi, H. Saitoh and N. Fujii, *Journal of Applied Polymer Science*, 1996, **60**, 2339-2346.

121. Z.-G. Wang, L.-S. Wan, Z.-M. Liu, X.-J. Huang and Z.-K. Xu, *Journal of Molecular Catalysis B: Enzymatic*, 2009, **56**, 189-195.

122. U. Hanefeld, L. Gardossi and E. Magner, *Chemical Society Reviews*, 2009, **38**, 453-468.

123. T. Subbiah, G. S. Bhat, R. W. Tock, S. Parameswaran and S. S. Ramkumar, *Journal of Applied Polymer Science*, 2005, **96**, 557-569.

124. F. A. Quiocho and F. M. Richards, *Biochemistry*, 1966, **5**, 4062-4076.

125. J. Jegan Roy and T. Emilia Abraham, *Chemical Reviews*, 2004, **104**, 3705-3722.

126. T. Matsunaga and S. Kamiya, *Appl Microbiol Biotechnol*, 1987, **26**, 328-332.

127. Y. L. Khmelnitsky, I. N. Neverova, R. Momtcheva, A. I. Yaropolov, A. B. Belova, A. V. Levashov and K. Martinek, *Biotechnol Tech*, 1989, **3**, 275-280.

128. A. L. Crumbliss, S. C. Perine, J. Stonehuerner, K. R. Tubergen, J. Zhao, R. W. Henkens and J. P. O'Daly, *Biotechnology and Bioengineering*, 1992, **40**, 483-490.

129. J. Kim, J. W. Grate and P. Wang, *Trends in Biotechnology*, 2008, **26**, 639-646.

130. L. Bayne, R. V. Ulijn and P. J. Halling, *Chemical Society Reviews*, 2013, **42**, 9000-9010.

131. M. Verma, C. Barrow and M. Puri, *Appl Microbiol Biotechnol*, 2013, **97**, 23-39.

132. A. A. Vertegel, R. W. Siegel and J. S. Dordick, *Langmuir : the ACS journal of surfaces and colloids*, 2004, **20**, 6800-6807.

133. W. Shang, J. H. Nuffer, V. A. Muñiz-Papandrea, W. Colón, R. W. Siegel and J. S. Dordick, *Small*, 2009, **5**, 470-476.

134. P. Asuri, S. S. Karajanagi, H. Yang, T.-J. Yim, R. S. Kane and J. S. Dordick, *Langmuir : the ACS journal of surfaces and colloids*, 2006, **22**, 5833-5836.

135. W. Shang, J. H. Nuffer, J. S. Dordick and R. W. Siegel, *Nano Letters*, 2007, **7**, 1991-1995.

136. M. Lundqvist, I. Sethson and B.-H. Jonsson, *Langmuir : the ACS journal of surfaces and colloids*, 2004, **20**, 10639-10647.

137. R. M. Blanco, J. J. Calvete and J. Guisán, *Enzyme and Microbial Technology*, 1989, **11**, 353-359.

138. F. López-Gallego, G. Fernandez-Lorente, J. Rocha-Martin, J. Bolivar, C. Mateo and J. Guisan, in *Immobilization of Enzymes and Cells*, ed. J. M. Guisan, Humana Press, 2013, vol. 1051, ch. 5, pp. 59-71.

139. P. M. Mendes, C. L. Yeung and J. A. Preece, *Nanoscale Research Letters*, 2007, **2**, 373-384.

140. K. L. Christman, V. D. Enriquez-Rios and H. D. Maynard, *Soft Matter*, 2006, **2**, 928-939.

141. D. I. Rozkiewicz, W. Brugman, R. M. Kerkhoven, B. J. Ravoo and D. N. Reinhoudt, *Journal of the American Chemical Society*, 2007, **129**, 11593-11599.

142. K. I. Fabijanic, R. Perez-Castillejos and H. Matsui, *Journal of Materials Chemistry*, 2011, **21**, 16877.

143. A. Bernard, J. P. Renault, B. Michel, H. R. Bosshard and E. Delamarche, *Advanced Materials*, 2000, **12**, 1067-1070.

144. A. Schwarz, J. S. Rossier, E. Roulet, N. Mermod, M. A. Roberts and H. H. Girault, *Langmuir : the ACS journal of surfaces and colloids*, 1998, **14**, 5526-5531.

145. M. Escalante, Y. Zhao, M. J. W. Ludden, R. Vermeij, J. D. Olsen, E. Berenschot, C. N. Hunter, J. Huskens, V. Subramaniam and C. Otto, *Journal of the American Chemical Society*, 2008, **130**, 8892-8893.

146. C.-C. Wu, D. N. Reinhoudt, C. Otto, V. Subramaniam and A. H. Velders, *Small*, 2011, **7**, 989-1002.

147. S. Xu and G.-y. Liu, *Langmuir : the ACS journal of surfaces and colloids*, 1997, **13**, 127-129.

148. K. Salaita, Y. Wang and C. A. Mirkin, *Nat Nano*, 2007, **2**, 145-155.

149. A. Kumar and G. M. Whitesides, *Applied Physics Letters*, 1993, **63**, 2002-2004.

150. Y. a. W. Xia, G. M. , *Annu Rev Mater Sci*, 1998, **28**.

151. C. D. James, R. C. Davis, L. Kam, H. G. Craighead, M. Isaacson, J. N. Turner and W. Shain, *Langmuir : the ACS journal of surfaces and colloids*, 1998, **14**, 741-744.

152. A. Bernard, E. Delamarche, H. Schmid, B. Michel, H. R. Bosshard and H. Biebuyck, *Langmuir : the ACS journal of surfaces and colloids*, 1998, **14**, 2225-2229.

153. E. Delamarche, A. Bernard, H. Schmid, B. Michel and H. Biebuyck, *Science*, 1997, **276**, 779-781.

154. E. Delamarche, A. Bernard, H. Schmid, A. Bietsch, B. Michel and H. Biebuyck, *Journal of the American Chemical Society*, 1998, **120**, 500-508.

155. M. Geissler, A. Bernard, A. Bietsch, H. Schmid, B. Michel and E. Delamarche, *Journal of the American Chemical Society*, 2000, **122**, 6303-6304.

156. S. R. Coyer, A. J. García and E. Delamarche, *Angewandte Chemie International Edition*, 2007, **46**, 6837-6840.

157. M. Jaschke and H.-J. Butt, *Langmuir : the ACS journal of surfaces and colloids*, 1995, **11**, 1061-1064.

158. R. D. Piner, J. Zhu, F. Xu, S. Hong and C. A. Mirkin, *Science*, 1999, **283**, 661-663.

159. C. Henderson, in *Encyclopedia of Microfluidics and Nanofluidics*, ed. D. Li, Springer US, 2008, DOI: 10.1007/978-0-387-48998-8_330, ch. 330, pp. 375-379.

160. S. A. M. Carnally and L. S. Wong, *Nanoscale*, 2014, **6**, 4998-5007.

161. J. Hyun, J. Kim, S. L. Craig and A. Chilkoti, *Journal of the American Chemical Society*, 2004, **126**, 4770-4771.

162. K.-B. Lee, J.-H. Lim and C. A. Mirkin, *Journal of the American Chemical Society*, 2003, **125**, 5588-5589.

163. J. D. Gerding, D. M. Willard and A. Van Orden, *Journal of the American Chemical Society*, 2005, **127**, 1106-1107.

164. R. Garcia, A. W. Knoll and E. Riedo, *Nat Nano*, 2014, **9**, 577-587.

165. D. Wang, V. K. Kodali, W. D. Underwood Ii, J. E. Jarvholm, T. Okada, S. C. Jones, M. Rumi, Z. Dai, W. P. King, S. R. Marder, J. E. Curtis and E. Riedo, *Advanced Functional Materials*, 2009, **19**, 3696-3702.

166. K. M. Carroll, A. J. Giordano, D. Wang, V. K. Kodali, J. Scrimgeour, W. P. King, S. R. Marder, E. Riedo and J. E. Curtis, *Langmuir : the ACS journal of surfaces and colloids*, 2013, **29**, 8675-8682.

167. M. Zelzer and R. V. Ulijn, *Chemical Society Reviews*, 2010, **39**, 3351-3357.

168. M. P. Conte, N. Singh, I. R. Sasselli, B. Escuder and R. V. Ulijn, *Chemical communications*, 2016, **52**, 13889-13892.

169. M. J. Webber, E. A. Appel, E. W. Meijer and R. Langer, *Nat Mater*, 2016, **15**, 13-26.

170. T. Aida, E. W. Meijer and S. I. Stupp, *Science*, 2012, **335**, 813-817.

171. R. de La Rica, K. I. Fabijanic, A. Baldi and H. Matsui, *Angewandte Chemie International Edition*, 2010, **49**, 1447-1450.

172. S. Zhang, *Nature Biotechnology*, 2004, **22**.

173. P. W. J. M. Frederix, G. G. Scott, Y. M. Abul-Haija, D. Kalafatovic, C. G. Pappas, N. Javid, N. T. Hunt, R. V. Ulijn and T. Tuttle, *Nature chemistry*, 2015, **7**, 30-37.

174. S. Maity, S. Nir, T. Zada and M. Reches, *Chemical communications*, 2014, **50**, 11154-11157.

175. L. Adler-Abramovich and E. Gazit, *Chemical Society Reviews*, 2014, **43**, 6881-6893.

176. C. H. Görbitz, *Chemistry – A European Journal*, 2001, **7**, 5153-5159.

177. M. Reches and E. Gazit, *Nat Nano*, 2006, **1**, 195-200.

178. L. Adler-Abramovich, M. Reches, V. L. Sedman, S. Allen, S. J. B. Tendler and E. Gazit, *Langmuir : the ACS journal of surfaces and colloids*, 2006, **22**, 1313-1320.

179. P. Tamamis, L. Adler-Abramovich, M. Reches, K. Marshall, P. Sikorski, L. Serpell, E. Gazit and G. Archontis, *Biophysical Journal*, 2009, **96**, 5020-5029.

180. I. Azuri, L. Adler-Abramovich, E. Gazit, O. Hod and L. Kronik, *Journal of the American Chemical Society*, 2014, **136**, 963-969.

181. N. Kol, L. Adler-Abramovich, D. Barlam, R. Z. Shneck, E. Gazit and I. Rousso, *Nano Letters*, 2005, **5**, 1343-1346.

182. X. Yan, P. Zhu and J. Li, *Chemical Society Reviews*, 2010, **39**, 1877-1890.

183. I. W. Hamley, *Angewandte Chemie International Edition*, 2014, **53**, 6866-6881.

184. J. Wang, K. Liu, L. Yan, A. Wang, S. Bai and X. Yan, *ACS Nano*, 2016, DOI: 10.1021/acsnano.5b06567.

185. X. Yan, Y. Cui, Q. He, K. Wang and J. Li, *Chemistry of Materials*, 2008, **20**, 1522-1526.

186. N. S. de Groot, T. Parella, F. X. Aviles, J. Vendrell and S. Ventura, *Biophysical Journal*, 2007, **92**, 1732-1741.

187. Z. Fan, L. Sun, Y. Huang, Y. Wang and M. Zhang, *Nat Nano*, 2016, **11**, 388-394.

188. H. Erdogan, E. Babur, M. Yilmaz, E. Candas, M. Gordesel, Y. Dede, E. E. Oren, G. B. Demirel, M. K. Ozturk, M. S. Yavuz and G. Demirel, *Langmuir : the ACS journal of surfaces and colloids*, 2015, **31**, 7337-7345.

189. J. Raeburn, A. Zamith Cardoso and D. J. Adams, *Chemical Society Reviews*, 2013, **42**, 5143-5156.

190. H.-J. Schneider and R. M. Strongin, *Accounts of Chemical Research*, 2009, **42**, 1489-1500.

191. C. P. McCoy, C. Rooney, C. R. Edwards, D. S. Jones and S. P. Gorman, *Journal of the American Chemical Society*, 2007, **129**, 9572-9573.

192. J. A. Lucey, T. van Vliet, K. Grolle, T. Geurts and P. Walstra, *International Dairy Journal*, 1997, **7**, 389-397.

193. F. Xie, L. Qin and M. Liu, *Chemical communications*, 2016, **52**, 930-933.

194. S.-L. Zhou, S. Matsumoto, H.-D. Tian, H. Yamane, A. Ojida, S. Kiyonaka and I. Hamachi, *Chemistry – A European Journal*, 2005, **11**, 1130-1136.

195. D. J. Adams, L. M. Mullen, M. Berta, L. Chen and W. J. Frith, *Soft Matter*, 2010, **6**, 1971-1980.

196. A. M. Castilla, M. Wallace, L. L. E. Mears, E. R. Draper, J. Doutch, S. Rogers and D. J. Adams, *Soft Matter*, 2016, DOI: 10.1039/C6SM01194B.

197. X. Yu, L. Chen, M. Zhang and T. Yi, *Chemical Society Reviews*, 2014, **43**, 5346-5371.

198. G. Cravotto and P. Cintas, *Chemical Society Reviews*, 2009, **38**, 2684-2697.

199. C. G. Pappas, P. W. J. M. Frederix, T. Mutasa, S. Fleming, Y. M. Abul-Haija, S. M. Kelly, A. Gachagan, D. Kalafatovic, J. Trevino, R. V. Ulijn and S. Bai, *Chemical communications*, 2015, **51**, 8465-8468.

200. C. G. Pappas, T. Mutasa, P. W. J. M. Frederix, S. Fleming, S. Bai, S. Debnath, S. M. Kelly, A. Gachagan and R. V. Ulijn, *Materials Horizons*, 2015, **2**, 198-202.

201. T. Naota and H. Koori, *Journal of the American Chemical Society*, 2005, **127**, 9324-9325.

202. S. Maity, P. Das and M. Reches, *Scientific Reports*, 2015, **5**, 16365.

203. A. Hawe, M. Sutter and W. Jiskoot, *Pharmaceutical Research*, 2008, **25**, 1487-1499.

204. M. Biancalana and S. Koide, *Biochimica et Biophysica Acta (BBA) - Proteins and Proteomics*, 2010, **1804**, 1405-1412.

205. M. Reches and E. Gazit, *Nano Letters*, 2004, **4**, 581-585.

206. V. Jayawarna, S. M. Richardson, A. R. Hirst, N. W. Hodson, A. Saiani, J. E. Gough and R. V. Ulijn, *Acta Biomaterialia*, 2009, **5**, 934-943.

207. S. Fleming, P. W. J. M. Frederix, I. Ramos Sasselli, N. T. Hunt, R. V. Ulijn and T. Tuttle, *Langmuir : the ACS journal of surfaces and colloids*, 2013, **29**, 9510-9515.

208. K. N. N. Berova, R. W. Woody, *Circular Dichroism: Principles and Applications*, Wiley, 2nd Edition edn., **2000**.

209. Q. Li, Y. Jia, L. Dai, Y. Yang and J. Li, *ACS Nano*, 2015, **9**, 2689-2695.

210. G. B. McGaughey, M. Gagné and A. K. Rappé, *Journal of Biological Chemistry*, 1998, **273**, 15458-15463.

211. E. Gazit, *The FASEB Journal*, 2002, **16**, 77-83.

212. M. P. Conte, K. H. A. Lau and R. V. Ulijn, *ACS applied materials & interfaces*, 2017, **9**, 3266-3271.

213. S. Debnath, S. Roy and R. V. Ulijn, *Journal of the American Chemical Society*, 2013, **135**, 16789-16792.

214. R. J. Williams, T. E. Hall, V. Glattauer, J. White, P. J. Pasic, A. B. Sorensen, L. Waddington, K. M. McLean, P. D. Currie and P. G. Hartley, *Biomaterials*, 2011, **32**, 5304-5310.

215. C. Vigier-Carrière, T. Garnier, D. Wagner, P. Lavalle, M. Rabineau, J. Hemmerlé, B. Senger, P. Schaaf, F. Boulmedais and L. Jierry, *Angewandte Chemie International Edition*, 2015, **54**, 10198-10201.

216. R. A. Pires, Y. M. Abul-Haija, D. S. Costa, R. Novoa-Carballal, R. L. Reis, R. V. Ulijn and I. Pashkuleva, *Journal of the American Chemical Society*, 2015, **137**, 576-579.

217. J. Zhou, X. Du, C. Berciu, H. He, J. Shi, D. Nicastro and B. Xu, *Chem*, 2016, **1**, 246-263.

218. D. Kalafatovic, M. Nobis, J. Son, K. I. Anderson and R. V. Ulijn, *Biomaterials*, 2016, **98**, 192-202.

219. Q. Ye, F. Zhou and W. Liu, *Chemical Society Reviews*, 2011, **40**, 4244-4258.

220. T. S. Sileika, D. G. Barrett, R. Zhang, K. H. A. Lau and P. B. Messersmith, *Angewandte Chemie International Edition*, 2013, **52**, 10766-10770.

221. D. R. Dreyer, D. J. Miller, B. D. Freeman, D. R. Paul and C. W. Bielawski, *Chemical Science*, 2013, **4**, 3796-3802.

222. H. Lee, J. Rho and P. B. Messersmith, *Advanced Materials*, 2009, **21**, 431-434.

223. D. G. Barrett, T. S. Sileika and P. B. Messersmith, *Chemical communications*, 2014, **50**, 7265-7268.

224. I. R. Sasselli, C. G. Pappas, E. Matthews, T. Wang, N. T. Hunt, R. V. Ulijn and T. Tuttle, *Soft Matter*, 2016, DOI: 10.1039/C6SM01737A.

225. M. Hughes, P. W. J. M. Frederix, J. Raeburn, L. S. Birchall, J. Sadownik, F. C. Coomer, I. H. Lin, E. J. Cussen, N. T. Hunt, T. Tuttle, S. J. Webb, D. J. Adams and R. V. Ulijn, *Soft Matter*, 2012, **8**, 5595-5602.

226. M.-I. Aguilar, in *HPLC of Peptides and Proteins: Methods and Protocols*

Humana Press Inc., Totowa, NJ, 2004.

227. E. Matayoshi, G. Wang, G. Krafft and J. Erickson, *Science*, 1990, **247**, 954-958.

228. A. G. L. Olive, N. H. Abdullah, I. Ziemecka, E. Mendes, R. Eelkema and J. H. van Esch, *Angewandte Chemie*, 2014, **126**, 4216-4220.

229. Z. Adamczyk and P. Weroński, *The Journal of Chemical Physics*, 1996, **105**, 5562-5573.

230. C. G. Pappas, I. R. Sasselli and R. V. Ulijn, *Angewandte Chemie International Edition*, 2015, **54**, 8119-8123.

231. N. J. Greenfield, *Nature protocols*, 2006, **1**, 2876-2890.

232. Y. Xia and G. M. Whitesides, *Angewandte Chemie International Edition*, 1998, **37**, 550-575.

233. B. D. Gates, Q. Xu, J. C. Love, D. B. Wolfe and G. M. Whitesides, *Annual Review of Materials Research*, 2004, **34**, 339-372.

9. Table of Figures

10. Appendices

10.1. Appendix A - Primary Characterisation of the Compounds Employed in Chapter 3

10.1.1. Reversed-phase High Performance Liquid Chromatography (HPLC)

A Dionex P680 HPLC system was used to analyze the dipeptides. Aliquots of 30 µL were injected with a flow rate of 1 mL min^{-1} into a Macherey-Nagel C-18 column (250 mm of length and 4.6 mm of internal diameter) containing silica particles (diameter: 5 µm, pores diameter: 10 nm). The gradient used was a linear exchange between water/acetonitrile (95:5, 0.1% TFA) at 4 min to water/acetonitrile (5:95, 0.1% TFA) at 35 min. This concentration was kept constant until 40 min when the gradient was decreased to 20% (v/v) acetonitrile in water at 42 min. The intensity of each identified peak was determined by UV detection at 255 nm. The estimated purity from HPLC integrated peak areas was 99.15%, 98.88% and 99.34% respectively for $FFNH_2$, FF and FY.

a)

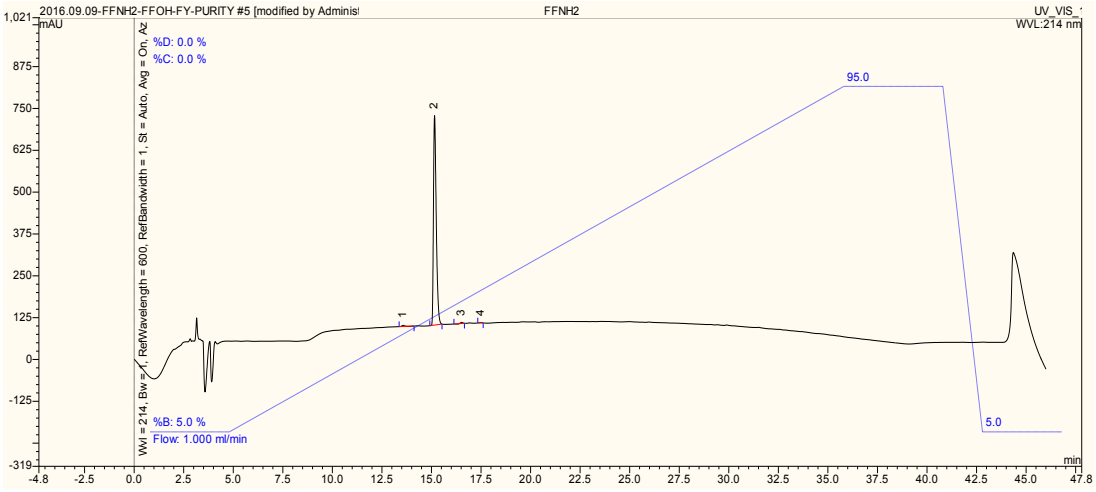

b)

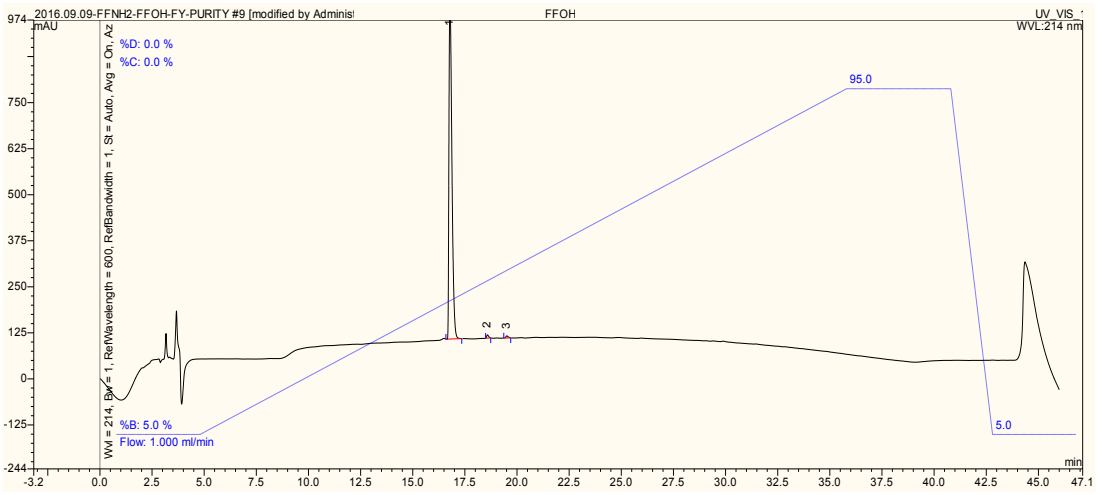

c)

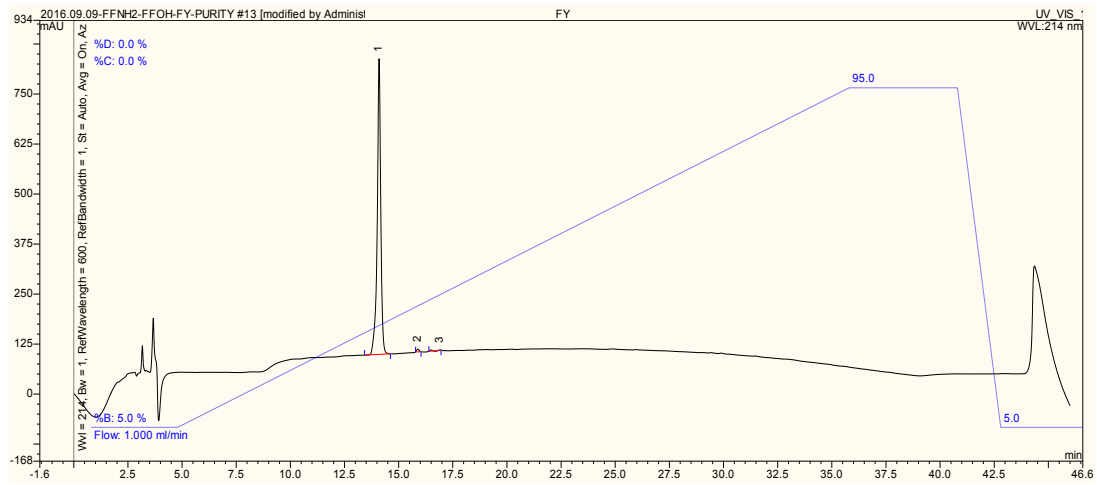

Figure 73 HPLC traces of the dipeptides FFNH2 (a), FF (b) and FY (c).

10.1.2. Nuclear Magnetic Resonance (NMR) Spectroscopy

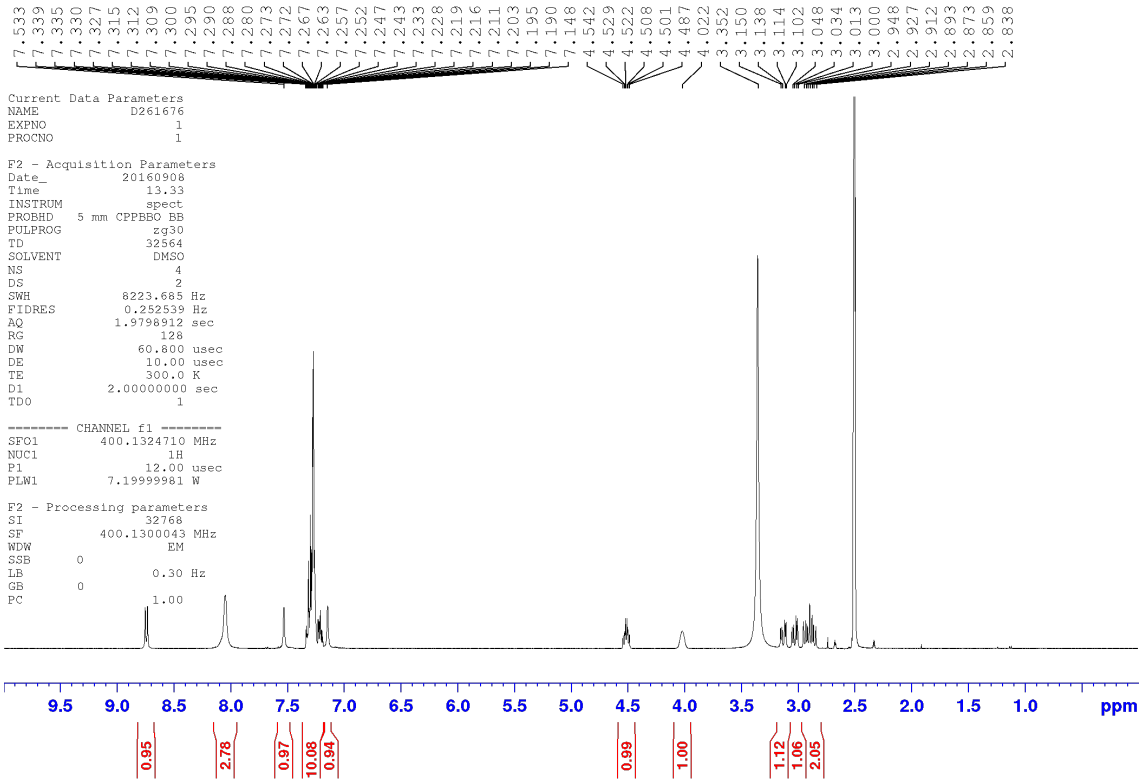

Figure 74 1H NMR of $FFNH_2$ (400 MHz, (CD3)2SO). 8.75 (1 H, d), 8.1 (2 H, s), 7.5 (1 H, s), 7.2-7.35 (10 H, m), 7.15 (1 H, s), 4.5 (1 H, m), 4 (1 H, s), 3.14 (1 H, dd), 3.01 (1 H, dd), 2.9 (2 H, 2dd). The intense peak around 3.4 ppm is due to residual H_2O in the solvent.

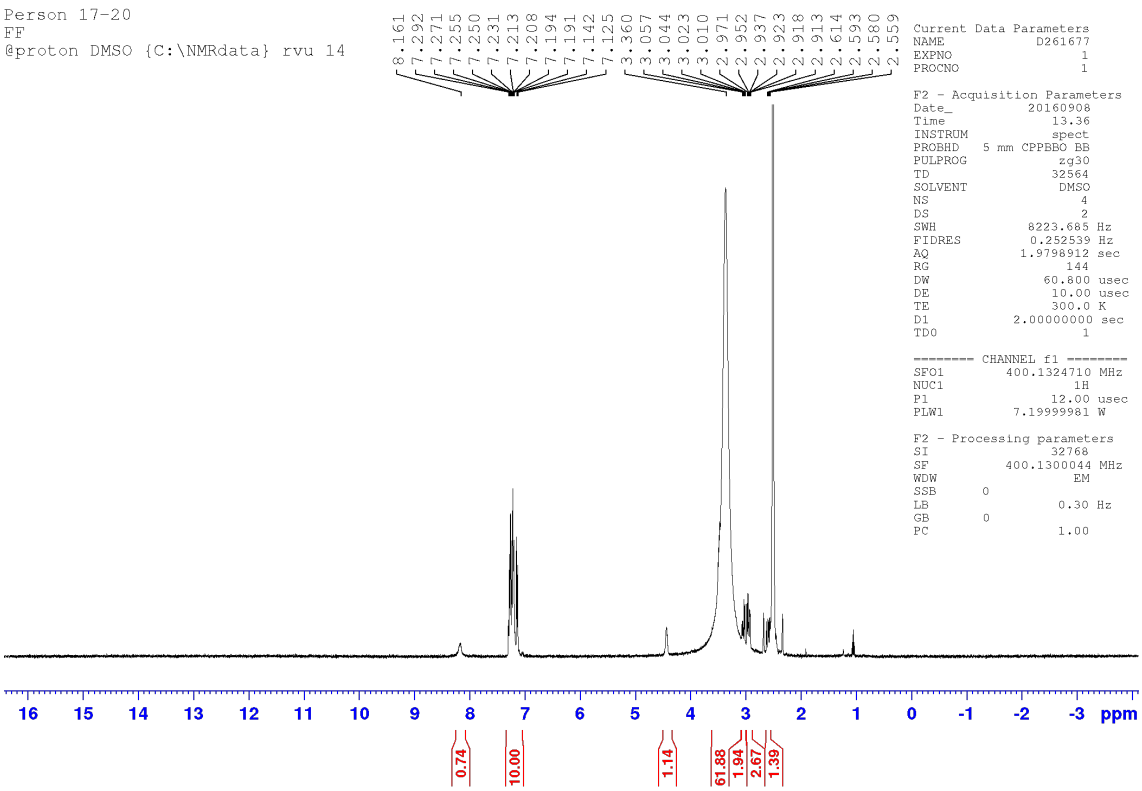

Figure 75 ^{1}H NMR of FF (400 MHz, $(CD_3)_2SO$). 8.2 (1 H, s), 7.2 (10 H, m), 4.5 (1 H, s), 3.02 (1 H, dd), 2.95 (1 H, dd), 2.6 (2 H, 2dd). The intense peak around 3.4 ppm is due to residual H_2O in the solvent.

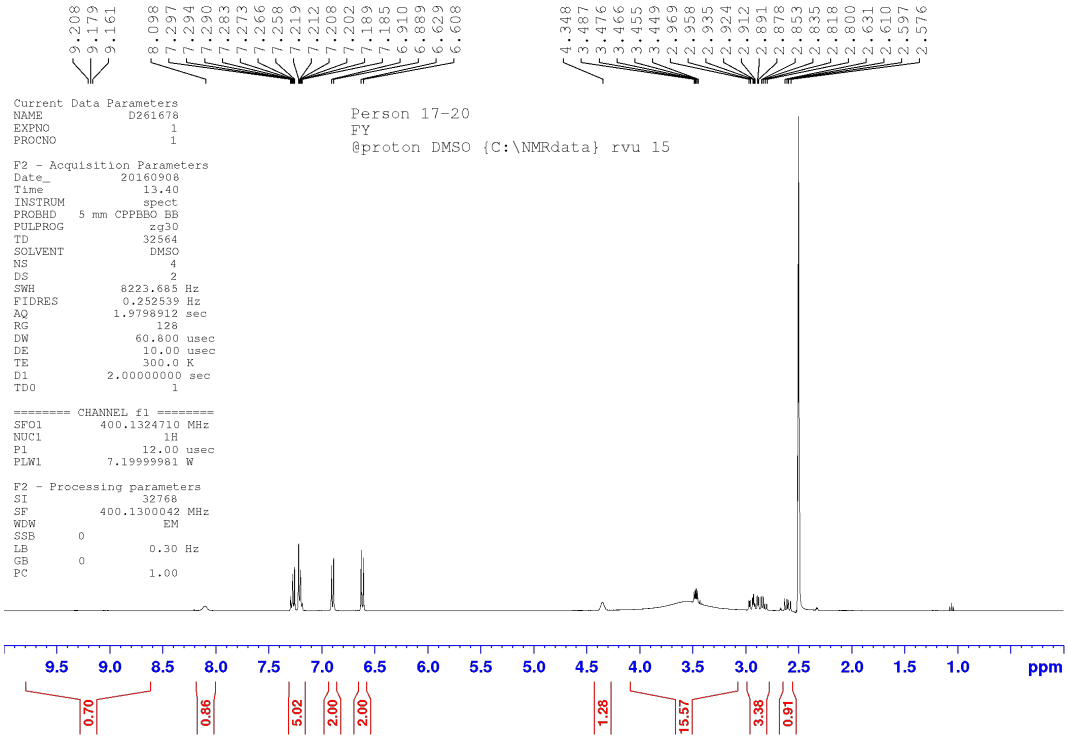

Figure 76 1H NMR of FY (400 MHz, (CD3)2SO). 8.1 (1 H, s), 6.9 (2 H, dd), 7.2-7.3, (5 H, m), 6.6 (2 H, dd), 4.3 (1 H, s), 2.9 (3 H, m), 2.6 (1 H, m).

10.1.3. Liquid Chromatography – Mass Spectroscopy (LCMS)

An Agilent LCMS 6130 single quad dual source mass spec was used to analyse the dipeptides. Aliquots of 10 µL were injected with a flow rate of 1 mL min^{-1} into a Agilent Poroshell 120 EC-C18 4.6mm x75mm x 2.7um. The gradient used was a linear exchange between water/acetonitrile (95:5, 5 mM ammonium acetate) at 1.48 min to water/acetonitrile (0:100, 5 mM ammonium acetate) at 8.5 min. This concentration was kept constant until 13.5 min when the gradient was decreased to 5% (v/v) acetonitrile in water at 16.5 min. The intensity of each identified peak was determined by UV detection at 254 nm. The results of the positive and negative scans are reported for the three dipeptides.

FY: predicted MW = 328.36; experimental (negative scan) = 327.0; experimental (positive scan) = 329.1;

FF: predicted MW = 312.36; experimental (negative scan) = 311.1; experimental (positive scan) = 313.1;

FF-NH_2 predicted MW = 311.38; experimental (negative scan) = 310.1; experimental (positive scan) = 312.0

```
Print of window 80: MS Spectrum
Data File  : D:\DATA\SEPT16\2016-09-08 1\MC_FY.D
Sample Name : MC_FY
======================================================================
Acq. Operator   :                                  Seq. Line :   5
Acq. Instrument : Instrument 1                      Location : Vial 11
Injection Date  : 9/8/2016 3:33:27 PM                    Inj :   1
                                                  Inj Volume : 10.000 µl
Acq. Method     : D:\DATA\SEPT16\2016-09-08 1\PORO_AMMACE_254.M
Last changed    : 2/12/2015 2:09:30 PM
Analysis Method : C:\CHEM32\1\METHODS\REPORTING_PORO2000.M
Last changed    : 9/8/2016 1:42:01 PM
                  (modified after loading)
Additional Info : Peak(s) manually integrated
```

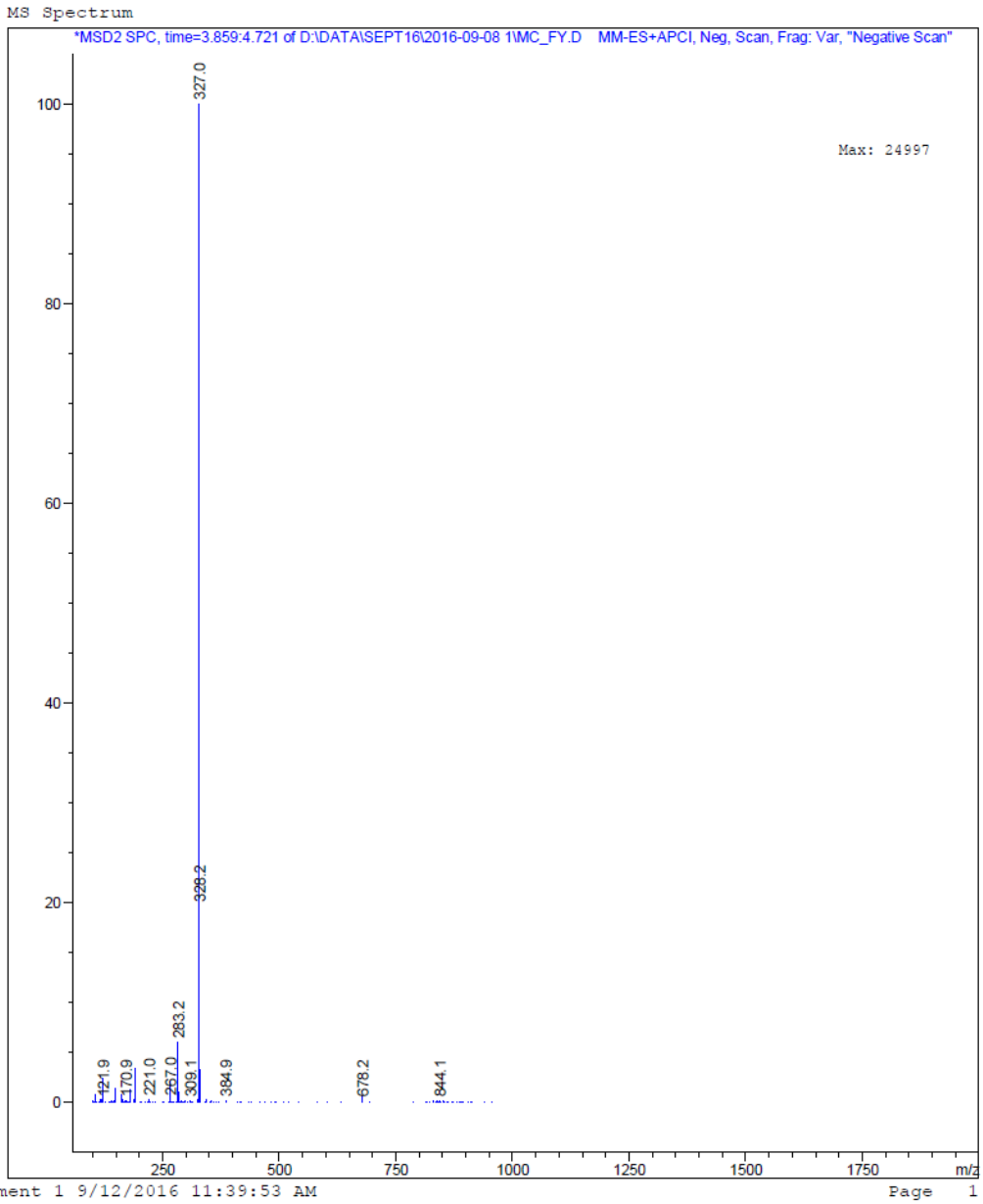


```
Instrument 1 9/12/2016 11:39:53 AM                    Page   1 of 1
```

Figure 77 Negative scan for FY.

```
Print of window 80: MS Spectrum
Data File  : D:\DATA\SEPT16\2016-09-08 1\MC_FY.D
Sample Name : MC_FY
======================================================================
Acq. Operator   :                                  Seq. Line :   5
Acq. Instrument : Instrument 1                      Location : Vial 11
Injection Date  : 9/8/2016 3:33:27 PM                    Inj :   1
                                                  Inj Volume : 10.000 µl
Acq. Method     : D:\DATA\SEPT16\2016-09-08 1\PORO_AMMACE_254.M
Last changed    : 2/12/2015 2:09:30 PM
Analysis Method : C:\CHEM32\1\METHODS\REPORTING_PORO2000.M
Last changed    : 9/8/2016 1:42:01 PM
                  (modified after loading)
Additional Info : Peak(s) manually integrated
```

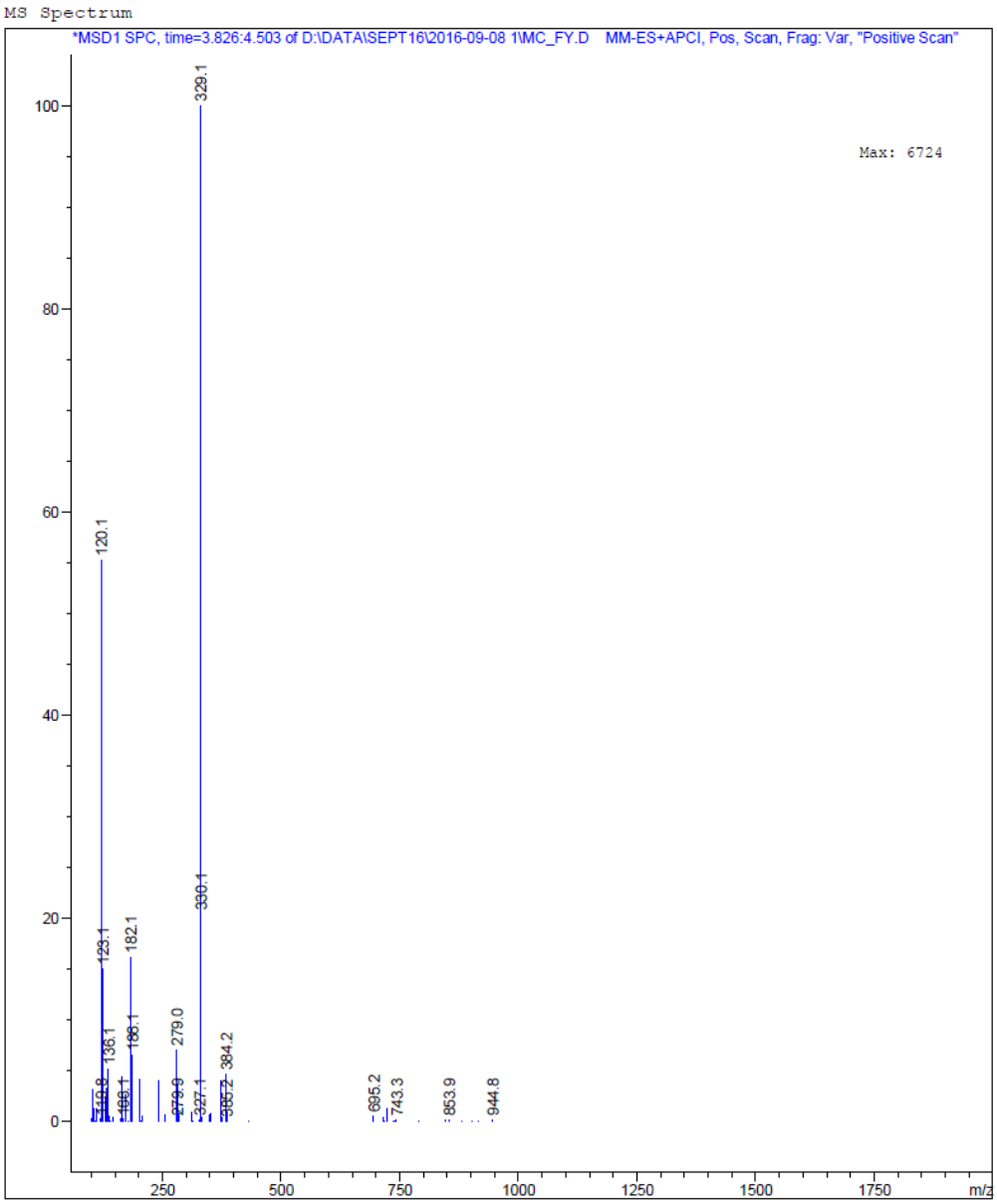


```
Instrument 1 9/12/2016 11:38:51 AM                    Page   1 of 1
```

Figure 78 Positive scan for FY.

```
Print of window 80: MS Spectrum
Data File  : D:\DATA\SEPT16\2016-09-08 1\MC_FF.D
Sample Name : MC_FF
======================================================================
Acq. Operator   :                                  Seq. Line :   4
Acq. Instrument : Instrument 1                      Location : Vial 10
Injection Date  : 9/8/2016 3:13:35 PM                    Inj :   1
                                                  Inj Volume : 10.000 µl
Acq. Method     : D:\DATA\SEPT16\2016-09-08 1\PORO_AMMACE_254.M
Last changed    : 2/12/2015 2:09:30 PM
Analysis Method : C:\CHEM32\1\METHODS\REPORTING_PORO2000.M
Last changed    : 9/8/2016 1:42:01 PM
                  (modified after loading)
Additional Info : Peak(s) manually integrated
```

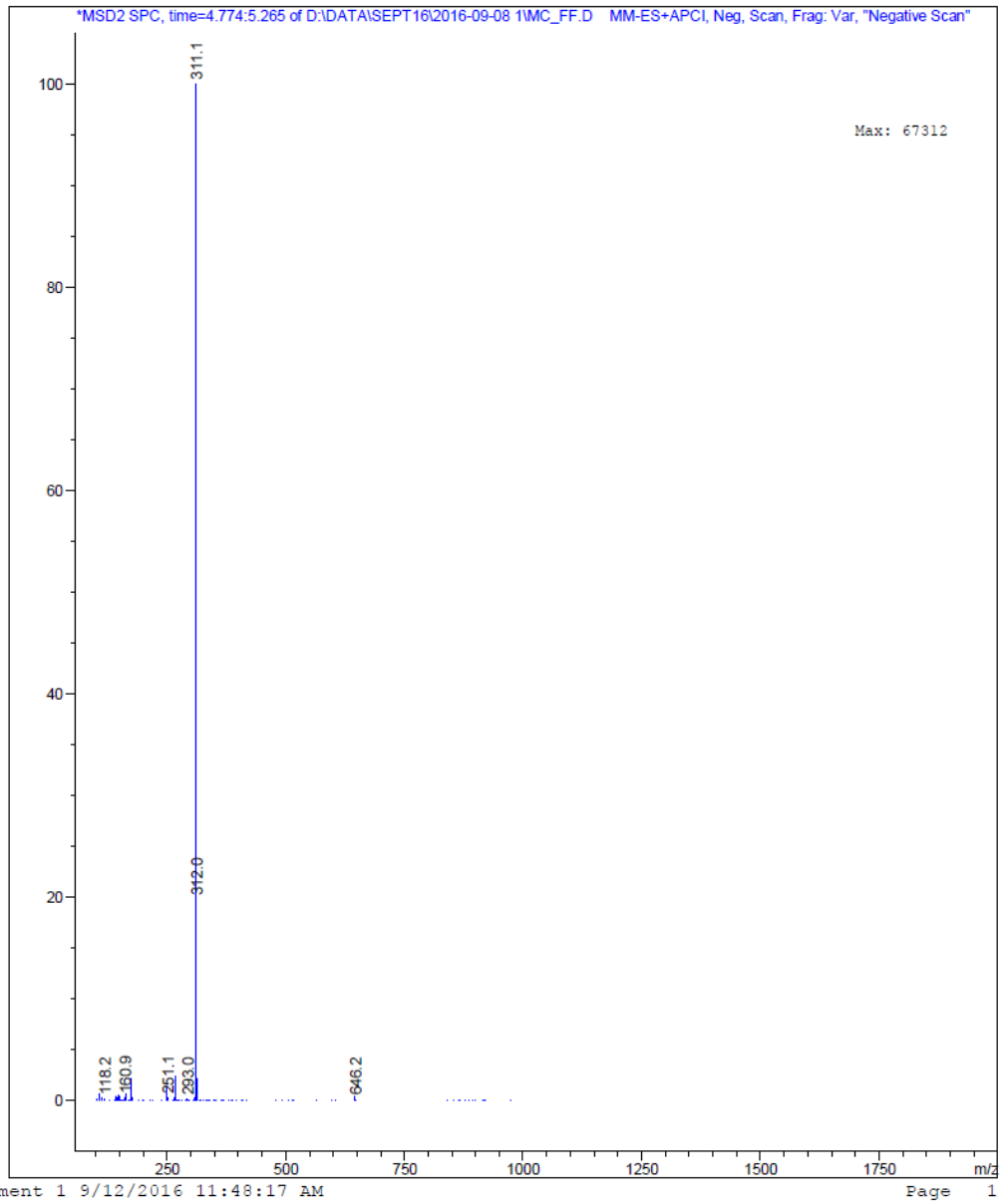


```
Instrument 1 9/12/2016 11:48:17 AM                    Page   1 of 1
```

Figure 79 Negative scan for FF.

```
Print of window 80: MS Spectrum
Data File  : D:\DATA\SEPT16\2016-09-08 1\MC_FF.D
Sample Name : MC_FF
======================================================================
Acq. Operator   :                                  Seq. Line :   4
Acq. Instrument : Instrument 1                      Location : Vial 10
Injection Date  : 9/8/2016 3:13:35 PM                    Inj :   1
                                                  Inj Volume : 10.000 µl
Acq. Method     : D:\DATA\SEPT16\2016-09-08 1\PORO_AMMACE_254.M
Last changed    : 2/12/2015 2:09:30 PM
Analysis Method : C:\CHEM32\1\METHODS\REPORTING_PORO2000.M
Last changed    : 9/8/2016 1:42:01 PM
                  (modified after loading)
Additional Info : Peak(s) manually integrated
```

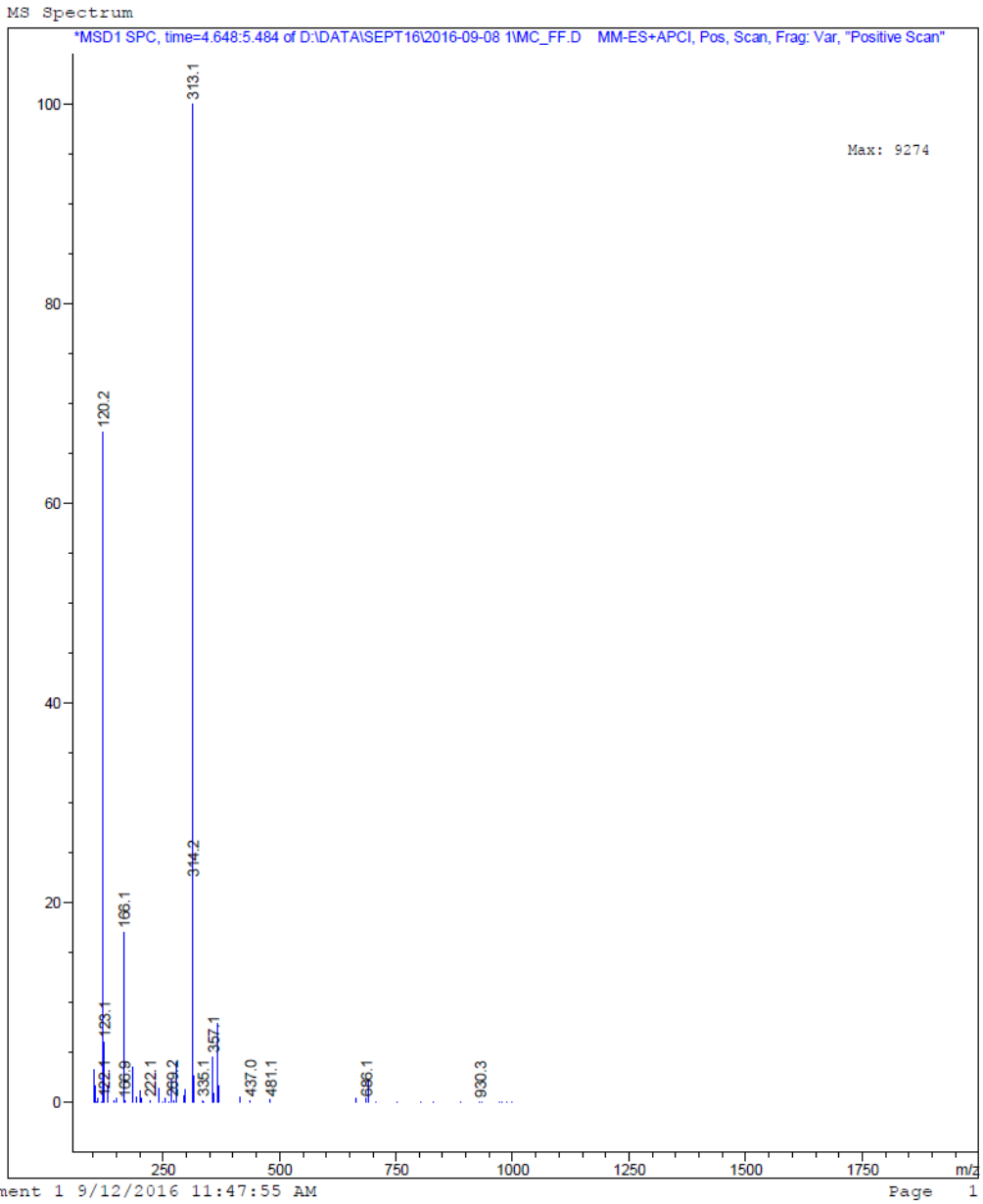


```
Instrument 1 9/12/2016 11:47:55 AM                    Page   1 of 1
```

Figure 80 Positive scan for FF.

```
Print of window 80: MS Spectrum
Data File  : D:\DATA\SEPT16\2016-09-08 1\MC_FFNH2.D
Sample Name : MC_FFNH2
======================================================================
Acq. Operator   :                                Seq. Line :   3
Acq. Instrument : Instrument 1                    Location : Vial 9
Injection Date  : 9/8/2016 2:53:26 PM                 Inj :   1
                                                Inj Volume : 10.000 µl
Acq. Method     : D:\DATA\SEPT16\2016-09-08 1\PORO_AMMACE_254.M
Last changed    : 2/12/2015 2:09:30 PM
Analysis Method : C:\CHEM32\1\METHODS\REPORTING_PORO2000.M
Last changed    : 9/8/2016 1:42:01 PM
                  (modified after loading)
Additional Info : Peak(s) manually integrated
```

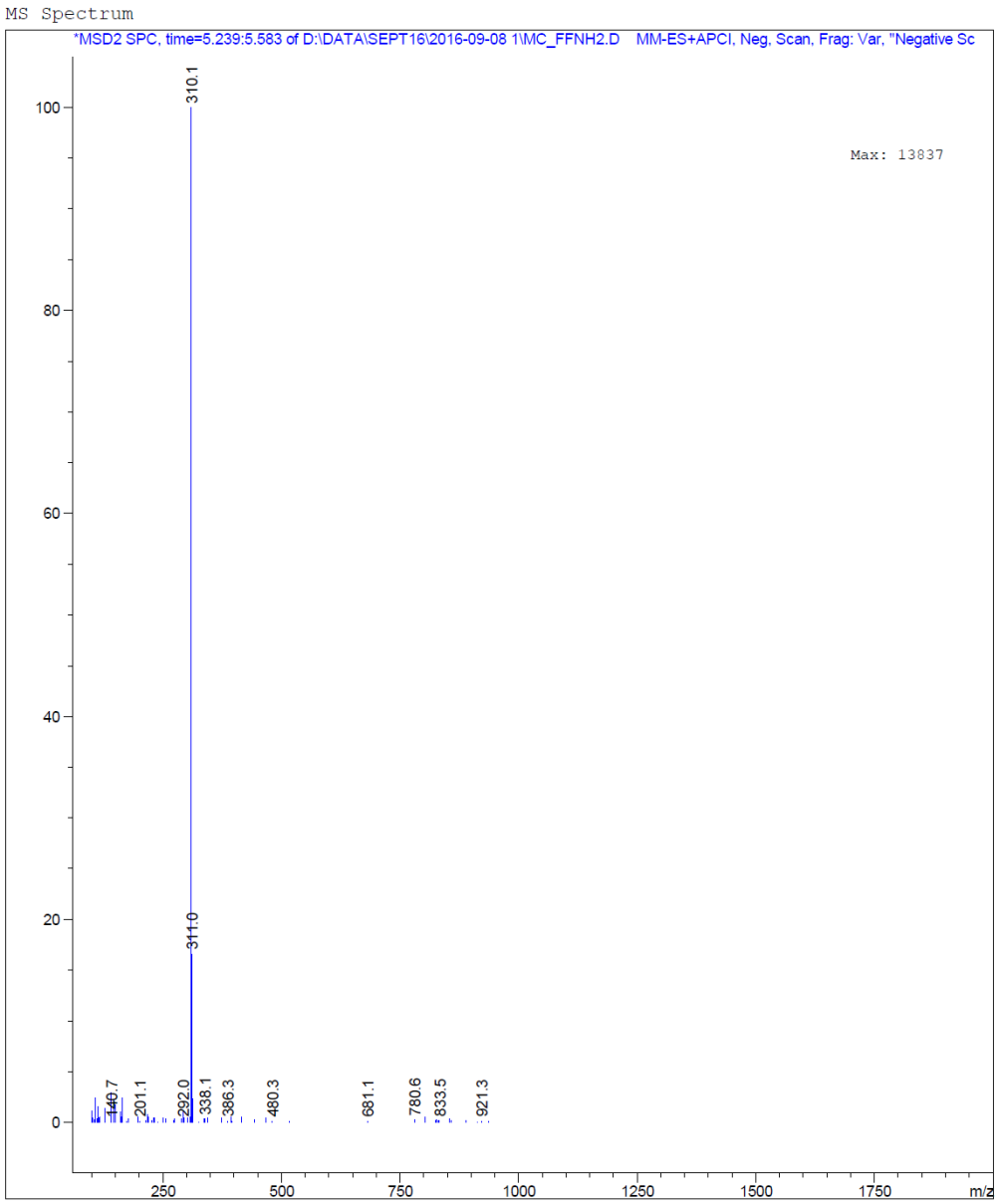


```
Instrument 1 9/12/2016 11:45:58 AM                    Page   1 of 1
```

Figure 81 Negative scan of $FFNH_2$.

```
Print of window 80: MS Spectrum
Data File  : D:\DATA\SEPT16\2016-09-08 1\MC_FFNH2.D
Sample Name : MC_FFNH2
======================================================================
Acq. Operator   :                                  Seq. Line :   3
Acq. Instrument : Instrument 1                      Location : Vial 9
Injection Date  : 9/8/2016 2:53:26 PM                    Inj :   1
                                                  Inj Volume : 10.000 µl
Acq. Method     : D:\DATA\SEPT16\2016-09-08 1\PORO_AMMACE_254.M
Last changed    : 2/12/2015 2:09:30 PM
Analysis Method : C:\CHEM32\1\METHODS\REPORTING_PORO2000.M
Last changed    : 9/8/2016 1:42:01 PM
                  (modified after loading)
Additional Info : Peak(s) manually integrated
```

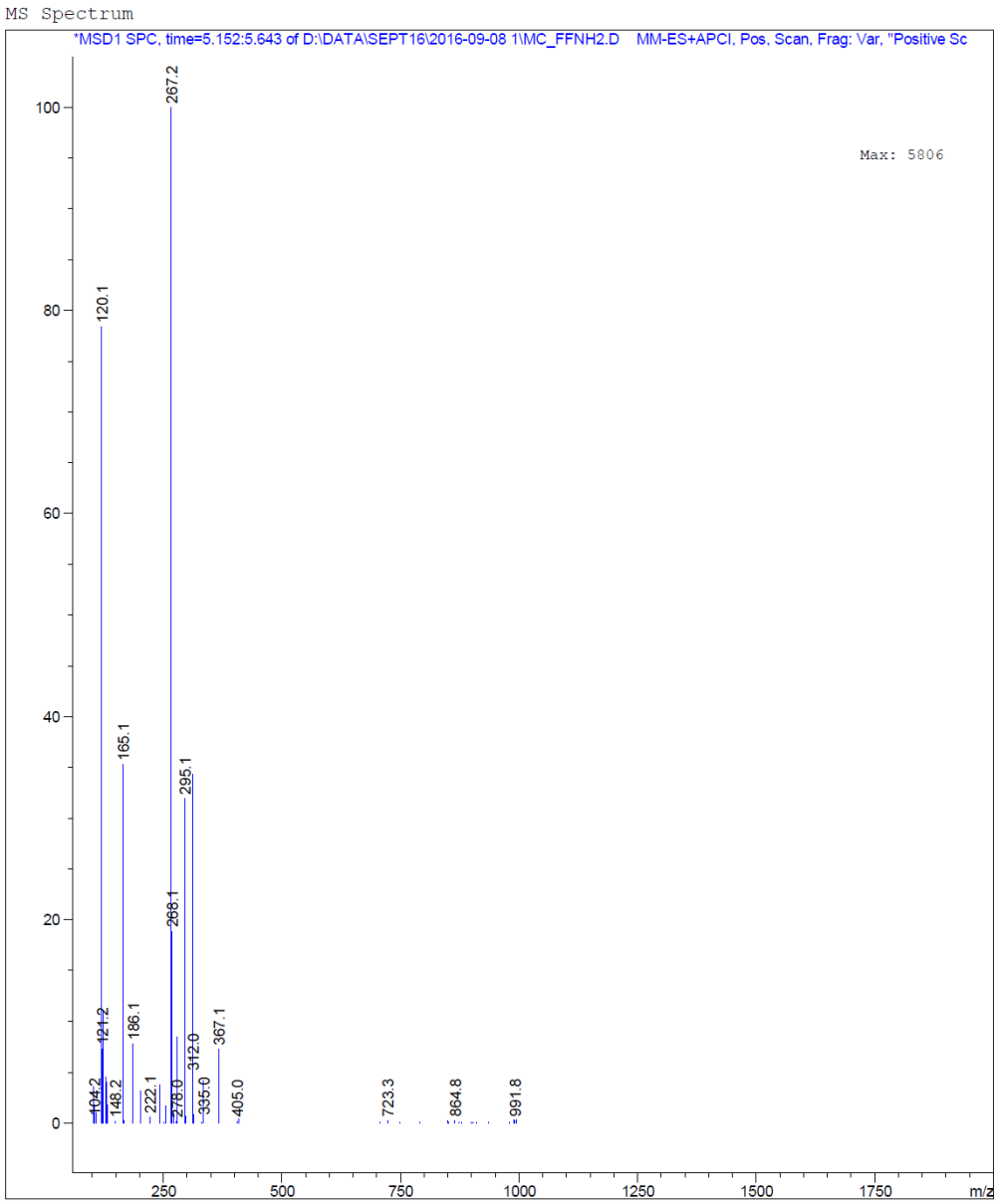


```
Instrument 1 9/12/2016 11:45:29 AM                    Page   1 of 1
```

Figure 82 Positive scan for FF-NH_2 .

10.2. Appendix B - Characterisation of the Enzymatically Formed Gel of Fmoc-TF-NH_2 (Chapter 4)

Samples were analysed on an LCMS system comprised of an Agilent 1200 LC system coupled to an Agilent 6340 ion trap mass spectrometer. Samples were injected onto an Agilent Zorbax column (SB-C8, 5 uM, 2.1x50 mm) using a linear gradient of 5-95% acetonitrile in water (1% formic acid) at a flow rate of 200 µL/min over 10 minutes.

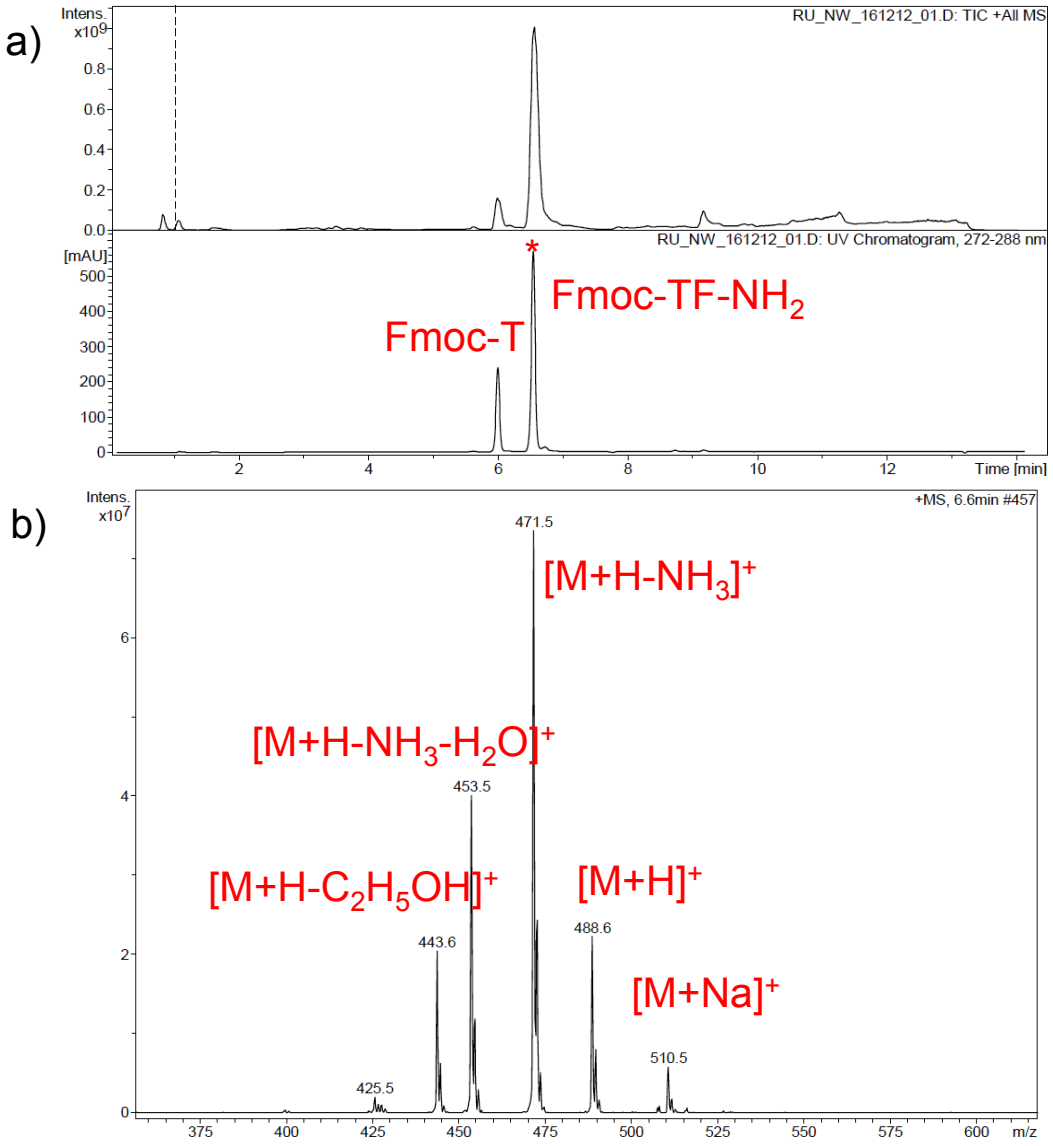

Figure 83 HPLC chromatogram (a) and mass spectrum (b) of a control sample formed by enzymatic reaction between Fmoc-T and FNH_2 with free enzyme in solution to confirm the formation of the conversion product Fmoc-TF-NH_2. Figure (a) shows the Total Ion Current (TIC) chromatogram (top) and the base peak chromatogram (bottom) with the two peaks relative to the precursor Fmoc-T and the conversion product Fmoc-TF-NH_2. In the mass spectrum (b), the product peak is visible at 488 m/z, as [M+H]+. Also visible is the peak of the sodium salt at 510 m/z [M+Na]+. The other peaks are fragment and their description is provided in the picture.